Review

The Enabling Technologies for a Quasi-Zero Emissions Commuter Aircraft

Danilo Ciliberti [1],*[iD]**, Pierluigi Della Vecchia** [1][iD]**, Vittorio Memmolo** [1][iD]**, Fabrizio Nicolosi** [1]**, Guido Wortmann** [2] **and Fabrizio Ricci** [1]

[1]   Department of Industrial Engineering, University of Naples "Federico II", Via Claudio 21, 80125 Naples, Italy;
     pierluigi.dellavecchia@unina.it (P.D.V.); vittorio.memmolo@unina.it (V.M.); fabrnico@unina.it (F.N.);
     fabrizio.ricci@unina.it (F.R.)
[2]   Rolls-Royce Deutschland Ltd. & Co. KG, Günther-Scharowsky-Straße 1, 91058 Erlangen, Germany;
     guido.wortmann@rolls-royce-electrical.com
*   Correspondence: danilo.ciliberti@unina.it

Abstract: The desire for greener aircraft pushes both academic and industrial research into developing technologies, manufacturing, and operational strategies providing emissions abatement. At time of writing, there are no certified electric aircraft for passengers' transport. This is due to the requirements of lightness, reliability, safety, comfort, and operational capability of the fast air transport, which are not completely met by the state-of-the-art technology. Recent studies have shown that new aero-propulsive technologies do not provide significant fuel burn reduction, unless the operational ranges are limited to short regional routes or the electric storage capability is unrealistically high, and that this little advantage comes at increased gross weight and operational costs. Therefore, a significant impact into aviation emissions reduction can only be obtained with a revolutionary design, which integrates disruptive technologies starting from the preliminary design phase. This paper reviews the recent advances in propulsions, aerodynamics, and structures to present the enabling technologies for a low emissions aircraft, with a focus on the commuter category. In fact, it is the opinion of the European Community, which has financed several projects, that advances on the small air transport will be a fundamental step to assess the results and pave the way for large greener airplanes.

Keywords: aerodynamics; propulsion; aero-propulsive interactions; energy storage; airframe

1. Introduction

Aviation contributes to global carbon emissions only from 2.0% to 2.5%. Of this small contribution, more than 90% of the carbon emissions come from commercial operations of large passenger aircraft, which carry more than 100 passengers per trip. Nonetheless, a significant reduction of aviation emissions—including NO_X and noise—is the objective of developed countries because of normative restrictions, long time to consolidate a new technology in aviation, and the global impact of pollutants emissions [1].

In the year 2011, the European Commission formulated ambitious goals in the "Flightpath 2050—Europe's Vision for Aviation" [2] for the European aviation for the year 2050. Two of the ambitious goals are:

- "90% of travellers within Europe are able to complete their journey, door-to-door within 4 h".
- "In 2050 technologies and procedures available allow a 75% reduction in CO_2 emissions per passenger kilometre to support the ATAG target and a 90% reduction in NO_X emissions. The perceived noise emission of flying aircraft is reduced by 65%. These are relative to the capabilities of typical new aircraft in 2000".

Furthermore, the Commission expects that "in 2050, the innovative, sustainable and highly competitive European aviation industry has cemented its place as the world leader".

At time of writing, there are three ongoing European funded projects [3] related to the Small Air Transport (SAT) sector to make economic growth compatible with sustainability and environmental constraints, while keeping the aviation industry competitive and innovative. In this sense, the Horizon 2020 period will be decisive for delivering the innovations defining this century's fleet and its environmental footprint. In fact, results of the Clean Sky 2 (CS2) program will be applicable to 75% of the world fleet needing replacement up to 2050 and CS2 technology will be able to address aviation emissions totalling over 70% of the worldwide civil air fleet [4].

One of the major ambitions of SAT markets is to meet Flightpath 2050 whereby "90% of travellers within Europe are able to complete their journey, door-to-door within 4 h", fitting perfectly and meeting a need that would otherwise go unserved [5]. Today, commuter aircraft have the agility to take off and land in tiny regional or remote utility airports, provide a reduced fuel consumption compared to bigger aircraft, have a fast turnaround time, and can be deployed on routes that would not be geographically or economically viable by rail or road, nor by larger aircraft such as regional turboprops or jets. For this perspective, SAT has a noble role in its operational and societal functions. In fact, SATs help 'connect the dots' and serve local communities and locations that would otherwise be isolated or confined to much slower road or rail transport. There are also many areas of the world where rail is not an option as the infrastructure simply does not exist. Moreover, SAT aircraft could be employed as a low cost/short range cargo for standard pallets (LD3, half pallet) delivery in remote areas [6].

Although the impact of the emissions of general aviation aircraft is tiny with respect to the global anthropic emissions, the SAT segment is seen as the bridge to overcome the gap from experimental aircraft to commercial aviation. It is believed that the success of many technologies can be better proven and demonstrated at the level of SAT rather than on large passenger transportation. This is the case of alternative propulsion system, which has been already introduced on light aircraft and has received a great deal of attention over the past years. Thus, the SAT segment can be a viable feasible platform to develop a systematic approach to fully design such aircraft system, define a best practice, and trace a technological roadmap for larger platform and aircraft demonstrators.

By "near-zero" or "quasi-zero" emissions, the intention is a significant abatement of CO_2, NO_X, and noise emissions with respect to a hypothetical aircraft designed with technologies available in the year 2000, from 50%—if the new aircraft is to enter in service in 2035—to the above cited target values indicated in the Flightpath 2050 document.

To achieve the near-zero emissions target, several technologies and approaches are reviewed in this document. These enabling technologies define the design space of ELICA (ELectric Innovative Commuter Aircraft), a Clean Sky 2 project focused on the conceptual design of a 19-passenger commuter aircraft based on alternative propulsion concepts, targeting 50% CO_2 emissions [7]. The authors of this paper participate in the ELICA consortium, which is made up of industrial, academic, and start-up partners from Germany, Italy, and Belgium.

The technologies presented in this paper include advanced propulsion and energy systems such as all-electric and hybrid-electric propulsion systems and high-power batteries and fuel cells for propulsion, which are discussed in Section 2. Apart from the energy sources, airframe–propulsor integration shall increase the impact of advanced propulsion systems, as in the case of distributed propulsion, which use multiple propulsors to achieve beneficial aerodynamic–propulsion interaction [1,8–11]. Moreover, boundary layer ingestion and laminar flow technology may contribute to improve the aerodynamic efficiency by reducing the aircraft parasite drag. These and other aerodynamic technologies are discussed in Section 3. Finally, airframe offers various key technologies to further improve performance versus weight ratio and even favour safety. That is the case of smart intelligent systems to monitor the whole airframe in IoT (Internet of Things) and Industry 4.0 perspectives. In addition, some challenging but promising advancements are forecasted

by introducing novel and multifunctional materials. Technologies related to airframe are presented in Section 4. Conclusions are drawn in Section 5.

When possible, at the end of each sub-section the authors commented on the feasibility of the presented technology for the commuter aircraft category. One of the limitations of this work is that each technology is analysed alone, therefore the impact of technologies' integration within the aircraft architecture is left to the designer.

2. Propulsion and Energy Storage Technologies

The power needed to propel an aircraft increases at more than the airspeed squared. Thus, high powers and large energies are needed to fly at high speeds over long distances (Figure 1). The maximum power required for an aircraft is the power at take-off and it scales with aircraft weight. Requirements that determine the power levels include considerations of runway length, airport elevation and ambient temperatures, climb rate, and cruise efficiency.

Fuel efficiency has always been a primary design criterion for commercial aircraft since it is an important determinant of aircraft range, size, and economics. Overall, the fuel burn per seat mile of gas turbine-powered commercial aircraft has been reduced by 70% since service started in the 1950s, at an average rate of about 2% per year since 1970. About half the gain has been the result of improvements to the airplane, the rest is due to the engine.

The typical mission profile for a 19-pax air transport is shown in Figure 2. It represents the design mission of the Do-228NG. Energy and power consumption during each flight phase have been simulated by UNINA with its preliminary design software [12,13] and are shown in Figure 3.
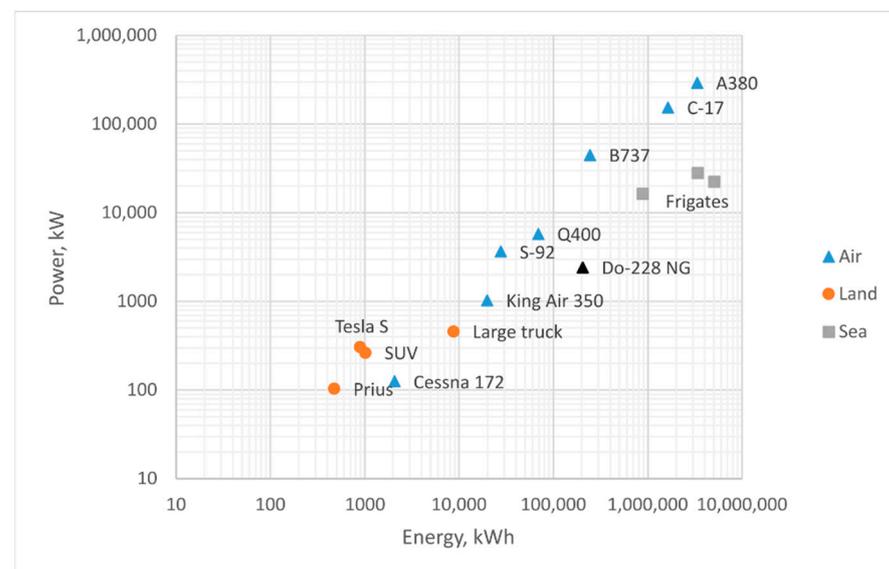

Figure 1. Do-228NG design mission profile.

Most of the fuel is stored in the wings. This arrangement has several advantages: the fuel is located close to the aircraft centre of gravity to minimise its shift as fuel is burned; the wing structural weight is reduced because the fuel weight partially offsets the bending moment produced by wing lift; no space useful for payload, which is carried in the fuselage, is lost.

In the search for alternative energy sources, aircraft weight and drag penalties must be considered if sources less dense than jet fuel (e.g., hydrogen and natural gas) are to be employed. For example, given the low density of hydrogen, the drag and weight increase from the tanks needed for cryogenic liquid hydrogen will offset the gain in energy density for high-speed aircraft. Similarly, battery-powered concepts in which the batteries will

be installed in the fuselage need to be compared with aircraft having similar net payload capabilities.

Aircraft burning fuel during their mission will lose weight. This is an advantage for long range aircraft (more than 3000 nmi), because the decreased weight leads to further increase in range. For ranges lower than 1000 nmi, the weight loss does not significantly affect the energy consumption [1]. However, a battery-powered aircraft needs to be sized to account for landing at maximum take-off weight. For Li-Air batteries, the weight will even increase during flight (see Section 2.4).
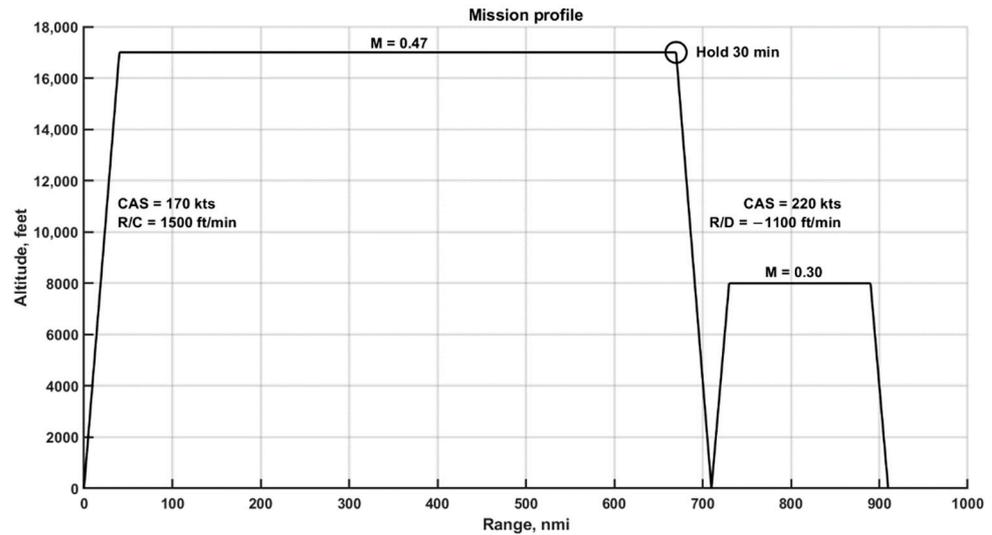
Figure 2. Simulation of Do-228NG power and energy required per flight segment.
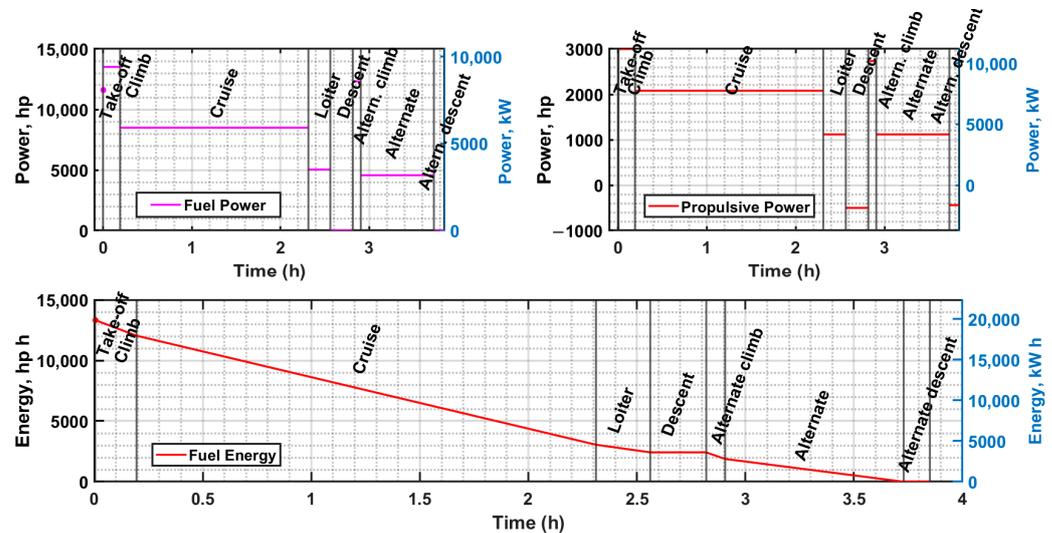
Figure 3. Power and energy required for vehicles ranging from small cars to large commercial aircraft [1,14].

Apart from economic considerations on the development and operations of energy sources alternative to fuel, the following advances in propulsion are identified and discussed in the following sub-sections:

- conventional propulsion
  - evolution of current gas turbines
  - sustainable aviation fuels
- electric propulsion
  - all-, hybrid-, turbo-electric propulsion
  - power electronics

- ○ batteries
- ○ fuel cells
- ○ hydrogen-fuelled aircraft

The best results will be obtained by integrating the enabling technologies. For instance, turbo-electric propulsion will be effective if coupled with distributed electric propulsion, which is discussed in Section 3.1.

2.1. Conventional Propulsion

Gas turbines convert the fuel chemical energy into a rotating shaft mechanical energy. An aircraft engine converts the shaft power into propulsive power with a propeller (turboprop engine) or with a propulsive system made of a ducted fan and a nozzle (turbofan engine). If the propulsor consists of a two large, contra-rotating, tandem propellers system, it is sometimes called "unducted fan" or "prop-fan". Propeller contra-rotation is a way to recover part of the energy loss due to the flow swirl in the propeller wake. The mechanical complexity, weight, and maintenance costs of such a feature often shadow the aerodynamic advantage, so that many propeller-driven airplanes employ a single propeller per engine.

Alternative (piston) engines are commonly used on very light and ultra-light aircraft, due to their compliance with the required power-to-weight and pressure ratio, simplicity, robustness, and the possibility to use automotive gasoline or diesel fuel. Commuter aircraft category are propeller-driven by definition [15]. Power-to-weight ratio favours turboprop engines as a conventional propulsive system for commuter aircraft.

2.1.1. Evolution of Current Gas Turbines

Recent studies have considered the practical limits for simple cycle gas turbines given the potential for new materials, engine architectures, and component technologies. Their estimates provide a possible improvement of 30–35% in overall efficiency with respect to engines currently in service. It may be possible to achieve thermodynamic efficiencies of 65–70% and propulsive efficiencies of 90–95%. Improvements in turbomachinery performance and reduction in cooling losses could improve thermodynamic efficiency by 19% and 6%, respectively. This gain will not be achieved only by the adoption of such new technologies in existing engines, but it will require the optimisation of the thermodynamic cycle from specific levels of component performance characteristics, temperature capability, and cooling. The practical limits to propulsive efficiency cannot be addressed at the engine level alone, but require integration within the airframe and airplane configuration [1].

As concerns propeller efficiency, it is a matter of aerodynamics studies. The adoption of high-fidelity numerical simulations at design level and the addition of a swirl recovery system should provide the achievement of the abovementioned increase in propulsive efficiency. Furthermore, it is known that the flow accelerated through a propulsor contains energy that is pushed away from the aircraft. Thus, a large propeller accelerating a large air mass is more efficient—i.e., it has a lower specific fuel consumption—than a turbofan engine providing a significant acceleration to a small air mass for a given thrust.

Improvement of thermodynamic efficiency requires larger pressure at compressor exit and higher turbine inlet temperatures, while reducing structural weight and aerodynamic losses. Improvements in materials and manufacturing should continue the trend of the last 40 years, which provided forged titanium alloys, several nickel superalloys, single-crystal turbine airfoils, forged high-temperature powder metal alloys, coatings for environmental protection and for thermal barriers, and, most recently, titanium aluminides. Advanced materials can reduce fuel burn by decreasing the engine structural weight and further improvements are expected with long lasting turbine blade resisting at 1700 °C. This includes ceramic matrix composites (CMCs) and other monolithic ceramics, which should enter into service within a few years. Challenges include low fracture toughness, low thermal conductivity, and manufacturing cost. If their thermal resistance could be brought to about 1500 °C, they would dramatically reduce or eliminate cooling in many parts of the engine, significantly increasing efficiency and lowering its weight [1].

Advances in high-temperature metallic alloys, such as nickel-based alloys as well as new materials classes such as niobium and molybdenum, have temperature capability comparable to that of CMCs and much higher fracture toughness and thermal conductivity, with a higher density. They seem suitable for static cooled parts such as combustors or turbine vanes. Further studies on manufacturing and coatings are needed [1].

Coatings can add value to many engine parts. They are required at high temperature for environmental protection. For cooled parts, a thermal barrier coating can significantly increase the temperature capability and reduce cooling requirements. Erosion coating can extend part life and retain performance. Ice-phobic coating can reduce the threats posed by ice formation. Further progress in coatings of all types can be expected given sufficient investment [1].

Different manufacturing techniques, such as additive manufacturing, offer the possibility to produce structures or properties that would otherwise be unrealisable or prohibitively expensive. Some manufacturers claim to achieve improved performance with fewer parts and saving millions of dollars per plane by using additive manufacturing on jet engines [16].

At the time of writing, it is difficult to further quantify the impact of the evolution of the gas turbine. If the overall engine efficiency 30% increase is directly linked to fuel burn, then it may be argued that carbon and presumably also NO_X emissions will be reduced by the same amount in the 2035–2050 timeframe. This improvement is consistent with the 2% fuel burn reduction achieved from the 1970s. Historical data show a 25% reduction in jet engines cruise thrust specific fuel consumption over 40 years, with turboprop gaining from 10% to 30% more efficiency over regional jets and large turbofans. However, fuel consumption and emissions from cruise data are not sufficient to describe the impact of the advancing technology. As concerns turbofan engines, it has been shown [17] that during the last 40 years, thrust specific emissions during a landing–take-off cycle have been almost constant. Moreover, despite significant investments in aero engine technology, emissions saving rates are decreasing over time. This is due to several factors: emissions of carbon monoxide and hydrocarbons significantly increase at low thrust settings (landing), while NO_X high emissions at high thrust settings (take-off) and high thermal efficiency is counterbalanced by high bypass ratios engines. The emissions of CO_2 follow the same trend of thrust-specific fuel consumption with engine ratings. Similar conclusions may be drawn for turboprop engines. In addition, the impact of emissions at low altitudes, especially in take-off and landing phases, may be critical because of the highly urbanised areas near the airports and photochemical reactions in the low troposphere [18].

This explains why even if all the above-mentioned technological improvements are successfully integrated into a turboprop engine, they will not be sufficient to cope with the target of quasi-zero emissions.

2.1.2. Sustainable Aviation Fuels

Sustainable aviation fuels (SAFs) are alternative to petroleum-based jet fuels, fully compatible with the existing aircraft and fuel infrastructure, miscible with conventional jet fuels, and sustainable in the sense that they have a smaller carbon footprint in their entire life cycle and are acceptable also from a socio-economic point of view. While burning SAF will produce nearly the same amount of CO_2 per unit of fuel as conventional jet fuel, the use of SAF reduces net life cycle carbon emissions because SAFs enable reusing or recycling carbon that is already present in the biosphere. If their commercialisation takes place on a large scale, aviation can significantly lower its net carbon emissions more quickly and effectively than improving operations, infrastructure, and aircraft. This reduction can also be achieved without impacting the timeframe or suitability of other potential carbon-lowering approaches.

Jet fuel is a generic term that encompasses many specific variants, such as Jet A, Jet A-1, JP-5, and JP-8. In most cases, the other names imply specific variants of the fuel, as often detailed in the specifications. Jet A is the most common form of jet fuel used by

commercial aviation in the United States, while Jet A-1 predominates in the rest of the world [1].

To be fully compatible with conventional jet fuels, SAF must have high energy per unit mass, high energy per unit volume, low freezing point, low vapor pressure, materials compatibility, low toxicity, and must be stable and non-volatile. These properties ensure safety and compliance to the required performance. Any synthetic fuel that has such characteristics is also called a "drop-in" fuel, in the sense that it can substitute conventional jet fuel without changing the existing aircraft fuel system or airport infrastructure.

Sources other than petroleum include woody biomass, hydrogenated fats and oils, recycled waste, and other renewable sources. The American Society for Testing and Materials (ASTM) International has developed standards ASTM D4054 and D5766 to approve new bio-based aviation fuels, and currently, six production pathways have been certified for blending with conventional aviation fuel. These are reported in Table 1. Additional pathways are currently in the ASTM certification process.

Table 1. Approved sustainable aviation fuels as per ASTM D5766 [19].

Name	Abbrev.	Description	Feedstocks [1]	Max blend	FRL [2]
Fischer–Tropsch Synthetic Paraffinic Kerosene	FT-SPK	Biomass is converted to synthetic gas and then into bio-based aviation fuel.	Wastes (MSW, etc.), coal, gas, sawdust	50%	7
Fischer–Tropsch Synthetic Paraffinic Kerosene and Aromatics	FT-SPK/A	A variation of FT-SPK, where alkylation of light aromatics creates a hydrocarbon blend that includes aromatic compounds.		50%	7
Hydroprocessed Fatty Acid Esters and Free Fatty Acid	HEFA	Lipid feedstocks, such as vegetable oils, used cooking oils, tallow, etc., are converted using hydrogen into green diesel, and this can be further separated to obtain bio-based aviation fuel.	Vegetable oils: palm, camelina, jatropha, used cooking oil	50%	9
Hydroprocessing of Fermented Sugars—Synthetic Iso-Paraffinic kerosene	HFS-SIP	Using modified yeasts, sugars are converted to hydrocarbons.	Sugarcane, sugar beet	10%	5–7
Alcohol-to-Jet Synthetic Paraffinic Kerosene	ATJ-SPK	Dehydration, oligomerisation, and hydro processing are used to convert alcohols, such as iso-butanol, into hydrocarbon.	Sugarcane, sugar beet, sawdust, lignocellulosic residues (straw)	50%	7
Co-processing		Biocrude of lipidic feedstock in petroleum refinery processes.		5%	6–7

[1] SAF technical certification [20]. [2] Fuel Readiness Level [21].

Actual potential for local bio-fuels production are 0.3% of US [1] and 4% of Europe jet fuel demand [19]. The price of SAF obtained from exhausted cooking oil ranges from 950 to 1015 €/ton, versus the 600 €/ton of the conventional jet fuel. Some sources of SAF are used to produce the biodiesel powering road vehicles, thus enabling a competition that is expected to grow in the coming years. Current consumption in Europe is very low compared to the potential production capacity [19].

The European Union define SAFs as biofuels whose life cycle's greenhouse emissions are reduced with respect to fossil fuels by at least 50% for production plants older than 5 October 2015, 60% for production plants built later, and 65% for installations from year 2021. Furthermore, raw materials cannot be sourced from land with high biodiversity or high carbon footprint. The consideration of the life cycle is important because even if a biomass grows by absorbing the same amount of CO_2 produced during its combustion and hence yielding to a zero net carbon footprint, the cultivation, harvesting, transportation, and conversion of biomass into fuel produce further carbon emissions that cannot be recovered [19].

Depending on the biomass source and difference in production chains, a HEFA biofuel should reduce the direct greenhouse gas emissions by about 50%, from the 89 gCO_{2eq}/MJ to the 40–50 gCO_{2eq}/MJ. Further details are reported in Table 2. It is here remarked that these estimates do not include indirect effects such as land use change (e.g., a cropland previously used for agriculture) [19]. Having the same basic molecular structure (i.e., hydrocarbons), the burning of SAF produces the same amount of CO_2 of conventional jet fuel. The so-called "pump-to-wake" contribution to greenhouse emissions is practically the same. The overall emissions, the so-called "well-to-wake", can be reduced up to 90% since most of the emitted carbon is absorbed by new biomass [1].

Table 2. Greenhouse emissions savings (excluding carbon emissions from land use change) [19].

SAF	Feedstocks	Direct Emission Savings *	Average
FT-SPK-A	Agricultural residues	89–94%	81%
	Forestry residues	88%	
	Municipal Solid Waste (MSW)	68%	
	Short-rotation woody crops	81%	
	Herbaceous energy crops	87%	
HEFA	Tallow	78%	61%
	Used cooking oil	85%	
	Palm fatty acid distillate	76%	
	Soybean	53%	
	Rapeseed/Canola	48%	
	Camelina	54%	
	Palm oil—closed pond	61%	
	Palm oil—open pond	29%	
SIP	Sugarcane	62%	65%
	Sugarbeet	68%	
Iso-butanol for ATJ	Agricultural residues	71%	67%
	Forestry residues	74%	
	Sugarcane	69%	
	Corn grain	54%	
	Herbaceous energy crops (switchgrass)	66%	
	Molasses	69%	
Ethanol for ATJ	Sugarcane	69%	48%
	Corn grain	26%	

* With respect to 89 gCO_{2eq}/MJ jet fuel baseline.

2.2. Electric Propulsion Architectures

Electric propulsion systems convert electric energy into mechanical energy, which is converted into thrust by a propeller or a fan. They are an effective way to reduce pollutant emissions as long as the energy sources are renewable. Electric propulsion can be all-electric, hybrid-electric, or turbo-electric. There are several variants of the logic schemes of an electric propulsion system [13,22–24]. In the following, multiple hybrid propulsion systems are evolved from a conventional propulsion system and their benefits over the conventional system are discussed in a qualitative way. The systems are focused on aircraft application. However, they could also be used to drive cars or trains.

The assessment starts with a conventional propulsion system by considering functional aspects only. This means that only different subsystem and component types and their impact on the hybrid system are considered. The number and the size of individual subsystems or components are not considered as this would lead to a large number of systems, which cannot be compared in a meaningful manner in this report. In the following, the system is extended step by step with electric components until the most complex hybrid system is presented at the end. Figure 4 shows the setup of a conventional propulsion system.
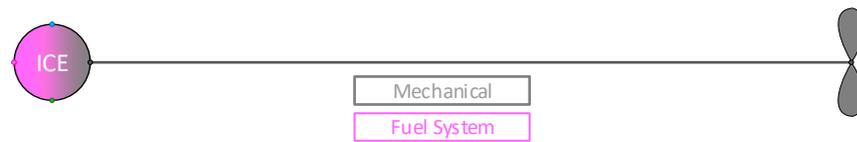
Figure 4. Conventional propulsion system.

The system consists of an internal combustion engine (ICE), which transforms fuel to mechanical power. This may be a piston or a gas turbine engine. The right side shows a propulsor, which consumes the mechanical power to propel the vehicle. The entire propulsion system may contain multiple of these subsystems; however, only one unit is considered to limit the number of propulsion systems to draw. There may also be gears and multiple shafts involved in the mechanical transmission, but this is not of interest for this high-level assessment.

Hybrid propulsion systems can be split into two categories: serial hybrid and parallel hybrid systems. In serial hybrid systems, the entire propulsive power is transformed from one form to another. In parallel hybrid systems, only a share of the total propulsive power is transformed to a second energy form. The easiest way to extend the conventional propulsion system from Figure 4 to a parallel hybrid system is to add an electric energy storage, which can supply power to the propulsor shaft. The setup of this parallel system is shown in Figure 5.
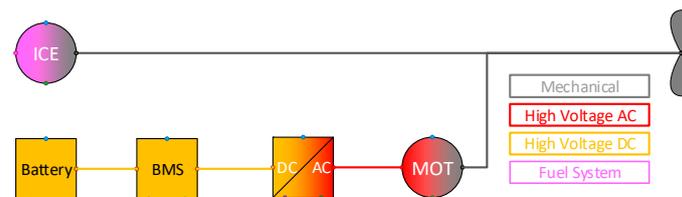

Figure 5. Parallel hybrid propulsion system.

The idea of adding an electric energy storage is its buffering capability. The storage can supply additional power during short time mission segments. Hence, the ICE can be downscaled to an average continuous load and the peak loads are covered by the additional power from the electric energy storage. The higher load of a downscaled ICE is beneficial for its efficiency but disadvantageous for the lifetime of temperature-limited parts such as turbines. When the ICE is operated at a higher relative load, the cycle temperatures and pressures are higher, which results in lower turbine lifetime and shorter maintenance intervals. No studies have been found in literature that state to which extent and under which circumstances the net balance of those two effects is positive or not.

In this case, the electric energy storage is implemented as a battery, but it could be any electric energy storage or a fuel cell. The battery power is supplied to an inverter, which drives an electric motor. The mechanical power of the motor is supplied to the propulsor shaft. When the power electronics are designed accordingly, the energy flow can be bidirectional. Hence, the battery can be charged when the system is operative by absorbing mechanical power from the ICE. This can be done during mission segments where the propulsor does not require much power.

The second group of hybrid propulsion systems are serial hybrid systems. In these systems, the entire propulsive power is transformed to a second power form. To transform the conventional propulsion system shown in Figure 4 to a serial hybrid system, two electric machines are added. The system setup is shown in Figure 6.
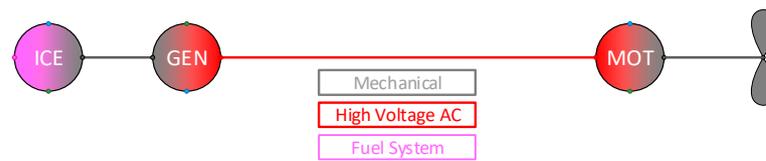
Figure 6. Electric shaft system.

The generator (GEN) transforms the mechanical power of the ICE to electrical power. The motor (MOT) on the right transforms the electric power back to mechanical power which is then supplied to the propulsor. This system is called "electric shaft", as there is no control input to manipulate the power transmission. The generator design, the rotational speed, and the power of the ICE determine the voltage, current, and the frequency in the AC transmission system. The motor configuration determines the rotational speed and the mechanic power of the propulsor. As the design of the electric machines is not considered to be modifiable during operation, the combination of the two electric machines has a constant transmission function like a mechanical gear stage. To adjust the load share between multiple propulsors connected to one engine, a variable pitch mechanism is required. With such a mechanism, the torque and power demand of each propulsor can be adjusted. This works for ship and aircraft propellers. For trains and cars, this mechanism is not possible. Moreover, this system requires a particular start-up sequence with very low load to enable the spool up of the propulsors together with the engines and the generators. This requirement reduces the application to hybrid-electric aircraft with variable pitch propulsors as they can feather the propulsor and spool up with a low torque load. Trains and cars would start to move during the start-up and the higher share of viscous propeller losses—compared to the aircraft—results in high loads even with feathered propellers.

The advantages introduced with the two electric machines are the simplicity of connecting multiple propulsors and generators to the AC transmission system as well as the simplicity of routing cables through the vehicle instead of rigid shafts. The drawback of this system is the cogging torque limit of the electric machines in such a setup. When the transmitted torque exceeds the cogging torque of synchronous machines, the machine gets desynchronised, which leads to the loss of power transmission and excessive mechanical forces.

The electric shaft system can also be extended with an electric energy storage to provide additional power during short mission segments. An example system setup with a battery energy storage is shown in Figure 7.
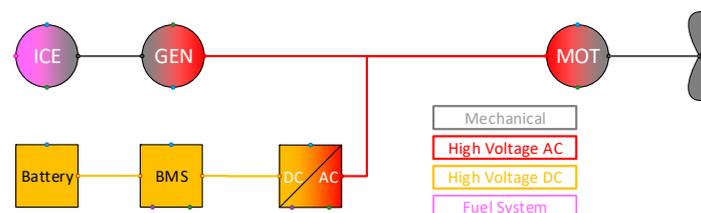
Figure 7. Electric shaft with electric energy storage.

With an electric energy storage, the ICE can be downscaled to increase its efficiency and to reduce its weight. When an energy storage is utilised that can operate at high frequency cycles, it can be used to compensate the reactive power in the AC transmission system. Moreover, the power electronics of the energy storage would allow to remove the cogging torque limitation of the electric machines. This allows to reduce the size of both electric machines and the cables. In this case, however, all the electric components are a single point of failure as the system would not be able to operate at rated power without the reactive power compensation.

To further extend the electric shaft system, a set of power electronic devices can be added to the AC transmission. The rectifier transforms the AC power from the generator to DC power. The DC power is transmitted to the propulsors, where an inverter transforms

the power back to AC power. In the aerospace industry, this system, without an energy storage, is called the turbo-electric propulsion system. It is shown in Figure 8.
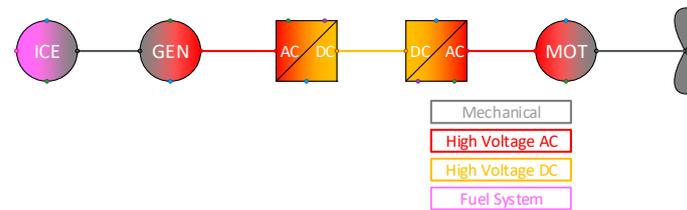

Figure 8. Turbo-electric propulsion system.

The introduction of the power electronic devices allows to operate the ICE and the propulsor at almost independent rotational speeds. Hence, the system could be compared to a mechanical gear stage with a variable transmission ratio. This allows to control multiple propulsors independently from each other, without the use of variable pitch mechanisms at the propulsors. In this way, multiple fixed pitch rotors could be controlled independently from each other. Of course, this system can also be extended with an electric energy storage, which supplies the DC link. A possible system setup is shown in Figure 9.
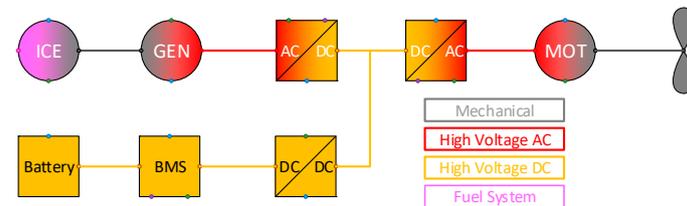
Figure 9. Serial hybrid propulsion system.

This serial hybrid propulsion system with a DC link and an electric energy storage concludes the series of hybrid-electric propulsion systems from the functional point of view. Three main hybrid topologies have been presented so far: the parallel hybrid system, the electric shaft topology, and the DC link topology. In the last step, the electric shaft and the DC link topology are qualitatively compared with each other. Table 3 summarises the comparison of the two topologies with respect to operational aspects, system level aspects, and component level aspects.

In contrast to the electric shaft, the DC link topology allows to decouple the rotational speeds of the electric machines in the propulsion system. Hence, fixed pitch rotors can only be operated independently in a DC link topology. The electric shaft topology has a torque limit, which must not be exceeded during operation to ensure synchronisation of all electric machines.

Both topologies can be extended with electric energy storage subsystems to benefit from buffering capability. The supply of electric non-propulsive loads is feasible in both topologies. The system complexity is significantly different. The electric shaft topology involves a lower number of components and only passive components. The electric machines do not require control or communication (except for health monitoring and safety) and, hence, no complex hardware, which is a significant benefit over the DC link topology.

The electric shaft benefits from lower losses in the electric machines, as the iron losses from the high frequency switching signals of the power electronics do not occur. Only iron losses from the low frequency machine currents occur in the motor. As there are no power electronic devices, the losses in the electric shaft topology are lower than in a DC link topology. However, the masses of the electric machines and the cables will be higher as the machines must be designed for the maximum peak torque to avoid desynchronisation and the cables must be sized for the reactive power in the system. For long distances between the electric machines, the electric shaft topology has the disadvantage that the power factor decreases with longer cable lengths.

Table 3. Comparison of the electric shaft and the DC link topology.

	Electric Shaft	**DC Link**
Operational aspects		
Electric machine rotational speeds are decoupled	No	Yes
Power split between multiple propulsor motors is variable without variable pitch mechanism	No	Yes
Peak torque capability	Low	High
System level aspects		
Battery integration possible	Yes	Yes
Non-propulsive power offtake possible	Yes	Yes
System complexity (number of components, control complexity)	Low	High
Component aspects		
Losses in electric machines	Low	High
Losses in power electronics	None	High
Mass of electric machines	High	Low
Mass of power electronics	None	High
Mass of cables	High	Low

2.3. Powerplant Integration and Technological Trends

A turbo-electric concept does not rely on electric energy storage. The overall efficiency of such powertrain is lower than the conventional gas turbine configuration, because of additional energy conversion and transmission losses. This is apparent from Figure 8. Therefore, the effectiveness of turbo-electric architecture relies on its integration in the airframe, leading to beneficial aero-propulsive interactions that are unfeasible to obtain with a conventional powertrain. In fact, electric propulsion enables the possibility to distribute the propulsors on the wing—distributed electric propulsion (DEP)—and to cancel most of the fuselage wake with boundary layer ingestion (BLI), which are discussed in Section 3.

A key benefit of DEP is the reduction of motor size and power required as there are many more motors. Moreover, electric motors can be easily scaled down, in contrast with gas turbines. The potential applications and timeframe for turbo-electric concepts rely on the advance in the specific power of components. Current electric generators installed on in-service aircraft have a specific power around 2.2 kW/kg. Future trends are shown in Figure 10, where most of the data are derived from research studies on possible future large passenger airplanes [1]. An average growth of 0.33 kW/kg per year is forecasted, such that a specific power of 10 kW/kg is expected in the next 25 years.
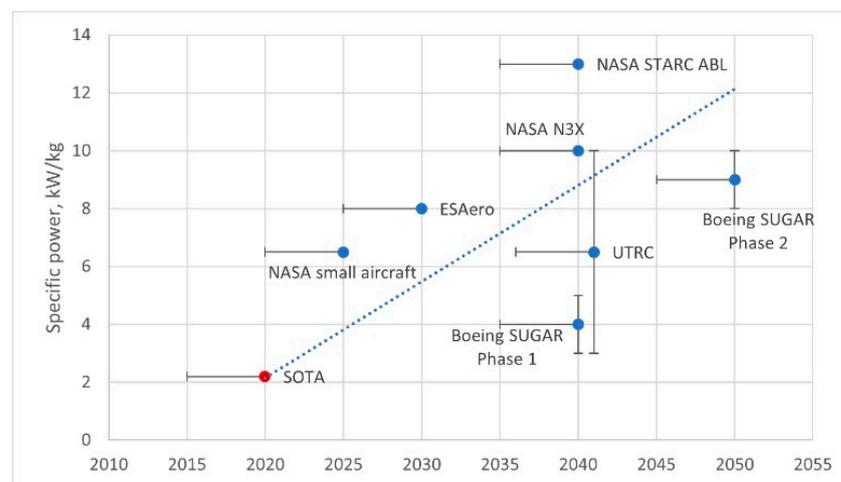
Figure 10. Trend of electric drives specific power. Reproduced from data presented in Ref. [1].

For commuter and general aviation aircraft, it is claimed that the electric motor power, including power electronics, will be below 1 MW and the required specific power should be around 7 kW/kg [1]. In April 2015, Siemens announced the development of a direct-drive (2500 rpm), 260 kW aircraft electric motor weighing a little over 50 kg [25]. The motor specific power is in the order of 5 kW/kg, and it is capable of powering aircraft with a maximum take-off gross mass of 2000 kg. The potential availability of such an engine suggests that twin-engine commuter aircraft could be powered by electric motors using current technology. It will be the energy source that will determine the potential range of such aircraft and hence their economic viability. This is the argument of the following sections.

2.4. Power Electronics, Distribution, and Thermal Management

Power electronics already play a key role for aircraft electrical power systems and that role becomes more critical with turbo-electric propulsion systems. Power electronics are used for power conversion (including motor drives) and power distribution (circuit protection).

Silicon carbide (SiC) power electronics enable MW-class aircraft power due to their improved efficiency and high voltage performance characteristics compared to today's silicon-based power electronics. SiC is also a more reliable technology than silicon in commercial aircraft environments. Specific power for silicon-based power electronics systems today is approximately 2.2 kW/kg for aircraft applications and their use for circuit protection is limited to 25 A at 270 V DC (7 kW). Higher-powered circuit protection is provided by mechanical breakers and relays up to about 500 A at 270 V DC (135 kW) using state-of-the-art equipment. It is envisioned that in 20 years, SiC-based power electronics systems for aircraft applications will have a specific power of 30 kW/kg—unpublished data from Rolls-Royce—for power conversion and circuit protection using electronic components up to 200 A at ±270 V—essentially 540 V, for a power capacity of 108 kW—or using mechanical breakers up to 1000 A at ±270 V (540 kW). High specific powers will be facilitated by advances in components that make power electronics heavy: switching components, materials, switching topologies, passive filter components such as transformers, packaging, and thermal management components [1]. Especially the passive components (e.g., filters and the DC capacitor) and connection interfaces and housing make the power electronics large and heavy. The power density of power electronic devices can be increased significantly by increasing the switching frequency and by integrating the inverter into the electric machine. Increasing the switching frequency is enabled by SiC technology, which has very low switching losses. High switching frequencies reduce the amount of energy for which the passive filters and capacitors must be sized for.

As concerns power distribution, the standard system works at 115 VAC 400 Hz. Smaller and older aircraft use a 28 VDC system and smaller airports may only have a 28 VDC power source. A third option is the 270 VDC standard. The 270 VDC system for aviation was first defined in MIL-STD-704B 17 Nov. 1975 [26]. As matter of fact, a higher DC voltage enables lighter cables and converters. The ±270 V (or 540 V) standard seems to be the target for the foreseeable future, since at this voltage, there are no electric sparks due to the breakdown of the dielectric—which is air—whatever the altitude and the gap between the electrodes. This limit is defined by the Paschen curves. The ±270 voltage is used on the Boeing 787 today, while the US Air Force is investigating its use for future high-power aircraft.

As future turbo-electric system concepts include kilovolt-class power distribution systems, new types of insulation systems and electrical conductor spacing rules and practices are required. In fact, as micro-voids in the insulation coat of the cables will reduce the breakdown field, eventual partial discharges will degrade the coat. Thus, the time-to-failure due to a disruptive discharge is a crucial safety issue. The health of the electric insulation is monitored by insulation monitoring devices (IMD). These measure the total insulation resistance between the conductors (plus and minus) and the aircraft structure. The insulation

resistances will degrade over time until a lower threshold is reached at which components need to be maintained. The IMD can measure the insulation resistance of the entire system, even those of the electric machines behind a power electronic device. The measurement can be performed once per minute and while the system is operating. Thus, the failure of the insulation due to partial discharge and ageing can be predicted quite well. In addition, a higher temperature of the air medium between electrodes will reduce the thermodynamic pressure, thus lowering the pressure–distance product and trigger an electric discharge [27]. This is the reason for the 270 VDC standard being below the 327 V minimum of the air Paschen curve.

The ability of aircraft to manage heat will be a limiting factor for the high-power electrical power systems needed for turbo-electric propulsion. The thermal management system itself will require electrical power to operate and that power demand will need to be accounted for, along with the demands of other non-propulsive power systems.

2.5. Batteries

Batteries are electrochemical cells that store chemical compounds holding a voltage difference between the electrodes. The battery, which is usually made up of several individual cells in series, provides electric energy with a chemical reaction when the electric circuit at its poles is closed. Electrochemical cells convert the energy stored in the chemical bonds directly into electricity, without producing heat or thermal energy as an intermediate stage of the energy conversion process. Because of this, electrochemical cells are not subjected to the Carnot limitations, hence their efficiency as energy in releasing energy can be very high. The total chemical energy that may be converted to electric energy is equal to the exergy of the electrode materials [28]. The working principle of an electrochemical cell is illustrated in Figure 11.
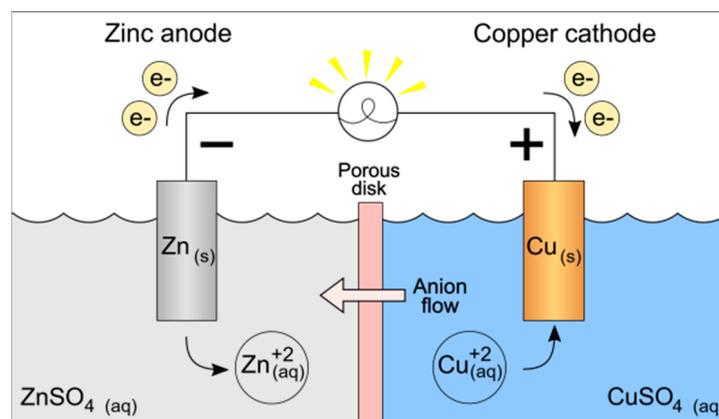

Figure 11. Working principle of a galvanic cell. CC BY-SA [29].

No combustion takes place; hence, batteries are theoretically an alternative to the fossil fuels since no emissions are generated during flight. However, when compared to the jet fuel as energy storage, the current battery technology loses its attraction. The most important parameter is the equivalent specific energy, which determines how much energy can be stored per mass unit. Jet fuel stores about 13,000 Wh/kg, while actual batteries are below 250 Wh/kg. For regional hybrid-electric turboprop specific energies higher than 500 Wh/kg, ideally 800 Wh/kg is needed. For an all-electric system, the required specific energy may be around 2000 Wh/kg, if the actual design ranges are to be kept [13,23,30].

A trend on specific energy derived from NASA/Boeing SUGAR study indicates that an increment of 7.6% per year is needed to achieve 750 Wh/kg by 2030 [31]. Although additional improvements are foresighted, it is unlikely that an electrochemical cell or a super capacitor will achieve more than 1500 Wh/kg, while even 500 Wh/kg achieved by 2035 seems optimistic. Current trends in battery technology concern lithium-ion, lithium-sulphur, and lithium-oxygen cells. Expected achievements by 2035 at cell level are reported

in Table 4 and illustrated in Figure 12. While theoretical specific energies are much higher than those reported, in practice, the attained value will be significantly lower because of the added weight of current collectors, electrolytes, separators, battery cases, and terminals. Even if specific energies of 1500 Wh/kg were achieved, such high specific energies will require major breakthroughs. Furthermore, the requirement to simultaneously achieve long cycle life, low cost, and acceptable safety greatly increases the complexity of the overall challenge [1]. At pack level, the specific energy will further decrease due to the additional weight of casing and connectors. Packaging of electrochemical cells is necessary to achieve the desired voltage. A single Li-ion cell has a nominal voltage from 3.3 V to 4.0 V, depending on the component bound to the lithium [28].
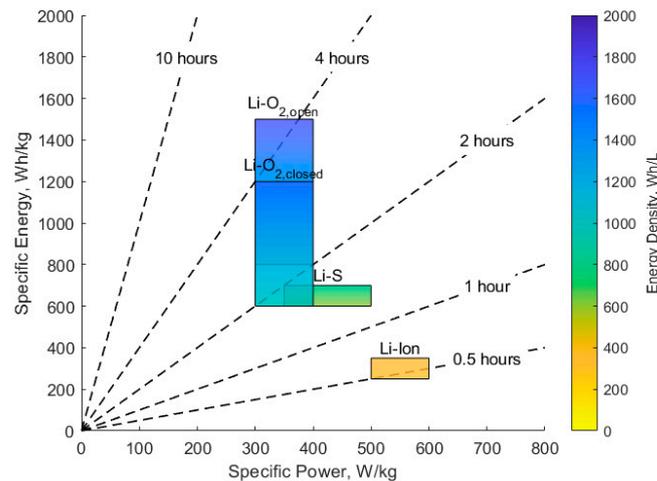
Figure 12. Ragone plot (in linear scales) of the forecasted battery cells technology by 2035.

Lithium-ion batteries currently dominate the market in both consumer electronics and electric vehicles. Batteries can be scaled to meet power and energy requirements for aviation, as lithium-ion battery systems with power capability greater than 10 MW and energy storage capacity greater than 10 MWh have already been demonstrated in stationary energy storage for electric utility applications [1]. The maximum theoretical specific energy that can be obtained by chemical reaction is about 550 Wh/kg. In practice, for a single cell it is around 210 Wh/kg, while for a cells' pack, it is about 150 Wh/kg [32,33]. As regards safety, Li-ion batteries have proven to be susceptible to thermal runaway, a process where the heat from a failing cell causes itself and surrounding cells to fail, thereby generating more heat. This happened to the Boeing 787 Dreamliner of Japan Airlines and, together with an emergency landing to another 787 of All Nippon Airways, prompted the US Federal Aviation Administration to ground the entire 787 fleet in 2013 [34]. Moreover, in case of overcharging, the high local temperatures can release oxygen from the cathode. If the oxygen reacts with the flammable organic electrolyte, there is a serious risk of combustion and even explosion. Therefore, improvements of Li-ion batteries should also focus on lighter casing and safer electrodes and electrolytes. This should lead to specific energies between 250 and 350 Wh/kg at cell level by 2035 [35].

The lithium-sulphur (Li-S) combination is being investigated to increase the specific energy of lithium batteries. The chemical reaction provides a maximum of 2500 Wh/kg, while specific energies of 300–350 Wh/kg at cell level and 200–250 Wh/kg at pack level are available [33]. Li-S batteries with specific energy of 600 Wh/kg have been tested in controlled environments; hence, it is expected that such values could be achieved by 2035 for electric aircraft propulsion systems. The practical application of Li-S batteries is actually hindered by a very low life cycle and low efficiency that does not permit the full extraction of the chemical energy. Both of these drawbacks could be overcome by the application of nano-structures and graphene at the electrodes [35].

Table 4. Trends in future batteries at cell level by year 2035 [35].

	Unit	Li-ion	Li-S	Li-O$_{2,open}$	Li-O$_{2,closed}$
Specific energy	Wh/kg	250–350	600–700	800–1500	600–1200
Specific power	W/kg	500–600	350–500	300–400	300–400
Energy density	Wh/L	600–800	300–350	1000–1700	1000–1600
Charge/discharge efficiency	%	90–95	70–90	60–85	60–85
Cycle life #	cycles	1000–3000	1000–2500	500–1000	500–1000
Degree of discharge	%	70–90	90–100	70–90	70–90
Lifetime	yrs.	7–15	7–14	5–10	5–10
Cost ($ 2010)	$/kWh	250–350	250–500	400–800	300–700
Uncertainty	-	low	medium	high	high

The lithium-oxygen (also known as lithium-air) technology is the most promising concept for new batteries. The maximum theoretical specific energy is about 3450 Wh/kg, with actual battery packs for ground vehicles ranging from 300 to 700 Wh/kg and 400 Wh/kg at system level, including the gas delivery system [36]. A value of 1500 Wh/kg at cell level is forecasted by 2035 [35], although some authors claim a theoretical value of 11,000 Wh/kg [37], quite close to the jet fuel value. Ref. [37] also states theoretical specific energy values of aluminium, magnesium, iron, and zinc cells to about 8000, 6800, 1800, and 1300 Wh/kg respectively. However, the same report, dating back to 1979, expects a 290 Wh/kg value for the Li-air battery and no attractive commercial applications. Similar to the Li-S battery, Li-air cells have problems with safety, low charge and discharge rates, poor energy efficiency, and limited life cycles. This is due to the nature of the battery, which needs gaseous oxygen to work. The oxygen may be extracted from the air (open-cycle) and this will theoretically reduce the mass of the battery, since one of the compounds is already present in the air. In practice, the presence of impurities as CO_2 and moisture requires a separator and possibly a purifier to get pure oxygen for the chemical reaction. At high altitudes, the oxygen must be compressed to counteract its lower density at ambient conditions. In such an open-cycle process, the mass of the battery increases while discharging, due to the additional oxygen bounded to the electrodes, a curious effect for the aviationist used to the airplane's weight decreasing with fuel burn. Such increase is about 0.2 g/Wh [35].

Alternatively, a closed-cycle process eliminates the need for the oxygen separator, compressor, and purifier, but a pressure vessel is needed to keep the oxygen at the desired pressure value. The vessel would naturally pressurise during the charge cycle with only small losses due to heat of the compression. However, all of the battery reactants will be located within the pressure vessel, with the presence of flammable electrodes and pure oxygen, leading to a non-trivial safety issue. This is complicated by the difficulty of cooling or heating the battery inside the vessel. In fact, the forecasts provide better achievements for the open-cycle battery [35].

A major technological breakthrough in battery systems will be required to achieve the specific energies required for battery-powered electric and hybrid aircraft propulsion systems before these systems can make a significant contribution to reducing carbon emissions in aviation [1]. Clearly, the improvements in battery technology will bring benefits to all aircraft classes, regardless of their size, with a concern for the weight and volume of the Li-air closed-cycle process system on small airplanes.

2.6. Fuel Cells

Fuel cells convert the chemical energy of a fuel into electrical power without any combustion. The exhaust from fuel cells is totally carbon-free if hydrogen is used as the fuel. However, if a hydrocarbon fuel is used, the exhaust still contains CO_2 in direct proportion to the amount of fuel consumed, but there are no NO_X or particulate emissions [1]. Fuel cells are similar to batteries, yet they are open thermodynamic systems, which may operate without stop. They are continuously supplied with fluid fuels and oxidants, their

electrodes are not part of the reaction process and, hence, do not need to be regenerated or recharged. In general, the oxidant is air at sea level pressure, while the fuel is hydrogen or a hydrocarbon. Fuel cells produce a maximum voltage of the order of 1 V, therefore higher values of the output voltage are achieved by having several fuel cells in series, or "stacks". Typically, fuel cells are in stacks of 20–30 units, which provide operational voltages close to 30 V [28].

Two types of fuel cells that have been developed for automobile transportation and stationary power generation applications can be considered for aviation. The proton exchange membrane (PEM, Figure 13a) fuel cells operate at 80 °C to 120 °C and require pure hydrogen as the fuel; if a hydrocarbon fuel is used, it must be reformed to produce pure hydrogen without any CO, which easily poisons PEM fuel cells. This type of fuel cell works perfectly when sized to replace the APU as it provides multiple advantages, such as water generation from the exhaust of the fuel cell. However, when sized for primary propulsion, these advantages turn into problems. Especially the low efficiency of 55 to 60% in combination with the operating temperature from 80 °C to 120 °C make the cooling particularly challenging. Instead, solid oxide fuel cells (SOFCs, Figure 13b) operate from 750 °C to 1000 °C and can use a variety of hydrocarbon fuels, including jet fuels. Fuel cells have been investigated for a variety of aviation applications:

- Auxiliary power units (APUs) [38,39]
- Low-altitude aircraft propulsive power [40]
- High-altitude long-endurance aircraft
- Airport applications
- Ground support equipment
- Mobile lighting
- Mobile generators
- Unmanned air vehicles [41–45]
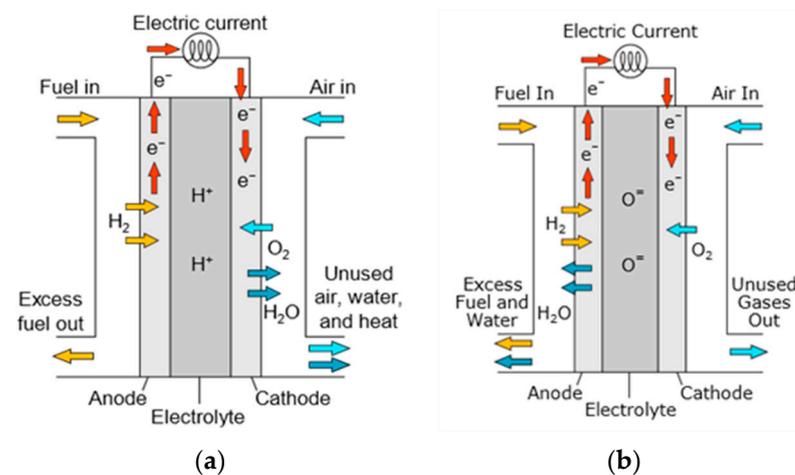
Figure 13. Scheme of two types of fuel cells: (**a**) PEM fuel cell; (**b**) SOFC fuel cell.

Hydrogen is an attractive fuel because of its enormous amount of specific energy (about 40,000 Wh/kg against the 13,000 Wh/kg of kerosene); it is stable, uniformly available on Earth, the outputs of the chemical reaction with oxygen are pure water and heat, it can be produced by electrolysis of water, and it can be directly fuelled into a PEM fuel cell. As drawbacks, it is a flammable and explosive gas, so it must be carefully stored and transported in special containers. It is the lightest element in the universe, it has a very low density at ambient conditions (0.08 kg/m^3 against the 1.225 kg/m^3 of air), and it must be compressed or liquified to be stored in a significant amount. The hydrogen molecule is so tiny that it may diffuse through metal containers such as steel and cause embrittlement and decarburisation. In practice, it can weaken and break the metal structure of its container [28].

As concerns hydrogen storage or production on aircraft, there are at least four solutions available. Pure hydrogen may be stored as a compressed gas in a pressurised tank or as a liquid in a cryogenic tank. It may be also safely stored as a metal hydride, a heavier compound that is stable at ambient conditions that can be safely heated to separate the hydrogen. Finally, the hydrogen can be extracted from a hydrocarbon-like jet fuel, a process known as reformation. It has been shown that the reformation process is the lightest solution to generate hydrogen on-board for long range applications [46]. The high specific energy of kerosene as a hydrogen source is advantageous in terms of system mass saving, while the hydride tank is the heavier solution, due to the significant mass of the metal compound (more than 90% [39]) which does not participate in the chemical reaction, but it only serves to store the hydrogen at ambient conditions. However, from the point of view of system efficiency, the reformer is the worst option because of the lower heating value of the kerosene with respect to pure hydrogen. The metal hydride solution is also penalised by the heat needed to extract the hydrogen from the compound, because the heat produced by the fuel cell itself is not sufficient to enable this process, hence lowering the system efficiency. For these reasons, the pressurised hydrogen seems to be the most efficient solution, followed by the cryogenic tank [46].

To provide a significant abatement of the aircraft emissions, the use of hydrocarbon, both as hydrogen storage for a PEM or fuel for a SOFC, should be avoided, unless such hydrocarbon is obtained through biomass, thus significantly lowering the CO_2 emission during its life cycle, and its utilisation is advantageous in terms of aircraft performance and safety. Otherwise, the storage of pure hydrogen is advised, since it enables higher efficiency and the system mass—fuel cell, tank, air compressor, etc.—is competitive with the mass of a reformer system for short flight times (about 100 min) [46].

Since a fuel cell can be continuously fuelled to produce electric power, it can be represented as a power conversion unit [1]—hence its contribution to aircraft powerplant performance can be evaluated in W/kg—while the entire system made up of chemicals, including storage tank and accessories, plus fuel cell can be valued with the specific energy [41]. Current SOFC power systems have a specific power of less than 100 W/kg compared to about 1000 W/kg for internal combustion engines. SOFCs are being developed for both large-scale stationary power applications (more than 100 kW) and small-scale (1 to 10 kW) APUs and residential applications. SOFCs work better under consistent, steady power conditions; for aviation applications, transient response times and on/off thermal cycles need to be improved. PEM fuel cells are presently being designed and built for automotive and APU applications, generally in 1 to 100 kW sizes. The hydrogen storage and operation at altitude remains a challenge [1]. Dealing with PEM issues related to the maturity of the technology, the fast cell ageing makes it less attractive than a conventional piston engine, while the management of toxic waste produced during the membrane production has high environmental and manufacturing costs. In addition, the environmental impact of fuel cell production needs to be inspected in detail. Moreover, the acquisition costs of PEM are still two orders of magnitudes above the alternatives employed in automotive industry. Current PEM specific power are around 100 W/kg, depending on flight time and assuming a constant electric power [46]. Because of their low specific power, fuel cells are often installed in a hybrid system with a battery or other power sources to provide a boost when required, while the fuel cell supplies a nearly constant load [38–40,42,47,48]. Specific power of hybrid SOFC systems range from 150 to 500 W/kg [39].

The efficiency and voltage of a fuel cell stack significantly reduce when high currents are required because of the low discharge efficiency, while for short range flights they can be attractive. An entire PEM fuel cell system (hydrogen storage, air compressor, electrolyze recharger, fuel cell, etc.) with a charge efficiency of 80% and a discharge efficiency of 50% may achieve more than 320 Wh/kg, a specific energy higher than today's advanced batteries or small internal combustion engines (about 200 Wh/kg) [41]. A less recent work [44] calculates a 125 Wh/kg specific energy for a long endurance, small UAV, a value comparable to the internal combustion engine usually installed, which generates

more noise and a bigger thermal signature. Others claim to have designed a UAV with a 360 Wh/kg fuel cell system [45]. Long range (>2000 km) UAVs would need a fuel cell system with 600 Wh/kg [43]. The by-product of a fuel cell may also be exploited to provide water and inerting gas to fill the emptying kerosene fuel tank, although these solutions are more attractive for commercial flights [46].

Thus, it seems that fuel cells alone are competitive only for small aircraft and yet even with low altitude and short-range applications, they would better be coupled with batteries, ultracapacitors, internal combustion engines, or gas turbines to cope with the high power required during transient manoeuvres. Table 5 and Figures 14 and 15 summarise the presented data and attempt to establish a trend in fuel cell performance, although not all authors explicitly declare specific power and energy—some results come from design studies and some are applications in a controlled environment or installations on small UAVs. A trend may be extracted from specific energy data (an increase of 65 Wh/kg per year), but not on specific power, due to the data scatter. In conclusion, it may be stated that fuel cells will be attractive if the entire electrical energy generation system provides a comparable or superior performance with future batteries specific energy (say 600 Wh/kg by 2035) and specific power, with equal safety.

Table 5. Fuel cells performance in aircraft applications. Specific energies and powers refer to the fuel cell system (including tank, etc.).

Authors	Year	Technology	Spec. Energy (Wh/kg)	Spec. Power (W/kg)	MTOM * (kg)	Notes
Kim et al. [49]	2012	PEM	165	n.a.	2.1	Sodium borohydride (NaBH$_4$) as hydrogen source. Battery supports fuel cell, but it has not been considered in the specific energy calculation.
Rhoads et al. [45]	2010	PEM	360	n.a.	13.4	24 h endurance
Bradley et al. [44]	2009	PEM	125	n.a.	12.5	24 h endurance
Bradley et al. [41]	2007	PEM	7.1	52	16.4	320 Wh/kg may be achieved if fuel cell powerplant scaled linearly (from 800 Wh/kg of compressed hydrogen, 80% charge efficiency, 50% discharge efficiency).
Renouard-Vallet et al. [46]	2012	PEM	330	n.a.	n.a.	Simulation with 50 kW of electric power and system mass (H2 tank) scaled for 200 min of operation.
Nicolay et al. [50]	2020	PEM	n.a.	1160	1261	Installing the Toyota MIRAI fuel cell stack with a specific power of 2.0 kW/kg.
Dudek et al. [51]	2013	PEM	530	117	5.5	Installing the AEROPACK by Horizon Fuel Cell Technologies.
Herwerth et al. [52]	2007	PEM-hybrid	n.a.	70	5	The fuel cell system without battery gives 51 W/kg, the fuel cell stack alone gives 600 W/kg.
Yang et al. [53]	2016	PEM-hybrid	n.a.	76	21.2	Battery is used for take-off and climb, while fuel cell is used for cruise.
Freeh et al.	2005	SOFC-hybrid	n.a.	230	n.a.	Weight and power data summarised by Santin et al. [39].
Bundschuh et al. [39]	2006	SOFC-hybrid	n.a.	155	n.a.	
Nether et al. [39]	2005	SOFC-hybrid	n.a.	326	n.a.	
Rajashekara et al. [39]	2006	SOFC-hybrid	n.a.	500	n.a.	
Mak and Meier [39]	2007	SOFC-hybrid	n.a.	360	n.a.	

* MTOM refers to the entire aircraft gross mass.
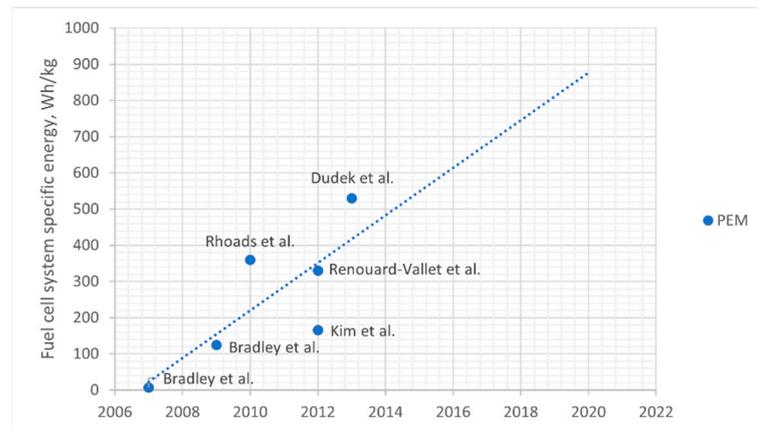
Figure 14. Specific energy of fuel cells systems for aircraft applications.
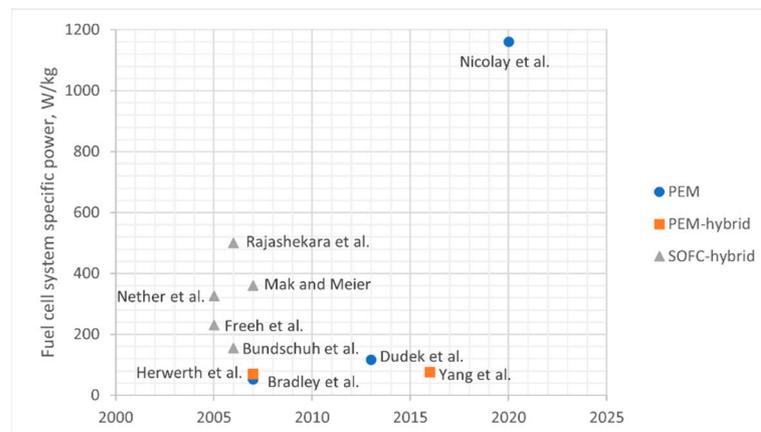
Figure 15. Specific power of fuel cells systems for aircraft applications.

2.7. Hydrogen-Fuelled Aircraft

Hydrogen-fuelled aircraft are dealt with in a different section of the present work to cover both the use of hydrogen as alternative power source for conventional and hybrid-electric propulsive systems and for fuel cells. In the first type of hydrogen combustion system, thrust is generated through the combustion of hydrogen in a modified jet engine, which eliminates most but not all greenhouse gases emissions. Overall, the transition would require less aircraft and engine redesign than hydrogen fuel cell propulsion, making it somewhat less disruptive to the current setup of the aerospace industry. On the other hand, hydrogen fuel cells (HFC) are a near-zero emission solution as the only output of fuel cells is water vapor, the impact of which can be minimised through careful aircraft operation. Moreover, considering the high efficiency of hydrogen fuel cells, the efficiency would be increased from 20% to 40% with respect to hydrogen combustion designs [54]. Considering these benefits, hydrogen applications in the aviation industry are approaching fuel cell solutions. Table 6 shows ongoing projects on applications of hydrogen applied to aircraft propulsion.

Hydrogen technology is not currently ready for a mature application in aviation industry. Some challenges should be faced before that moment. First, the propulsive system is a minor issue if compared to the fuel storage challenge due to the required light-weighting storage tanks for aviation application, which should, at the same time, have a safe and complex cryogenic cooling systems. To take advantage of hydrogen's high energy density, the cooling system of the tank is a critical element. A comparison between gravimetric (specific) and volumetric energy density among different technologies is reported in Table 7. Second, the cost of production methods for "green" hydrogen, which

is the result of an emission-free hydrogen production, competes with kerosene on a cost basis. Third, the production of "green" hydrogen is still not possible on a large scale.

However, a recent Clean Sky 2 study states that hydrogen propulsion has the potential to reduce CO_2 equivalent emissions up to 90% [55]. By equivalent CO_2 emissions it is meant a climate impact of non-CO_2 emissions comparable to CO_2 emissions; these include NO_X, water vapor, soot, contrails/cirrus formation. Hydrogen may also be used to produce synfuel (synthetic fuel), a SAF (see Section 2.1.2) like a biofuel, but with the potential of obtaining zero net carbon emissions (tank-to-thrust) if CO_2 is captured from air. The production of a synfuel from hydrogen requires electricity, which should be generated in a sustainable way. A synfuel has the potential to reduce the climate impact up to 60% relative to conventional (kerosene) aviation.

Table 6. Research and industrial projects applying hydrogen technologies.

Project	Range (km)	Seats	Power System	Status
HY4	1000	4	Hydrogen fuel cells and batteries	First flight in 2016 [56]
HES Element One	500–5000	4	Hydrogen fuel cells	Under development [57]
Alaka'i Skai	240	5	Hydrogen fuel cells	Under development [58]
Apus i-2	800	4	Hydrogen fuel cells	Under development [59]
NASA CHEETA	-	-	Hydrogen fuel cells	Applied research [60]
Pipistrel Airflow eSTOL	400–800	4–9	Hydrogen fuel cells	Scaled flight tested [61]
ZeroAvia	400	6	Hydrogen fuel cells	First flight in 2020 [62]
Airbus ZeroE	-	-	Hydrogen combustion engine	Demonstrator built [63]
NASA Concept B	3500	225	Hydrogen fuel cells	Feasibility study [64]

Table 7. Comparison of energy carriers and storage solutions in terms of gravimetric and volumetric energy density.

Technology	Gravimetric Energy Density (kWh/kg)	Volumetric Energy Density (kWh/L)
Fuel	12.0	10.4
Jet fuel + storage system	8.9	9.5
Current batteries	0.3	0.8
Hydrogen (liquid)	33.0	2.4
Hydrogen (liquid) + storage system	10.0–21.0	1.6–2.1

Hydrogen may be also directly used as a fuel with minor gas turbine evolution if the installation of a cryogenic tank (20 K) on aircraft to provide liquid hydrogen (LH_2) is feasible. The jet engine would require additional heat exchangers to heat the hydrogen from tank temperature to injection conditions [65]. Such feasibility may be achieved on short/medium range aircraft with lighter LH_2 tanks, bringing the system specific energy to 12 kWh/kg and climate impact reduction to 75% [55].

It is expected that a hydrogen-powered commuter aircraft should be a revolutionary design, with a fuel cell system with a specific power of 2 kW/kg and distributed electric propulsion to enhance the aerodynamic efficiency. It is also expected that such aircraft could be commercially available in the next 15 years. Such revolutionary design may have a 90% climate impact reduction, weigh 15% more, and cost 5% more (cost per available seat kilometre) [55].

Of course, airports will require minor changes in a short time frame (2035) if the transition to the hydrogen fuel technology is coordinated with regulators and airlines. By starting with few and small operators, major changes in airports are expected as hydrogen consumption increases and bigger aircraft shall be served [55].

3. Aerodynamic Technologies

Improvements in aerodynamics have a direct impact on the whole aircraft performance. From the beginning of aeronautics until today, research in the aerodynamic field has pushed aircraft technology to ever improved performance.

Such improvements can be achieved by both upgrading current designs and adopting innovative technologies, keeping in mind that such an introduction should not only guarantee a positive impact on aircraft main performance but should also strongly contribute to product cost and operability.

ICAO Doc. 9988 Appendix A [66] identifies several aerodynamic assets potentially leading to drag reduction:

- Basket improving viscous drag
  - Riblets
  - Active turbulence control
  - Natural laminar flow
  - Hybrid laminar flow control
- Basket improving non-viscous drag
  - Increased wingspan (increased aspect ratio)
  - Improved aero tools
  - Excrescence reduction
  - Variable camber with control surfaces
  - Morphing wing

Each one of the previous technologies, if properly actuated, can potentially provide a significant drag reduction, improving the aircraft performance. A technology may be suitable for a specific aircraft category rather than all.

Another potential asset, one of the most investigated technologies emerging in the last decade, is Distributed Propulsion (DP). It can be described as a propulsion system where the vehicle thrust is produced from an array of propulsors located across the air vehicle. While a formal definition of a DP system has not yet been established, in general, the distributed thrust capabilities of a DP system should serve an enabling role in improving the system-level efficiency, capabilities, or performance of the air vehicle. Otherwise, any aircraft with more than one propulsor could be classified as such. DP could improve aircraft aerodynamics not only in what concerns the drag coefficient, but also improving the lift characteristics. In the following sections, a selection of the most promising technologies to be applied on hybrid commuter aircraft is made.

3.1. Distributed Electric Propulsion

Distributed electric propulsion (DEP) concepts for aircraft systems have enabled new possibilities in the overall efficiency, capabilities, and robustness of future air vehicles. Distributed electric propulsion systems feature the novel approach of utilising electrically driven propulsors that are only electrically connected to energy sources or power-generating devices. As a result, propulsors can be placed, sized, and operated with greater flexibility to leverage the synergistic benefits of aero-propulsive coupling and provide improved performance over more traditional designs [67].

Several conventional aircraft concepts that utilise distributed electric propulsion have been developed, along with various short and vertical take-off and landing platforms. Careful integration of electrically driven propulsors for boundary-layer ingestion can allow for improved propulsive efficiency and wake-filling benefits. The placement and configuration of propulsors can also be used to mitigate the trailing vortex system of a lifting surface, by using a "tip-propeller" or leverage increases in dynamic pressure across blown surfaces for increased lift performance, the so-called "high-lift propellers" or blowing. Additionally, the thrust stream of distributed electric propulsors can be utilised to enable new capabilities in vehicle control, including reduced requirements for traditional control surfaces and increasing tolerance of the vehicle control system to engine-out or propulsor-out scenarios. Furthermore, the small propulsors of a DEP system can be installed to leverage an acoustic shielding effect by the airframe, which can further reduce noise signatures.

The rapid growth of flight-weight electrical systems and power architectures has provided new enabling technologies for future DEP concepts, which provide flexible opera-

tional capabilities far beyond those of current systems. While several integration challenges exist, DEP is a disruptive concept that can lead to unprecedented improvements in future aircraft designs. Several examples of disruptive configurations using DEP technologies can be seen in Figure 16.

| (a) | (b) |
| (c) | (d) |
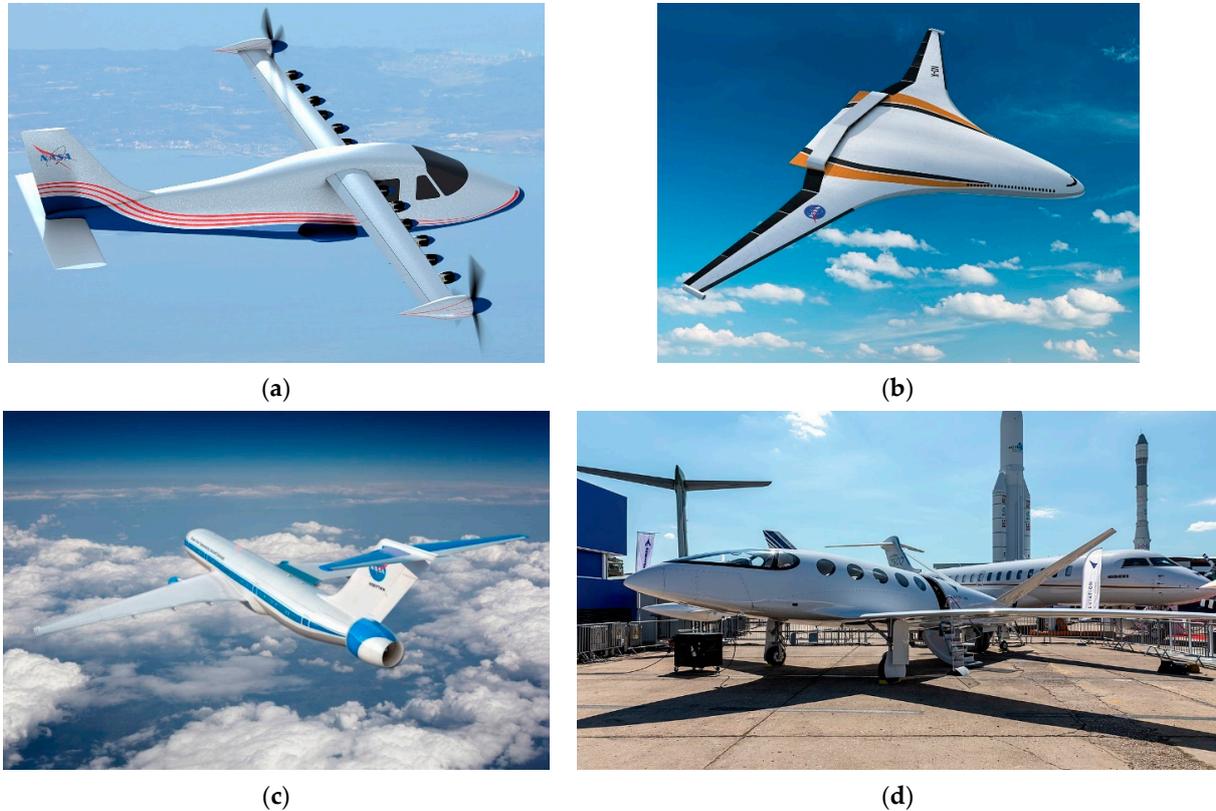
Figure 16. Disruptive configurations using DEP technologies: (**a**) NASA X-57; (**b**) NASA N-X3; (**c**) NASA STARC-ABL; (**d**) Eviation Alice/Matti Blume/CC BY-SA.

In recent years, the increased popularity of the DEP concept and the rapid developments in electrical machinery for aircraft applications have enabled a variety of new technologies and aircraft concepts to be developed. DEP aircraft concepts generally involve the use of multiple electric propulsors around an airframe with one or more independent electric generators or energy storage devices. Based on currently available and near-term electrical components and subsystems, there are now a number of electric aircraft concepts that are configured and even manufactured at various organisations throughout the world. However, due to the limited specific power or specific energy density of currently available hardware, the majority of early adopters of this technology have been found in small aircraft applications. With the enduring interest of increasing efficiency, decreasing operating costs, and encouraging environmental responsibility of larger commercial aircraft applications, there are now a number of organisations investing in and researching DEP aircraft systems for larger passenger and cargo-carrying capabilities [67].

One of the inherent features of a DEP-enabled aircraft is the tight integration of the propulsion system into the wing-body surfaces of the aircraft. With the increased number of propulsion units near the aircraft's aerodynamic surfaces, a level of aero-propulsive coupling will be present. The manifestation of this coupling depends largely on the type of propulsion unit in use—for example, propeller versus ducted fan—and the proximity of those propulsion units to the wings, tail surfaces, or fuselage. The upside to this facet of a distributed propulsion system is that with careful design, the propulsion-airframe integration can be advantageously used. The benefits of aero-propulsive coupling can be broken down into several categories. First, a wide range of vehicle configurations that

have been developed claim propulsive efficiency benefits due to boundary-layer ingestion. Second, the strategic placement of propulsors can reduce vehicle drag through a variety of mechanisms, including wake filling and vortex suppression. Finally, various applications have been developed which make use of the propeller or fan slipstream interacting with an aerodynamic surface to produce some form of enhanced lift or control authority [67]. Each of these categories of aero-propulsive coupling, which occur on a variety of distributed propulsion aircraft configurations, are discussed in the following sections.

Aircraft with distributed propulsion may also employ differential thrust as a mean to reduce or eliminate the vertical tail and be still compliant with regulations, although aero-propulsive interactions and system robustness must be carefully investigated, while different safety criteria could be applied [68–71]. Moreover, effects on aircraft stability and control due to DP technologies must be carefully evaluated from the preliminary design stage to avoid potential disadvantages of such integration.

3.2. Tip Propeller

Wing-tip vortex can be mitigated by installing a propeller at the wing tip. The main impact of propeller slipstream on wing performance is to increase the speed downstream of the propeller. A first simple assumption that can be done is that only the speed component normal to the propeller plane is increased. However, this assumption neglects the swirl in the propeller slipstream, whose interaction with the tip vortex of the wing causes a variation of induced drag, even more than the increase in axial speed.

In general, the induced drag can be approximated accordingly to Equation (1), because of the wing finiteness. By decreasing the induced angle α_{iw}, the induced drag C_{Di} is reduced. As shown in Figure 17, the presence of the wing causes a decrease of the angle of attack related to the downwash effect. The induced angle of attack due to the wing, also called downwash angle, α_{iw} can be approximated as in Equation (2). The effect of the increase in axial speed (red arrow in Figure 17) due to the presence of the propeller is shown. The variation of the axial speed causes an upwash effect countering the downwash due to the wing. The actuator disk theory provides the estimation of the axial induction factor a_p at the propeller disk as a function of thrust to weight ratio T_p/W and the diameter of the propeller D_p (Equation (3)) and finally the flow speed at the propeller V_p (Equation (4)):

$$C_{Di} = C_L \alpha_{iw} \tag{1}$$

$$\alpha_{iw} \approx \frac{w}{V_\infty} = \frac{C_L}{\pi A R e} \tag{2}$$

$$a_p = \frac{1}{2}\sqrt{1 + \frac{8}{\rho_\infty \pi V_\infty^2}\frac{T_p/W}{D_p^2/W} - 1} \tag{3}$$

$$V_p = a_p V_\infty. \tag{4}$$
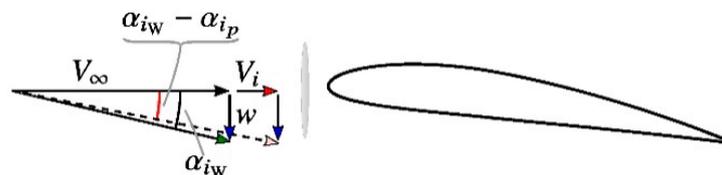
Figure 17. Induced angles due to wing and actuator disk.

Beyond the axial induction, the flow rotation due to the propeller slipstream must be accounted for too, as shown in Figure 18. Assuming a certain rotation direction of the propeller, the tangential induction is a measure of the ratio between the propeller angular speed Ω and the flow angular speed ω induced by the propeller rotation. It can be used to estimate the vertical velocity component of the flow due to the slipstream. The tangential induction due to a propeller can be computed with Equation (5). The tangential speed w_{swirl}

perceived in the propeller slipstream is the product of the tangential induction factor a_{pt} and of the tangential speed of the tip of the propeller ΩR, shown in Equation (6). Finally, the induced angle can be computed accordingly to Equation (7), where w is the wing-induced downwash and w_p is the propeller-induced downwash without swirl:

$$a_{p_t} = \frac{\omega}{2\Omega} = \frac{1}{2} - \sqrt{\frac{1}{4} - \frac{V^2}{\Omega^2 R^2}\left(1 + a_p\right)a_p} \tag{5}$$

$$w_{\text{swirl}} = a_{p_t}\Omega R \tag{6}$$

$$\alpha_i = \tan^{-1}\left(\frac{w + w_p + w_{\text{swirl}}}{V_\infty + V_P}\right). \tag{7}$$
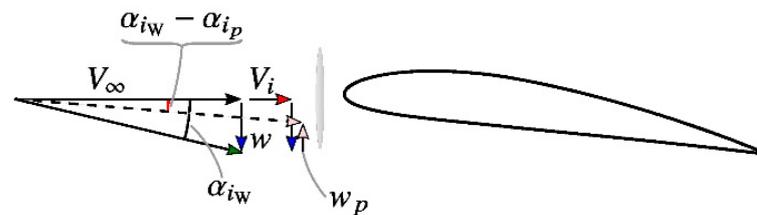

Figure 18. Induced angles due to wing and rotating disk.

It is clearly understandable that by properly rotating the tip propeller in the opposite direction relative to the tip-vortex (inner-up direction), it is possible to reduce the induced angle of attack and hence the induced drag. Numerical and experimental analyses clearly confirm this phenomenon.

In 1969, Snyder and Zumvalt [72] proposed that aircraft can be designed by using propellers at the wingtips in such a way that the lift-to-drag ratio can be varied by changing the effective aspect ratio in flight. An experimental program testing a wing with propellers mounted at the wingtips showed that the use of a propeller at the wingtip, turning in the direction opposite to that of the wing vortex, shifts the trailing vortex core outboard, decreases the wing drag coefficient, increases the maximum lift coefficient, and increases the effective aspect ratio. Conversely, rotating the propeller in the same direction of the tip vortex has the reverse effect. The test model was a reflect-plate, simply tapered wing, with an aspect ratio $AR = 8$, a tip-nacelle, and two options as propeller: (1) a typical 4-blade propeller; (2) an impeller, shaped like an "orange juice" extractor. As the authors stated, a limitation to the use of a propeller in affecting the wing trailing-vortex was the efficiency of the propeller: about 80% of the energy provides axial acceleration of the air and only about 20% is available to produce rotation (swirling to the flow) with which to supplement or to counteract the trailing vortex and the attendant downwash pattern. Earlier tests of an impeller had shown that the device does produce thrust, but the propulsive efficiency peaks at less than 50%. This type of propeller was chosen to serve as the inefficient propeller for these tests.

The main results were summarised in terms of lift coefficient, drag coefficient, and effective aspect ratio AR_e as function of vortex rotating direction and counter vortex rotating direction, number of revolutions per second. The effect of propeller position is shown in Figure 19. With respect to the baseline reference geometry, which was a pod with dummy spinner and $AR_e = 6.45$, the wingtip propeller allowed an increment of AR_e of about 35% at 175 rps. The impeller provided an even better result, almost three times the baseline.
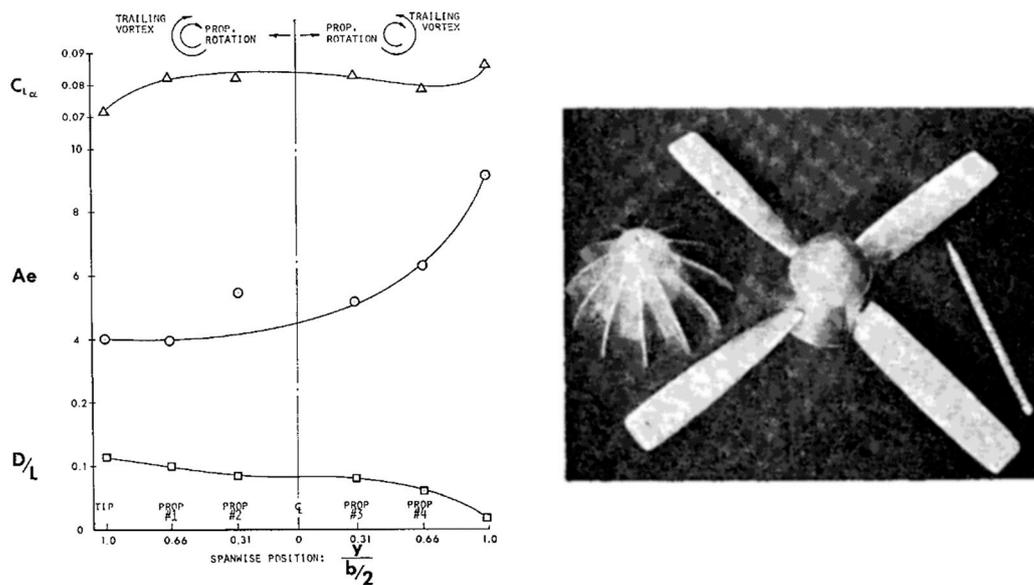
Figure 19. Effect of propeller position on wing characteristics. Reproduced with permission from Ref. [72] 1964 American Institute of Aeronautics and Astronautics.

By combining results coming from previous experiences, the authors also summarised the effects as function of engine position in spanwise direction, with the effective aspect ratio attaining the maximum value at wingtip, lift curve slope almost constant until 70% span then increasing by about 10% at wingtip, and drag-to-lift ratio decreasing at 0.02 at wingtip at $C_L = 1.0$.

Finally, the authors also highlighted the main disadvantages of this solution including difficulty (or impossibility) of trimming the aircraft for one engine-out operation and generation of aeroelastic problems due to the change of the torsional moment of inertia of the wing and the interaction of bending and torsional modes of flutter or vibration [72]. Today, these drawbacks could be partially overcome with new technologies, design, materials, powertrain strategies, and controls.

In 1989, at NASA, the wing-tip pusher propeller on a wing-body configuration with an $AR = 6.10$ was analysed in the NASA Langley wind-tunnel facility as shown in Figure 20. All tests were conducted at $M = 0.70$ and $Re = 3.82 \times 10^6$, from -2 to 4 degrees of angle of attack. The main results showed a drag reduction of about 20 drag counts for the counter-rotating wing-tip pusher propeller in the range of low values of the lift coefficient.
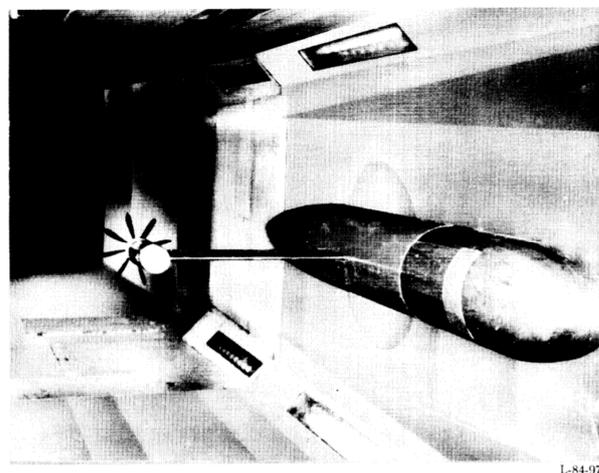
Figure 20. Wing-tip mounted pusher turboprop model in Langley 7- by 10-Foot Speed Tunnel. Reproduced from Ref. [73].

In the last decade, the NASA X-57 program also investigated the effect of tip-propeller on the X-57 Maxwell aircraft (Figure 16a). A lot of numerical studies were performed, highlighting potential benefits of a tip-mounted engine, useful in whole flight phases, reducing the induced drag. Results indicated an average drag reduction in the range of 20–40 drag counts during typical X-57 cruise condition, slightly dependent on the solvers and transitional model [74], in line with what was shown at NASA for a pusher wing-tip propeller [73].

Della Vecchia et al. [8] studied the effects of a high-efficiency tip-propeller on the Tecnam P2006T wing, varying the diameter and the thrust level in the range of typical cruise settings. They confirmed the previous results that a high-efficiency propeller ($\eta_p > 0.8$) allows smaller drag reduction than low efficiency propeller, improving the axial component and the available thrust. Moreover, the numerical analyses showed that, for a given propeller characteristics, by decreasing the diameter the drag reduction decreases in the whole range of lift coefficient, while by increasing the thrust level, the drag reduction increases (see Figure 21). This behaviour is due to the variation of rpm, which must increase when decreasing the diameter to provide the same level of thrust. Results globally show that, in the typical cruise attitude of the Tecnam P2006T, a drag reduction of about 10–15 drag counts can be attained for a propeller diameter equal to 1.78 m, which is the same propeller diameter actually installed on the aircraft.
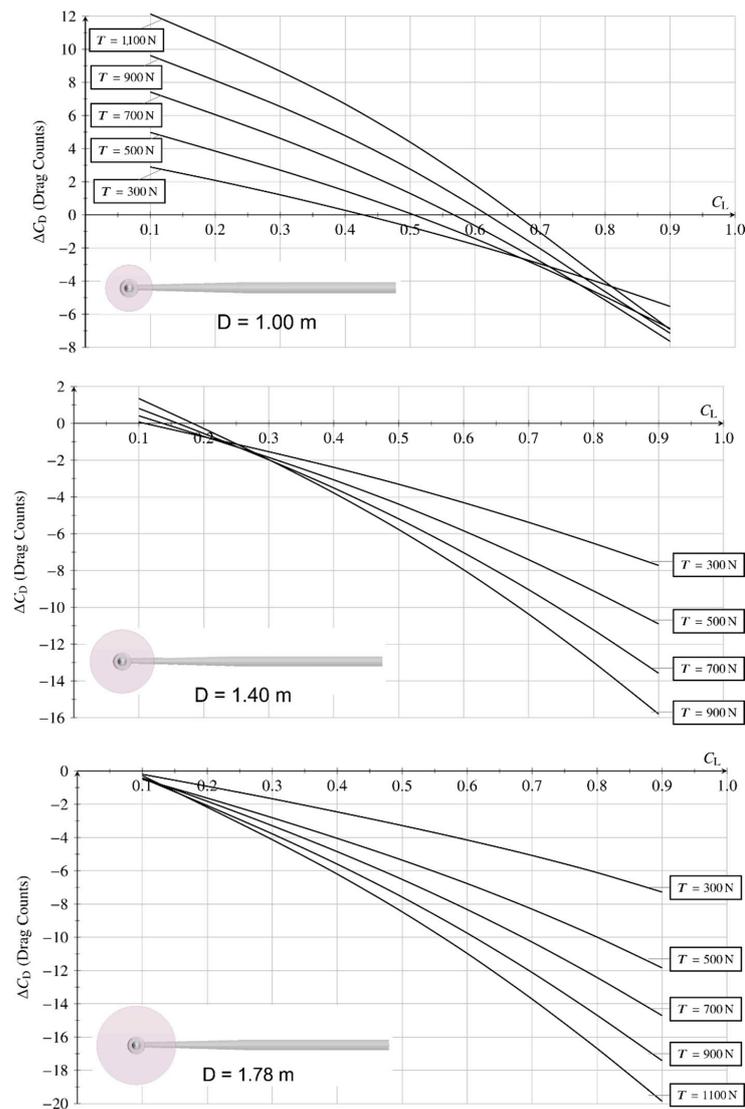

Figure 21. Drag reduction due to high-efficiency tip-propeller, $AR = 8.47$, $M = 0.23$, $Re = 6.9 \times 10^6$ [8].

At the Technical University of Delft, several numerical and experimental studies were conducted in the last two decades on the wing-tip-propeller, especially on low-and-medium aspect ratio wing from 3 up to 6.2 [75–77]. In one of the last studies, they experimented conventional wing mounted configuration versus wing-tip-mounted propeller configuration [77]. The majority of the measurements discussed in this paper were taken at a freestream velocity of 40 m/s. This velocity provided the best compromise between achievable Reynolds number and the operating range of the propeller, which was constrained by the output power of the electric motor. The resulting Reynolds number based on the wing chord was about $Re_c = 650,000$, while the Reynolds number based on the propeller diameter was $Re_D = 640,000$. The propeller was operated at four thrust settings, corresponding to advance ratios J of 0.7, 0.8, 0.9, and 1.0. The associated thrust coefficients C_T were equal to 0.123, 0.095, 0.053, and 0.014, respectively, while the Reynolds number at $r/R = 0.7$ was in the range of 130,000–180,000 (for $J = 1.0$ to 0.7). For Model II, additional measurements were taken at 28 m/s to achieve higher thrust coefficients. At this velocity, the propeller was also operated at advance ratios J of 0.5 and 0.6, resulting in thrust coefficients C_T of 0.168 and 0.144, respectively. The corresponding Reynolds numbers were 455,000 based on the wing chord, 450,000 based on the propeller diameter, and 90,000 to 170,000 based on the effective velocity and chord at $r/R = 0.7$ (for $J = 1.0$ to 0.5), see Ref. [77]. As expected, the results show a drag reduction when increasing the thrust setting level and the lift coefficient, leading to a drag decrement from 30 to 60 drag counts within a C_T range of 0.1–0.2 and with a cruise lift coefficient $C_L = 0.5$, which are typical conditions for general aviation and small regional aircraft.

At the University of Naples "Federico II", high-fidelity Navier–Stokes analyses were performed on a typical 40-passenger regional turboprop wing, to evaluate the tip-mounted propeller impact by varying the thrust level and the propeller diameter. High-efficiency propellers, suitable for cruise and climb performance, designed according to minimum-induced-loss procedure, were used to obtain required thrust, changing the rotational rate opportunely. Results are shown in Figure 22 in terms of wing drag reduction versus lift coefficient, for several thrust settings, propeller diameter, and rpm—which means C_T. For a given thrust value, what usually happens is that by decreasing the propeller diameter—i.e., increasing the C_T—the drag reduction increases. By increasing the thrust three times—from 4000 N to 12,000 N—the drag reduction increases by about five times. In conclusion, it can be stated that a properly counter-rotating, tip-mounted propeller can reduce the induced drag, improving the aerodynamic efficiency, but it is constrained by directional control and structural limits. It must be highlighted that those values of drag reduction in cruise conditions cannot be attained with a wingtip device or a winglet, which provides only slightly improvement in cruise, opening a challenge to introducing a propeller at the aircraft wingtip. Thus, numerical analyses show that a tip-mounted propeller provides aerodynamic benefits on all aircraft classes and it is worth further investigating in the commuter category.

3.3. High-Lift Propeller

A DEP system can be incorporated into the airframe to augment high-lift capabilities at low speed. One popular example is the NASA X-57 Maxwell aircraft (see Figure 16a), which is based on a Tecnam P2006T aircraft fuselage and reconfigured with a wing much smaller than that of the baseline aircraft. The smaller wing is achievable for this design due to the high lift provided by 12 small electric-powered propellers distributed along the leading edge of the wing and enabled during the take-off and landing flight phases. The purpose of having these distributed propellers is to increase the dynamic pressure, hence the lift, over the wing at low speed [10].

The high-lift propellers must be properly designed, aiming to improve the wing-blowing. According to Patterson [78], to improve the axial velocity and hence the high-lift capability, a near-uniform axial velocity must be produced aft of the propeller. At NASA, the high-lift propellers for the X-57 Maxwell were designed for this scope. The 12 high-

lift propellers have been installed on nacelles upstream of the wing leading edge and positioned in an alternating fore-and aft staggered pattern. The high-lift propellers are designed to fold smoothly onto the nacelle for the cruise configuration, which is referred to as the cruise wing. Preliminary results have shown a maximum achievable lift coefficient of about 4.3, almost double the unblown wing.
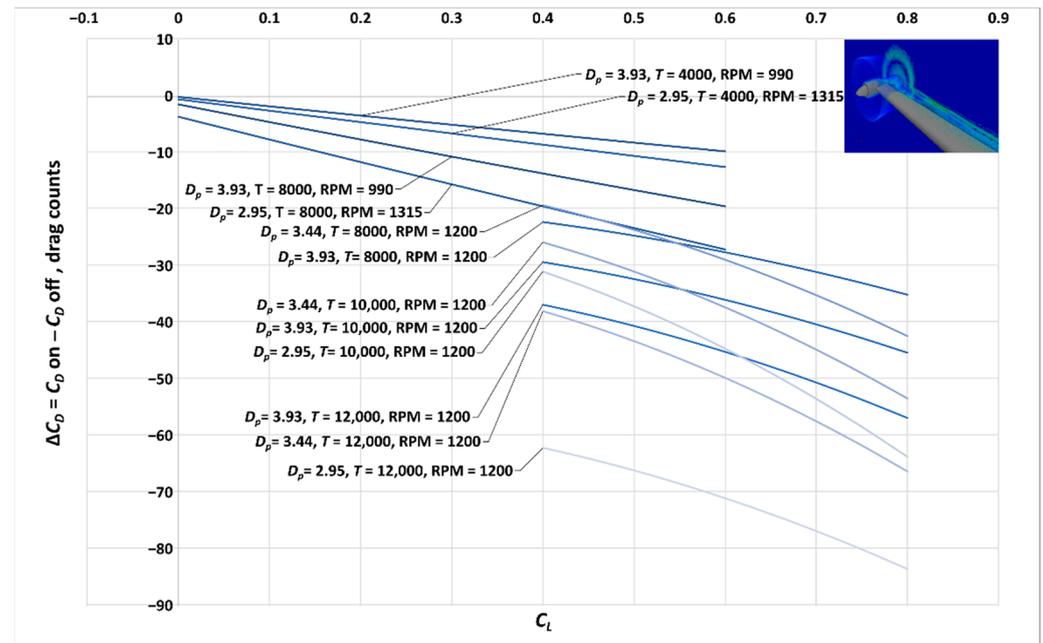
Figure 22. Wing drag improvement due to the propeller tip-mounted on an *AR* = 11 wing, *M* = 0.48, *Re* = 15 × 10⁶, thrust *T* in Newton.

Analyses were also performed to evaluate the effect of rotation direction of each propeller, highlighting how co-rotating propellers were better than counterrotating propellers, as explained in Ref. [79]. Moreover, in 2016, NASA prepared and tested a DEP high-lift propeller testbed, highlighting a good agreement between numerical and experimental data [80]. The max lift was about doubled with respect to the unblown solution, increasing from about C_L = 2.8 up to C_L = 6.0.

Della Vecchia et al. evaluated the wing high-lift propellers effect on the Tecnam P2006T baseline wing, splitting the same available power of 200 hp through several distributed propellers, considering 120 hp needed for cruise tip-mounted propellers [8], see Figure 23. Results showed a mild lift increment to about 1.0–1.5. This limited value was attributed to low engine power, reduced blowing, excessive wing planform area, and conventional propellers used for high lift. Moreover, a key aspect is the propeller diameter-to-chord ratio, D_p/c = 0.42, which was half of that of the NASA X-57 Maxwell (D_p/c = 0.9), see Figure 23.

At the University of Naples "Federico II", the aerodynamic effects of high-lift propellers on a typical 40-passengers regional aircraft were numerically analysed, varying the number of blown propellers, the thrust per propeller, the flap settings, blowing on the same wing area, see Figure 24. High-lift propellers were designed for each configuration according to MIL theory. Figure 25 shows the main achieved results: for a given reference wing, increasing the number of high-lift propellers leads to an increment of maximum lift coefficient, of drag coefficient, and of pitching moment. This behaviour slightly changes by deflecting a conventional flap: as can be seen in Figure 25a, the flap deflection, combined with propeller blowing, promotes the trailing edge wing separation, achieving maximum lift coefficient increment even before with a lower number of high-lift propellers. Conversely, drag coefficient increment exhibits a minimum in a certain range of the $T/(D_P^2 V^2)$ parameter, which is dependent on the number of high-lift propellers, see

Figure 25b. The pitching moment increment due to high-lift propellers is not negligible, as shown in Figure 25c.

(a)

(b)

(c)

(d)
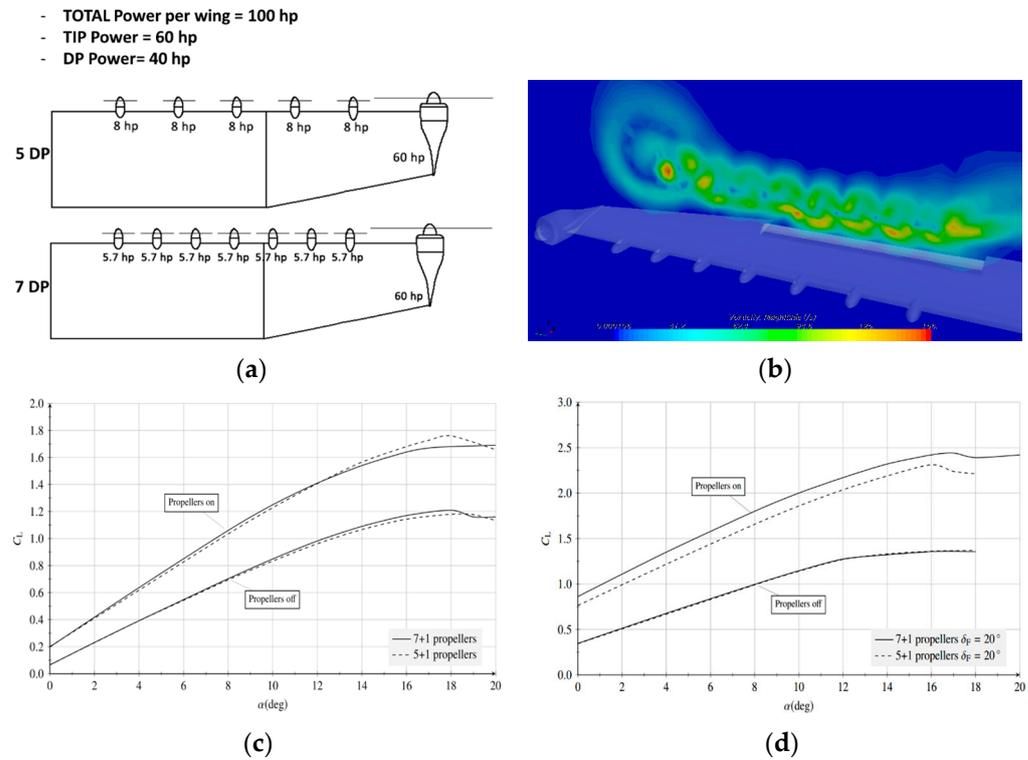
Figure 23. Tecnam P2006T wing simulated at $M = 0.08$, Re = 3.3×10^6, from Ref. [8]: (**a**) wing planform; (**b**) vorticity magnitude contour behind the wing; (**c**) lift coefficient in clean configuration; (**d**) lift coefficient in flapped configurations.
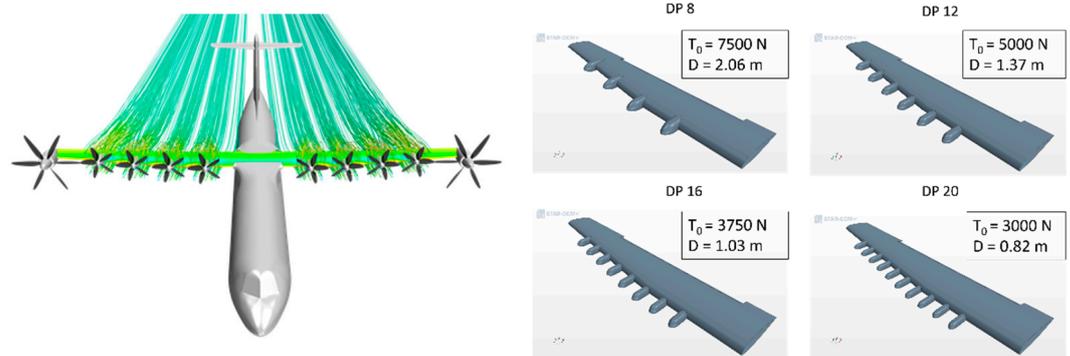
Figure 24. High-lift propeller on a typical 40-passenger regional turboprop wing, $AR = 11.07$, $M = 0.15$, $Re = 7.6 \times 10^6$, DEP 8, DEP 12, DEP16, and DEP 20 configurations, T_0 is the thrust per propeller.

All the results on high-lift propellers highlight how promising this technology can be. The main key factors to consider in the design stage are:

1. The operative speed must be as low as possible to obtain the main benefit.
2. The thrust levels must be as high as possible.
3. The propeller diameter over the chord ratio D_p/c must be as large as possible.
4. The propeller design must have an axial induction as constant as possible.
5. The propeller high-lift devices interaction must be carefully investigated with high-fidelity methods.

(a)

(b)

(c)
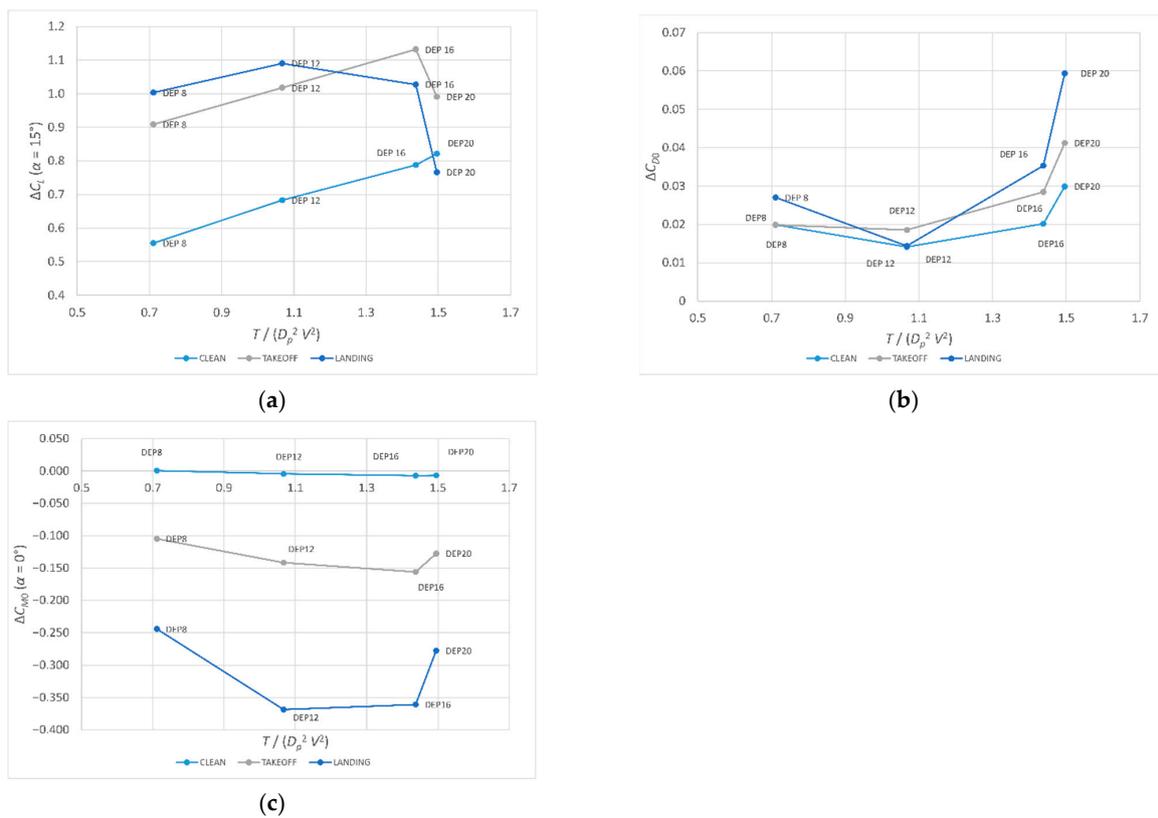
Figure 25. Effects of high-lift propellers on a typical 40-passenger regional turboprop wing, presented as difference values with respect to the unblown isolated wing, $AR = 11.07$, $M = 0.15$, $Re = 7.6 \times 10^6$, DEP 8, DEP 12, DEP16, and DEP 20 configurations: (**a**) lift coefficient change ΔC_L at $\alpha = 15°$; (**b**) parasite drag coefficient change ΔC_{D0}; (**c**) pitching moment coefficient change ΔC_{M0} at $\alpha = 0°$.

The effects of distributed propulsion on commuter aircraft sizing and emissions was discussed by the authors in Ref. [81]. As concerns larger aircraft, the reader may consult Refs. [13,24]. In these references, it is remarked that distributed propulsion as a means to enhance the airplane's high-lift capabilities is not effective on all aircraft categories. These recent investigations show that benefits are enabled on small aircraft within a limited range; otherwise, a weight snowball effect—mainly due to the low density of the electric energy source—will oversize the aircraft out of the commuter category. Moreover, regional turboprop airplanes may benefit from DEP, if the design mission range is reduced to the actual design range—i.e., below 300 nmi, where the airplane spends a significant part of its mission in climb and descent phases—to avoid an excessive gross weight that would put the aircraft out of the market because of manufacturing and operating costs.

3.4. Boundary Layer Ingestion

The primary benefit associated with boundary layer ingestion (BLI) is the potential for reduction in energy usage due to ingestion of the thin, low-momentum air region at the aircraft surface, known as the boundary layer. The ingestion of this low-momentum air leads to an increased propulsive efficiency and can also lead to wake-filling benefits when the air is re-energised and used to reduce the velocity deficit and turbulent mixing losses in the wake. For these reasons, BLI propulsors are located on the top of the trailing edge lifting surface, as in the case of DEP concepts, which deal with distorted inflow, or at the end of the fuselage, as in the case of an annular BLI concept (see again Figure 16c). BLI can reduce the required propulsive power by 4% to 8% [82,83].

Several conceptual DEP aircrafts aim to take advantage of BLI. First among these is the N3-X aircraft (see again Figure 16b), where the large fuselage boundary-layer provides an excellent opportunity to exploit this technology. Studies were performed to incorporate

the effects of BLI in the propulsion system design for the BWB aircraft and additional work has been done to investigate the potential for incorporating a boundary-layer ingesting crossflow fan into the N3-X propulsion system. Experimental and numerical work has also been performed to assess the effects of BLI on propulsion system performance and inlet distortion problems. Finally, the E-Thrust and Lilium aircraft propulsion systems also utilise BLI as a performance improving mechanism [67].

Another possibility to perform BLI is to install a propeller on the fuselage tail. Numerical and experimental analyses show a potential propeller efficiency improvement, demonstrating that the required power for BLI is lower with respect to the required power without BLI. Results from an experiment performed at TU Delft [84] on different architectures show a net force benefit with respect to the free-stream case of about 9% for wake ingestion—i.e., propeller detached from the body, in its wake—and 18% for BLI—i.e., propeller installed on the body stern—with a propeller efficiency improvement of 11% for wake ingestion and of 21% for the BLI configuration, at $J = 1$. Other works also concluded that BLI can bring sensible to significant emissions reduction [85,86], also on commuter aircraft [87].

3.5. Noise Mitigation for DEP Systems

Several studies [67,88–90] indicate that DEP architectures offer promising perspectives for noise reduction and appear as a viable solution for delivering the strict mid-to-long term environmental goals set in the ACARE addendum [5]. This may a priori seem counterintuitive if one considers the multiplicity of aerodynamic interactions taking place in a DEP system, which are generally synonymous of load fluctuations and noise production. Several factors are actually in favour of noise reduction [67].

Positive aerodynamic interactions—such as wing blowing—open indirect perspectives for quieter transport. Furthermore, the efficiency of electric motors does not depend much on their size, so that the overall conversion efficiency of a large number of electric motors driving many small propellers can be as good as that of a single motor driving a single large propeller. This means that either a smaller wing size for cruising can be used or that lower take-off and landing speeds are possible. The latter option is very promising in terms of noise emissions, since the aerodynamic noise radiated by the fixed parts of the airframe—landing gear and high-lift devices in particular—would typically radiate noise in proportion of the 5–6th power of the flight speed [91]. Moreover, a high lift-to-drag ratio could allow steeper take-off and landing trajectories, which further reduces the noise footprint affecting communities.

The noise emitted by electric machines is much less than that associated to the compressor, combustor, and turbine components. Huff et al. [92] reported that the noise generated by the electric motor system alone was 8–20 dB below the fan noise for a regional jet-sized aircraft, and 17–29 dB lower than that of a single-aisle commercial transport class aircraft. While the proximity of the propulsive system with the airframe is normally a source of important tonal noise, the multiplicity of propulsors opens interesting perspectives for noise control via an adequate clocking of the propellers [90,93]. The flexibility offered by DEP systems permits placing the propulsors over the airframe in such a way to enhance noise shielding effects. Posey et al. [94] achieved low-frequency noise reductions of the order of 20 dB across a significant community area. For turbo-electric distributed propulsion systems—i.e., when the electric power is provided by a common turbine—an effective by-pass ratio can be defined as the ratio of mass flow rate of all combined airflows to the one that enters the turbine. A high effective by-pass ratio is generally beneficial to noise reduction.

The main conclusion to be drawn from the above discussion is that, in order to properly address the noise reduction potential of DEP systems, all the relevant aspects must be tackled simultaneously: aero-propulsive benefits, noise shielding, tonal interference effects, as well as non-aerodynamic noise sources. Obviously, the noise resulting from the unsteady aerodynamic interactions between the multiple propulsors and the airframe must not

over-compensate the gains obtained from increased aero-propulsive efficiency. In that respect, quite innovative flow and noise control technologies have been proposed over the last decade, which may prove very efficient to reduce aerodynamic interaction noise and provide broadband acoustic absorption.

3.6. Laminar Flow

On most of today's aircraft, airflow is turbulent on almost the entire wetted surface. The result of this condition is a viscous drag which is larger than the one that could be obtained by forcing a laminar boundary layer on the whole surface of the airplane. To force a laminar boundary layer or at least promote it on a large portion of aircraft wetted surfaces, two different approaches can be adopted: Natural Laminar Flow (NLF) and Laminar Flow Control (LFC). With the former concept, laminar boundary layer is kept solely by shaping the surface in such a way as to produce a favourable pressure gradient. With the latter, airflow laminarity is preserved by applying distributed suction over the surface. A third concept exists, which makes use of both the approaches: with Hybrid Laminar Flow Control (HLFC), one combines the NLF and LFC concepts. In fact, HLFC makes use of a moderate amount of suction at the leading edge, in order to counteract an adverse pressure gradient, combined with a more extended un-sucked region in which a favourable pressure gradient is obtained through a suitable shaping of the aircraft surface. To a certain extent, the HLFC concept could be seen as an optimisation of the LFC one in the sense that it requires a significantly limited sucked region in order to keep the airflow boundary layer laminar [95].

For an airplane wing, three different instability mechanisms, leading to transition from laminar to turbulent boundary layer, can be distinguished:

- Tollmien–Schlichting waves—It is the most common way by which a laminar flow transits to turbulent. They are streamwise unstable waves that arise in boundary layers, hence these are driven by a viscous effect on the surface of a body. On a swept wing, they usually occur in the mid-chord region.
- Attachment-line contamination—It is essentially provoked by the boundary layer of the fuselage, which, by propagating from the junction between the fuselage and the wing inner panel, ends by contaminating the boundary layer of the latter, enabling the transition from laminar to turbulent flow.
- Cross-flow instability—It was first discovered during early studies on swept wings. This instability occurs in the region of high-pressure gradient of a swept lifting surface, for which boundary layer velocity profiles are three-dimensionally warped. For this reason, when projected into the perpendicular direction to the outer flow, a cross-flow profile can be obtained, which is inherently unstable since having at least one point of inflection.

Figure 26 shows which are the transition mechanisms on a swept wing and which region of a lifting surface they affect the most. More specifically, the mechanism through which transition occurs on a swept wing can depend on the size of the sweep angle at the leading edge. For lower leading-edge angles, transition is usually dominated by Tollmien–Schlichting waves, while cross-flow instability dominates for higher values [96]. Another investigation [97] showed that forward swept wings seem to behave much better with respect to cross-flow instability in transonic flow. This can be associated with their lower leading-edge sweep angle with respect to a backward swept wing with the same 50% chord line angle, which is the location at which shocks usually occurs for transonic wings.
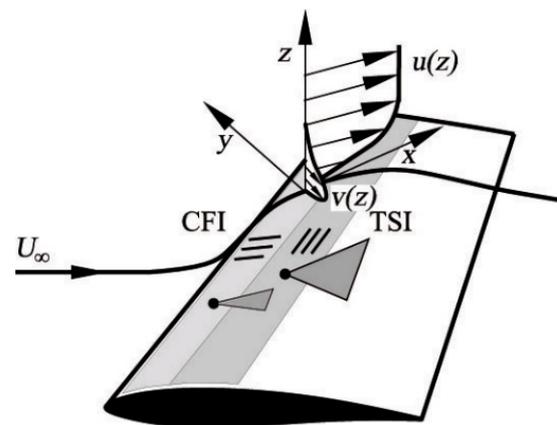
Figure 26. Transition mechanisms on a swept wing. Herbert.Oertel/CC BY-SA.

The following sub-sections focus on giving an overview on the so far performed research studies both for NLF and LFC, providing, when possible, information on actual flight tests and current applications of these technologies.

3.6.1. Natural Laminar Flow

One way to achieve laminar boundary layer on a large portion of an aircraft component without adopting active control devices consists in appropriately shaping its surface to obtain a favourable pressure gradient over the forward region, in order to delay transition. On the lifting surface and airfoils side, this usually results in a sharp leading-edge profile, which implies as a direct consequence a reduction in terms of lifting capabilities for the forward portion of the airfoil section, and so a deterioration in terms of high-lift and stall performances. Moreover, because of the dominant role of cross-flow instabilities for high swept wings flying at transonic speed and at a high Reynolds number, the use of this technology seems to be limited to small regional aircraft carrying fewer than 100 passengers, at least for conventional wing configurations and in absence of further flow control technologies.

The effectiveness of this type of technology has been successfully validated through several flight tests over the last decades, some of which were performed as part of the European Laminar Flow Investigation (ELFIN) project [98]. One of the main elements of the project consisted of a partial-span flight demonstration of natural laminar flow utilising a foam and fiberglass glove over existing wing structure. The aircraft chosen for this test was a Fokker 100 transport aircraft, whose starboard wing was modified with a full-chord, partial-span natural laminar flow glove simply bonded to it.

The main objective of this test was to evaluate the reduction in drag associated with the natural laminar flow and to establish the upper limits in terms of transition Reynolds number for a given leading edge sweep angle. Flight tests were performed for a total of twelve hours, leading to results comparable with the results from wind tunnel tests, confirming predictions of 15% drag reduction.

More recently, within the framework of the EU-funded Clean Sky I projects, more NLF demonstrators have been developed and tested. As part of the SFWA (Smart Fixed Wing Aircraft) project, the BLADE (Breakthrough Laminar Aircraft Demonstrator) demonstrator was flight tested [99]. The outer wing of an Airbus A340 was substituted with an NLF wing, characterised by a lower leading-edge sweep, in order to better control cross flow instabilities.

Currently, NLF has been adopted and realised only for light business jets such as the HondaJet [100,101]. Instead of adopting an existing NLF airfoil, such as the ones developed by NASA for business jet applications, a new NLF airfoil has been designed and studied to exactly match the requirements of the aircraft and to optimise its performance. The designed airfoil SHM-1 shows all favourable characteristics for such an application: high

drag-divergence Mach number, small nose-down pitching moment, low drag for cruise, and docile stall characteristics. All these achieved while keeping a 15% thickness, allowing to carry the necessary fuel without an increase in wing area.

It is the authors' opinion that an NLF airfoil can be installed on commuter aircraft, as the Reynolds number is clearly lower than business jet and large transport aircraft, but it is also advised that an NLF airfoil becomes useless with the application of distributed electric propulsion. In addition, NLF should require anti-contamination and monitoring systems, as described in the next sub-section.

3.6.2. Laminar Flow Control

Laminar flow control is an active boundary layer flow control technique aiming to maintain the airflow laminar over a surface for chord Reynolds numbers much greater than the ones that usually characterise transitional or turbulent configurations. In highly swept wings, which are usually required for flight at high subsonic and supersonic speeds, suction can control sweep-induced cross-flow disturbances that promote boundary layer transition. Most of the research so far has been on laminarisation through flow active control by application of a combination of NLF and LFC, that is the HLFC technology. In HLFC, suction is applied only at the leading edge of a swept lifting surface to annihilate cross flow instabilities. The aft region of the wing is then appropriately shaped—as for the NLF technique—to control pressure distribution and stabilise mid-chord Tollmien–Schlichting waves. In theory, Tollmien–Schlichting instabilities could be controlled by suction even further downstream. The reason why this is rarely taken into consideration, at least in conventional aircraft configurations, lies in the weight penalty one would incur in installing a suction system in the area of the wing box, in addition to the reduction in total available volume for fuel tanks. Despite this, the introduction of active laminar flow control technology on a limited portion of wing area still adds, with respect to NLF, additional mass, power consumption, and complexity to the aircraft. For this reason, the HLFC design requires multidisciplinary work on aerodynamics, structural engineering, production technology (closer tolerances), systems engineering, and airline operations (maintenance and damage repair, essentially). An HLFC installation would require a dedicated apparatus, comprising several systems. The following is a list of the systems that an HLFC aircraft would require. Except for the suction system, the remaining items would be necessary for an NLF application too, although they are probably less demanding in terms of power required and additional weight.

- Suction system—To keep a laminar boundary layer on the leading edge of a swept lifting surface, air must be removed from it through suction. This can be achieved both through the usage of a slotted wing surface or a perforated one, if a difference in pressure exists between the external surface and the chamber underneath the skin. Then, the sucked air can be guided through an outflow or can be used by another aircraft system requiring air. To achieve the aforementioned pressure difference, two approaches can be followed: one making use of an active system based on an electric motor-driven compressor, the other exploiting the natural difference in pressure between the inflow and outflow positions. Active systems have been successfully tested both in wind tunnel and actual flight tests, but they obviously pose some problems in terms of increased system weight, power consumption, maintenance, cost, and complexity. On the other hand, a passive system would not achieve the same performances and the same laminar efficiency. Several studies [102,103] have been carried out to address the problem of taking into account the design of HLFC suction systems during the preliminary aircraft design phase. Different sizing methodologies have been presented for an early estimation of components parameters, such as required power, mass, and dimensions. Pe [102] also addressed the problem concerning the number of compressors to be installed along with their positioning, concluding that for a long-range aircraft with HLFC technology, it is most beneficial, in terms of power usage and additional weight, to have one compressor for each side of a wing.

- Anti-contamination system—To keep the flow laminar over the leading edge, a very high surface cleanliness is required, since even small obstacles could undermine the effectiveness of the HLFC system and promote transition. Contamination of the leading-edge area due to impact of insects has been extensively investigated in the past, even for NLF application, for which such a system would be necessary too. It has been demonstrated that this type of contamination takes place below 500 ft, thus actions must be undertaken before taking off, at landing, and while taxiing to keep lifting surfaces clean. Several measures/concepts have been proposed during the last decades: paper coverings, scrapers/wipers, deflectors, soluble films, resilient surface, liquid spray systems. However, some of these solutions are too demanding in term of system complexity and additional weight, hence they have been regularly discarded. Krüger flaps have been proposed as a solution for such a problem, at least for the wings, thanks to their potential shielding capabilities. The price to pay would consist in restrictions in the design freedom for the high-lift system, and thus a deterioration of high-lift performance.
- Ice and rain protection—To avoid the formation/growth of ice on aircraft surfaces, anti- and de-icing systems are regularly installed on main lifting surfaces. For HLFC application on tails and other aerodynamic components, an ice protection system should be installed to avoid ice blocking the suction holes, degrading the laminar boundary layer.
- Monitoring system—An HLFC aircraft should be provided with a monitoring system, which would start the functioning of the HLFC apparatus once the design altitude has been reached, inform the pilot about the malfunctioning of the system and/or of the anti/de-icing and anti-contamination systems, and communicate with the fuel monitoring system to check the fuel consumption with respect to a laminar operation.

With respect to the last system, it is important to keep in mind the fundamental importance of such an apparatus. A failure of the HLFC systems would result in the inability to achieve the target fuel burn reduction, that, in turn, could imply the inability of the aircraft to reach the target destination due to insufficient fuel reserves.

Several European and US-based programs/research projects have performed flight tests involving HLFC technologies to assess their feasibility. In 1987, NASA and Boeing started a cooperative flight program on a B-757 transport aircraft [98]. The main objectives of the flight test program were to perform high Reynolds number tests on HLFC technology, develop a database on the effectiveness of such a concept, and test its integration with other aircraft systems (high-lift, anti-/de-ice, etc.). For these tests, the actual leading edge of the main wing of the B-757 was replaced with a new construction, consisting of a micro-perforated titanium outer skin, subsurface suction flutes, and ducts to collect sucked air. The new portion of leading edge was also equipped with a Krüger flap, working as a shield against contamination from insects. Tests were performed at $M = 0.80$ and for $C_L = 0.50$. The effectiveness of the HLFC system in delaying the boundary layer transition was successfully demonstrated, with laminar flow extended much beyond the 50% chord, which resulted in a 6% drag reduction for the aircraft.

At the turn of the 1980s, Dassault tested HLFC technology on a Falcon 50 [98]. A perforated suction apparatus was gloved over the inboard structure, close to the fuselage. Suction was performed through an ejector/plenum arrangement. An anti-icing system was integrated into the design, also accomplishing the task of insect contamination avoidance. A Guster bump installation, to avoid attachment line contamination, was also tested for several configurations. Tests confirmed the effectiveness of the integrated anti-ice/contamination avoidance system. The optimal Guster bump location for attachment line contamination avoidance was found to be 300 mm from the side of the fuselage. For this configuration, and with boundary layer suction active, the test article was observed to become fully laminar.

In 1998, another HLFC demonstration was prepared, this time under the leadership of Airbus [104]. For this experiment, the vertical tailplane of an Airbus A320 was equipped

with a complex HLFC system. The experiment was a big success, since an extensive laminarisation of the boundary layer over the vertical tail surface was observed, but the overall complexity of the system would have discouraged any aircraft manufacturer to put it into series production. Nevertheless, the positive results of the test have pushed the DLR to continue the study on such a technology, leading to a simplified concept characterised by a much less complicated suction system, called the ALTTA concept [105], which was tested in 2014 within the frame of the VERSUS project, again on the vertical tail of an A320 and, this time, through wind tunnel tests. It will be flight demonstrated within the EU project AFloNext. Boeing is currently testing HLFC for the horizontal tail and for the vertical fin of the 787-9, at least according to several news articles. A passive suction system was already patented by them in 2011 [106].

Risse [107] has proposed in his work a way to include HLFC on wings and tails in the preliminary overall aircraft design. The basis of this work was the integration of a preliminary design methodology for hybrid laminar flow control systems into an existing aircraft design framework. The framework in which this has been performed is MICADO [108], a multidisciplinary, requirement-driven design software composed by a series of program modules dedicated to different tasks, including optimisation. The approach through which HLFC systems design has been included into the existing framework is physics-based. A quasi-three-dimensional wing design approach and a database of optimised HLFC airfoils for different design conditions are used to incorporate HLFC aerodynamics into overall aircraft preliminary design. Drag is estimated through a transition prediction code, considering cross flow instabilities too. The chosen spanwise and chordwise distribution of the suction orifice, along with the pressure distribution coming from the aerodynamics computations, allows to perform an automatic estimation of the power requirements and of the masses of the suction system. The suction system architecture is made up of:

- a micro-perforated thick metal sheet;
- stringers parallel to constant chord lines, dividing the double skin into several chambers;
- an inner metal sheet with throttle orifices;
- a plenum with constant under-pressure.

In Ref. [107], a quantitative assessment of HLFC at aircraft level is also provided. Since HLFC shows its full potential on long distance flights, a conventional turbulent long-range aircraft configuration was selected as reference, characterised by a design range of 8150 nmi, a design passenger number equal to 470, and a cruise Mach number of 0.85. The reference design, performed through the MICADO framework, was then compared to the design coming from HLFC integration. In particular, three HLFC configurations are compared (HLFD-0, HLFD-1, HLFD-2), characterised by different values for the cruise Mach number (0.85, 0.80, 0.80, respectively) and the outboard leading-edge sweep ($34°$, $34°$, $28°$, respectively). Moreover, two different design approaches in terms of HLFC integration were examined, one involving retrofitting of laminar flow technologies (D1) and one considering the resizing of aircraft components (D2). Then, comparisons were performed in a step-wise fashion to identify the different design influences. References [107,108] show design evolution and impact on mission block fuel as a percentage relative to the reference. Here, two additional scenarios were also considered, both linked to the loss of laminarity during the mission: one at the 50% of the design range, the other for the whole length of the mission. A resizing of the aircraft for HLFC would imply greater benefits in terms of fuel burn reduction, more than 1%. Risse showed instead the relative percentage changes of key design parameters. It can be observed how the propulsion system and geometry are kept constant for the retrofit design (D1).

It is the opinion of the authors that the HLFC technology reviewed so far is too complex for an application on the commuter aircraft category.

3.7. Riblets

The previous section addressed the problematic aspects of keeping the boundary layer flow as laminar as possible in the chordwise direction. Laminar flow control could theoretically be used to extend laminarity even further along the mid-chord region, as highlighted by Ref. [96], but this would come at a high cost in terms of required power, weight penalty, and direct operative costs. Since at this stage a complete LFC seems not to be feasible, a significant proportion of skin friction drag due to turbulence remains. An improvement in this sense could result from the usage of techniques reducing the turbulent drag.

Riblets are small surface protrusions, aligned with the direction of the flow, which confer an anisotropic roughness to a surface (Figure 27a). There are also other passive techniques to be used in order to reduce the skin friction in turbulent boundary layers, such as dimples (Figure 27b), but several tests performed during the last years have shown little or no improvements in terms of turbulent drag reduction, along with a higher cost associated with their operation. On the other hand, the potential of riblets has successfully been proven, both in laboratory and during actual flight tests.

(**a**)   (**b**)
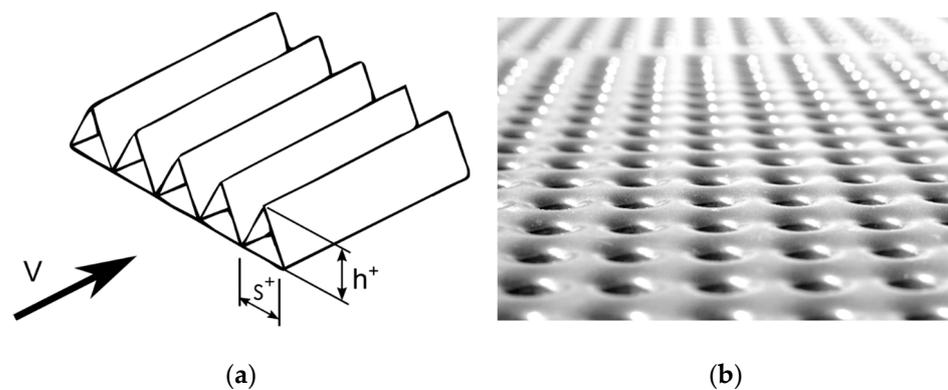
Figure 27. Technologies to reduce turbulent drag: (**a**) riblets; (**b**) dimples.

The correct explanation of the underlying physics of riblets is still a subject of discussion and a topic of research. It has been shown that riblets induce a displacement of the turbulence eddies with respect to the mean flow, leading to a reduction of the momentum transfer to the wall with a consequence drag reduction [109]. However, this mechanism is confined to a region that is very close to the surface and, in case the riblets are large enough to interact directly with the turbulence structure, they could even lead to an increase in drag [110].

Garcia-Mayoral and Jiménez [111] found that the riblets' groove dimensionless cross-sectional area A_g^+ is the most suitable parameter to characterise riblet performance with respect to different non-dimensional parameters, such as riblet spacing s^+ or riblet height h^+. In fact, the adoption of $l_g^+ = \sqrt{A_g^+}$ collapses riblets experimental data into a compact group of similar curves, meaning that A_g^+ can be used to better identify an arbitrary family of riblets. Garcia-Mayoral and Jiménez found that the best estimate for optimum drag reduction is $l_g^+ \simeq 11$, but also confirmed that drag reduction is heavily affected by riblet spacing, size, and orientation, which, in some cases, could even produce a drag increase.

From an aircraft perspective, Catalano et al. [110] have investigated the effects of the application of riblets to a wing-body configuration of a typical regional turbopropeller airplane, see Figure 28. For such configuration, the wing was equipped with NLF optimised airfoils for cruise condition, with the twist being optimised for low-speed performance. Different assumptions were then made to assess the effect of riblets in combination with NLF. Riblets were applied with the assumption of fully turbulent flow and eventually the flow was assumed to be laminar for a large portion of the wing because of NLF technology. Three different aircraft configurations were analysed to better determine the zones of the aircraft in which the effect of riblets is more effective: one with riblets only on the wing,

one with riblets applied on both the wing and the fuselage, and one with riblets applied on the whole aircraft. Finally, three different scenarios were considered: cruise condition with fully turbulent assumption, laminar cruise condition, and fully turbulent climb/descent. RANS simulations were performed to assess the effects of NLF and riblets, with a proper boundary condition to simulate the effect of the latter. Table 8 reports the results of the performed analysis in terms of saved weight percentage with respect to the weight obtained at the end of the cruise phase for the clean configuration. Two different design missions were examined, one with a cruise range of 350 nmi and one of 900 nmi.
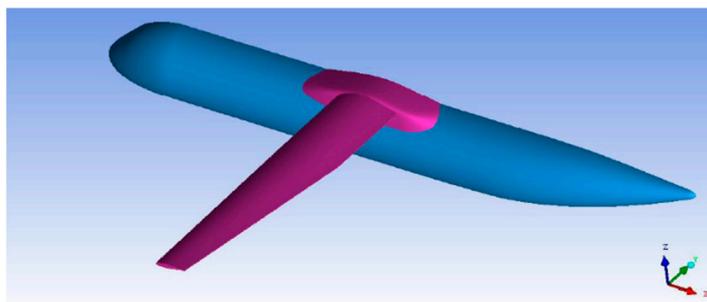

Figure 28. Aircraft configuration examined in Ref. [110].

Table 8. Weight savings for a design mission with cruise phase of 900 nmi and 350 nmi [110].

	Clean	Riblets Wing (%)	Riblets Body (%)	Riblets WB (%)	NLF (%)	NLF and Riblets WB (%)
$100\,\Delta W/W_f^c$ (900 nmi mission)	0	3.75	1.74	7.38	9.86	16.03
$100\,\Delta W/W_f^c$ (350 nmi mission)	0	1.6	0.74	3.15	4.20	6.82

From the data reported in Table 8, it is possible to state that NLF technology can allow to save much more weight than riblets, but, at the same time, the usage of riblets can provide a sensible contribution to drag decrease. Moreover, it is easy to conclude that riblets on the wing are much more effective than riblets on the fuselage.

Regarding actual flight investigations with riblets applied on aircraft surfaces, several tests have been performed during the last decades. In the 1980s, McLean et al. [112] tested the effect on drag reduction of a riblet film glued over the upper surface of one wing of a T-33 jet trainer. Several 3M riblet films, different in terms of spacing and height, were used on a portion of wing surface extending from the 7% to the 83% of the local chord. For a flight Mach number equal to 0.70, tests results reported that the presence of riblets contributed to slightly change the velocity profile on the wing surface, causing a lower velocity gradient. Results from two flights showed a skin friction drag reduction of 6–7%, in a range of s^+ varying from 10 to 15, while a not significant effect of h^+ were observed, at least for the riblet films tested.

In Ref. [113], Szodruch reported a flight evaluation of riblet performance on an Airbus A320. For this test, about 70% of the aircraft surface was covered with riblets. To estimate the total drag reduction, fuel burn savings were estimated during flight tests. According to Szodruch, for a Mach number range from 0.77 to 0.79, a 2% in total drag reduction was obtained, a really encouraging result considering it came from actual flight tests performed on a marketed commercial aircraft.

However, as previously highlighted, riblets pose some serious aerodynamics issues, such as their performance in off-design conditions. Other than that, several additional considerations must be made. Riblets, in fact, imply additional operative costs: maintenance of riblet shape and adhesiveness over operational life is required. Hydraulic fluids, dirt, insects, and hail can easily compromise their performance, and time required to install, remove, and

re-apply is surely not a negligible cost for an operator. For these reasons, the application of riblets does not seem suitable for a commuter aircraft, in the authors' opinion.

3.8. Ultra-High Aspect Ratio Wings

Improving an aircraft aerodynamics efficiency is directly related to drag reduction, either parasite drag or induced drag. Technologies for parasite drag reduction have already been presented in Sections 3.4 and 3.6. Induced drag is directly affected by the wing aspect ratio. It follows that an ultra-high aspect ratio wing (UHAR), with values well beyond the limits of actual operative commuters, would improve the aircraft aerodynamics efficiency. Moreover, by using an UHAR, laminar flow could be achieved more easily because of the reduced cross-flow component.

Using an UHAR wing as a means to improve an aircraft efficiency could be considered as the easiest and most straightforward solution. However, there are some drawbacks. Increasing the wing aspect ratio means either enlarging the wingspan or reducing the wing area. Both have their pros and cons. A higher value of the wingspan triggers the need for aeroelastic considerations. In large span wings, these phenomena, together with wing loads, require a sophisticated wing structure which, in turn, does not bring a high weight penalty. Practical issues, ranging from new manufacturing technologies up to everyday ground operations and constraints, should also be considered a priori in such a solution. With this purpose, innovative aircraft concepts such as the Strut-Braced Wing (SBW) [114] or Truss-Braced Wing (TBW) [115], illustrated in Figure 29, may be designed and optimised aimed to improve the wing aerodynamics, structural efficiency, flight performance, and pollutants emissions. Usually, long-range aircraft fly at transonic speed and at a lift coefficient lower than short range aircraft. Moreover, short-range aircraft spend a significant part of their flight in climb and descent, performing short cruise segments. Climb and descent are both characterised by a higher lift coefficient. Therefore, even if for long range aircraft drag reduction has a larger impact on fuel burn, it is evident that the larger benefits in decreasing induced drag can be obtained on a commuter aircraft.

Figure 29. SUGAR Volt truss-braced wing aircraft concept.

The ultra-high aspect ratio wing configuration is expected to be prone to aeroelastic issues with specific reference to wing elasticity influence on loads distribution and effectiveness of roll control and on aircraft static and dynamic stability. Therefore, the preliminary stage of aircraft design cannot neglect the multi-disciplinary interaction between aerodynamics, structures, stability, and control. As the simple cantilever wing layout is unfeasible for a wing aspect ratio as high as 20, strut-braced or truss-braced wing configurations must be considered. These configurations should provide fuel burn reduction of 10–20% compared to a conventional cantilever wing [115,116] for a long-range aircraft with additional innovative technologies such as riblets and natural laminar flow.

Lacking similar aircraft configurations in service, the classic preliminary design methods cannot comply with such a task. Therefore, low- and medium-fidelity methods, such as vortex or doublet lattice methods, should be applied to investigate the aerodynamics, stability, and control of a set of ultra-high aspect ratio wing configurations. In parallel, trade-off flutter, divergence, and control-reversal analyses should be carried out to define a "safety domain" of stable structural arrangements for the wing [117].

Recent investigations on a regional aircraft with a typical mission profile of 300 nmi have shown that by doubling the aspect ratio with a conventional layout will increase the operative empty weight of about 40% and the fuel burn of about 10%. The effect of reducing the induced drag was exceeded by the increase in weight. The UHAR wing becomes attractive if the design manufacturing technology is such that there is at least a 30% structural weight saving with respect to a conventional cantilever wing, as illustrated in Figure 30.

(**a**)	(**b**)
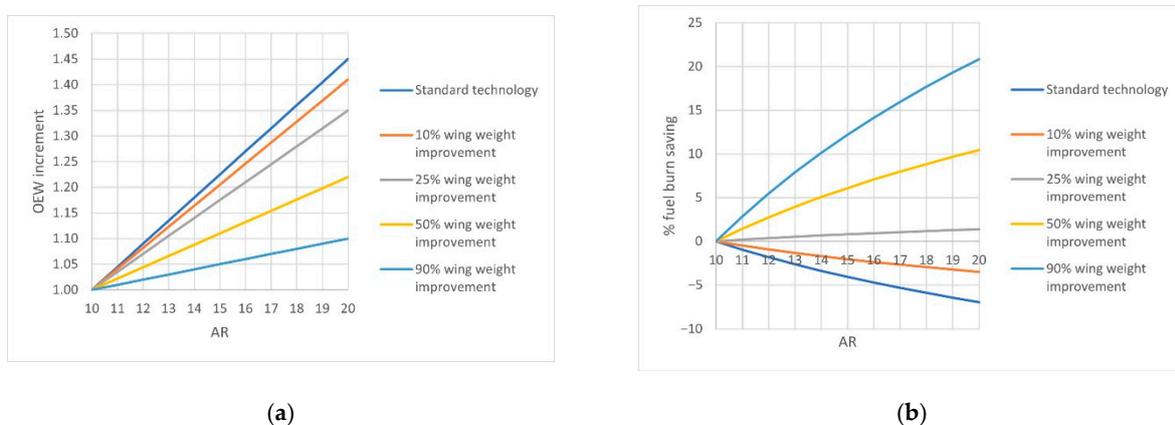
Figure 30. Example of potential weight increase and fuel burn variation due to aspect ratio variation: (**a**) change in operative empty weight; (**b**) change in fuel burn.

3.9. High-Lift Devices

Further improvement in aerodynamics is related to the design of high-lift devices. In SAT, Piaggio Aero and Evektor are working on the design of such system, improving the low-speed performance. Together with methods and tool improvements, a better high-lift device design can lead to a whole aircraft improvement. High-lift systems, which include wing flaps and slats, are under development for small aircraft in a first Clean Sky 2 research phase. After optimising the aerodynamic and integration design, these devices will be classified based on their high lift architectures to shortlist the best design. The EU-funded MOTHIF project [118] uses a specifically designed and manufactured wind tunnel model for testing variable positions of flap and for different angles of attack. Along with the flap separation control jet blowing system installed on the main wing box trailing edge, this will be installed in the Von Karman Institute (Belgium) subsonic wind tunnel and tested at the required Reynolds number. The project is concluded, but results have not been published yet.

An example of active control on high-lift device is shown in Ciobaca and Wild [119]. They tested in a wind tunnel both leading edge and trailing edge flap devices on the DLRF15 wing model. They appreciated a significant increase in maximum lift coefficient of about 0.3 with an increase of stall angle of about 5°, with respect to the baseline configuration, due to the combined flow control applications on the leading edge. Moreover, the trailing edge actuations showed a lift enhancement of $\Delta C_L \approx 0.6$ in the linear regime and $\Delta C_{L\max} \approx 0.4$.

The combined design of high-lift devices and high-lift propellers was carefully evaluated at NASA during the design of the X-57 wing. Starting from a wing with the GA(W)-1 LS-0417 airfoil at root and GA(W)-215 airfoil at tip, realised by scaling the thickness distribution of the 13% and 17% thick airfoils about the camber line [120], the flap high-lift device was designed accounting for the presence of high-lift propellers, their positions, and

their relative dimensions. Results of study on the propeller diameter to wing chord ratio D_p/c indicated that the blown to unblown C_L ratio increased as the chord was decreased. However, because of the increase in relative size of the high-lift nacelle to the wing, which impacted wing lift performance, the study indicated that a D_p/c ratio of 1.0 gives the overall best maximum lift on the wing with the X-57 DEP system. Investigations on flap design and high-lift propellers are still in progress to assess the proper chordwise and relative propeller height respect to the local chord line to mitigate the separation effects highlighted in Section 3.3.

4. Airframe Technologies

Airframe design directly affects the aircraft weight. That is the reason why a lot of new technologies were introduced in the last decades to pave the way towards low carbon air vehicles. New materials, along with new process technologies have been widely investigated with the aim of achieving a lighter airframe. However, on one hand, there is still a lack of understanding of new materials. As a consequence, almost every novel concept introduced so far (e.g., composite materials) has many drawbacks either preventing its full exploitation in terms of weight saving or introducing strict maintenance procedures. On the other hand, airframe design is a matter of weighting structure configuration with aerodynamic loads and performance. As a direct consequence, the configuration designed is not always the best structural layout possible. Many factors affect the airframe design and multi-disciplinary analysis is strongly needed. Moving from material and layout characterisation, the most promising key-enabling technologies are reported afterwards focusing the attention on how and how much they can impact the design at aircraft level, generalising the result even beyond the target platform.

4.1. Smart Intelligent Composite Structure

One of the major concerns of aerospace and transportation engineering over the last years has been related to efficiently adopting composite materials in view of increasing vehicle performance and safety along with energy savings. Indeed, composite materials have been widely introduced in structure manufacturing with the aim of designing stiffer and lighter components. That is mostly because they ensure tailoring the properties of the structure according to the specific load to be withstood in order to achieve the optimal ratio between strength/stiffness and weight. In addition, composite materials allow one-piece barrel manufacturing with an incredible weight saving thanks to unneeded bolts and connections. However, there are many other aspects preventing their full exploitation which directly reduce the benefits that pushed up the composite quotation as key-enabling technology.

Specifically, random events—such as certain low velocity impacts—may induce barely visible or invisible failure due to the complex mechanics behaviour of such an anisotropic and multilayer structure. Impact-induced damage in stiffened composite laminates is usually accommodated with constrained design and strictly maintenance tasks that increase operational costs above all else and decrease the advantages for which composites have been introduced massively. To overcome such drawbacks, an integrated structure providing monitoring of critical components appears the most promising solution. A condition-based approach could be able to relax the maintenance strategy minimising aircraft downtime as well. Moreover, the design constraints would be avoided with a further increase of structural performance resulting in a more environment-friendly aircraft. Although the latter possibility is a very long-time perspective, Structural Health Monitoring (SHM) systems, providing continuous or on-demand information about the structural efficiency, appear to be the key technology to achieve the first goal [121].

Aircraft health monitoring aims at enhancing flight safety allowing the reduction of maintenance and operational costs simultaneously [122]. A system that enables automatic detection, diagnosis, prognosis, and mitigation of adverse events arising from component failure, can be conceptualised in an integrated vehicle health management system. The cur-

rent practice of scheduled maintenance increases the cost of maintenance steeply, especially in the case of an aircraft operating beyond its designed service life. That is to say, preventive (or scheduled) maintenance requires a deep and strict inspection task program that could be relaxed by moving to predictive (or "on condition") maintenance. However, adopting a condition-based philosophy is only possible through an effective and reliable damage detection system. The aim of SHM is to detect and diagnose initiation of any defect, to analyse its effects, and to trigger maintenance workflows in order to maintain aircraft safety. That is possible through collecting various data by a network of sensors and analysing them by using data analytics algorithms aiming at providing diagnosis and prognosis in a reverse engineering approach [123]. It is worth noting that, under this general framework, SHM systems are employed on both structures and systems. SHM approaches and main characteristics deeply discussed in the present section, essentially look at the structural integrity by monitoring damage emerging and growing within airframe and assessing its remaining useful life. Instead, system health monitoring, approached in a following section looking into the specific case of landing gears, looks at functional aspects and any degradation in performance triggering maintenance tasks or replacement of affected components.

4.1.1. Composite Damage Mechanics

For reasons inherent in their internal structure, composite materials suffer much more than any other conventional metallic material of problems related to damage. Typical for composites are matrix cracking, delamination, fibre fracture, and interfacial debonding. These kinds of damage, especially those accidentally and suddenly induced and then occurring in fatigue problems, are very critical. As a consequence, composites are some of the most critical type of materials with respect to fatigue, where the crack initiation may even be due to accidental damage. The most problematic aspect is that damage can be produced even by events involving very small values of energies. As an example, delamination at interfaces between adjacent plies differently oriented might arise as a result of impacts with external objects involving energy of a few Joules. Although that damage results in a loss of stiffness, the failure cannot be likely detected through a simple or detailed visual inspection because it is characterised by small external indentation [124]. That is where many concerns have been raised related to the use of composite materials, which are becoming increasingly important in aircraft manufacturing. It is recognised that damage can be difficult to detect, resulting in a barely visible or invisible flaw, and demands for a specific design. In the modern aircraft, the damage tolerance approach involves the use of inspection procedures and structural design concepts to ensure safety, rather than the traditional correction factors used for ultimate loads [125]. The damage tolerance practise requires information on residual strength characteristics, sensitivities to damage growth and environmental degradation, maintenance practices, and in-service usage parameters and damage experiences. However, a sort of "defect factor" based on degree of detectability has been introduced for establishing minimum damage tolerance residual strengths for composite structures in requirements proposed for inclusion in Ref. [126]. The application of this philosophy results in introducing such knockdown factors affecting the design of composite structures by limiting material strength. That is due to such complex impact mechanics, which makes the real condition of the structure under loading unpredictable. The impact behaviour of composite materials has been studied experimentally by many authors [127] and the complexity of the physical phenomena demands detailed investigation to numerical modelling, making it difficult to extend analytical solutions to complex structures [128]. The low velocity impact damage has a significant effect on the strength and durability of the laminates; it is an inevitable event and needs appropriate design solutions to be addressed [129]. As a matter of fact, a lot of work is still necessary to improve the modelling of the damage developing during impact on composite laminates to better assess numerically their residual mechanical characteristics in order to optimise their design [130].

The influence and severity of damage caused by an impact event in composite structures is typically more difficult to be assessed, more severe, and even less visible than in metals. As a result, composite materials are sensitive to many aspects of in-service use for which it is difficult to provide design data. It is worth noting that due to the brittle behaviour of composite laminates every out-of-plane load or even drop of minor objects (e.g., tools used for assembly or maintenance) may lead to significant damage. This latter can be broadly divided in two groups [131]:

- intralaminar damage, where the flaw develops inside the ply (e.g., matrix cracking, fibre/matrix debonding or fibres breakages);
- interlaminar damage, when a discontinuity arises at the interface between two consecutive plies (e.g., delamination).

Although in this classification, composite structure failure is often characterised by multiple damage mechanisms arising locally and developing three-dimensionally, in fibre-reinforced laminates, delamination is the most common and critical damage mode under impact loading. However, it rarely occurs alone. The delamination usually arises between two adjacent layers with different fibres orientation [132] due to the high interlaminar stresses developing and the relatively low interlaminar strength available. This is combined with also very low through-thickness strength due to the low resistance of the matrix. As a consequence, low-velocity impact is usually followed by first matrix cracks developing in the plies and then delamination spreading along the ply interfaces growing from these cracks. Relevant efforts have been spent in the past years to understand how delamination arises and develops within the composite laminates. The complex mechanics results in the classic "peanut" shape which develops at almost every interface and penetrate through-the-thickness into the following layers achieving the typical "Christmas tree" structure [133,134].

Although improved knowledge about composite failure mechanics was achieved in the last years, a major concern still regards the detectability of damage. The impact evolution in composite laminates induces bending or shear stresses initiating micro cracks in the matrix located on the opposite side of the impact point. Then, micro cracks propagate into the nearby interface between dissimilar plies yielding to the delamination. These phenomena result in a very small surface indentation even when the through thickness damage is greater than an emerging flaw due to the mixed crack-delamination evolution. The morphology of damage typically obtained after composite structure being subject to low velocity impact is highlighted in Figure 31, which shows a classic ultrasonic non-destructive evaluation (NDE). Specifically, it regards the case of a 6 mm carbon fibre reinforced plate designed for a lower wing panel of a commercial aircraft and loaded by a low velocity impact of 85 J using a drop weight machine with one inch tip [135]. The peanut shape and the relevant extent of damage is evident from the c-scan image—in-plane view of the damage. Furthermore, the s-scan—section view of the damage—shows how the laminate is corrupted through the thickness by several instances of delamination arising among adjacent layers. This results in the typical impact cone due to the complex failure mechanics (cracks-delamination mixed failure). However, although the conformation of the damage appears evident, the only relevant item is the indentation on the upper surface, which is not visible as it is of the order of few hundred microns.

Such hidden damage is particularly dangerous because it drastically reduces the compression after impact (CAI) strength as well as the fatigue strength, which are both critical design parameters for aircraft structures. The loss of the latter may be up to 70% of the undamaged case depending upon the laminate layup and according to the fatigue load spectrum [136]. Generally, CAI strength after damage may result around 60% of the undamaged value. This is the reason why the compressive strain is usually limited in between 3000 and 4000 microstrains during design [137]. As a consequence, composite materials are not fully exploited up to now due to issues inherent to their internal mechanics. New methods of investigation have been developed to reduce the gap between theoretical and practical benefits in adopting composites, including SHM.

As discussed afterwards, the integration of this technology can benefit both composite design and aircraft maintenance strategies. However, before moving to the benefit of introducing this key-enabling technology, it is worth looking into the current composite damage tolerance approach.
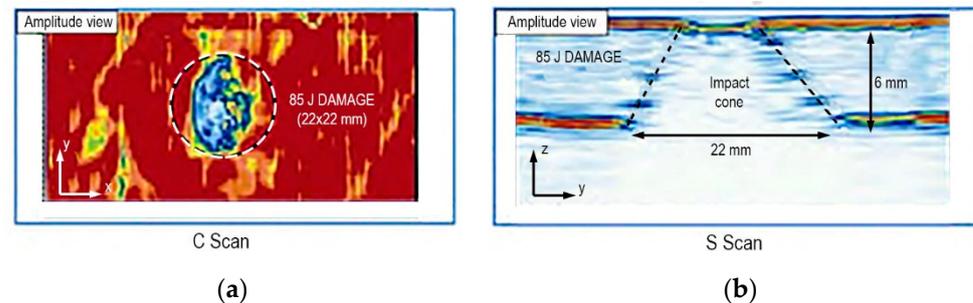
Figure 31. Low velocity impact damage: (**a**) typical peanut shape in the plane of the plate; (**b**) conical distribution of delamination through the thickness.

### 4.1.2. Composite Damage Tolerant Approach

The complexities inherent to composite response under low velocity impacts and the detectability of emerging damage require the design of aircraft structure to be appropriately addressed. Basically, in a damage tolerance approach, the presence of hidden failures due to barely visible damage is accounted for right from the design, generally accomplished by limiting the design strain level for ultimate and limit combined load design criteria [138]. Another common design approach limiting the benefits of composites is operated to preserve the collaboration of reinforcements. In this context, the typical problem regards the stiffened composite components where the stringers adopted for reinforcing thin-walled structures may be affected by not visible disbondings even when subjected to low energy impacts. As in the case of delamination, the punctual load leads to complex damage mechanics resulting in the separation between the stringer and the hosting structure, which prevents the collaboration between parts with a dangerous drawback for loading absorbing [123]. Hence, disbonding stoppers are usually included in the design to avoid separations between stiffeners and skin above the maximum size, ensuring safe structural collaboration [138]. As a matter of fact, connectors are eventually necessary where the introduction of composites would avoid or limit any type of connection between different parts to reduce weight as well as manufacturing and maintenance costs. Therefore, this rough damage tolerance approach breaks down many benefits encouraging the introduction of a composite airframe. There are indeed two primary damage tolerance requirements described in [139]: (i) damage growth characterisation and (ii) residual strength capability. The certification demands the demonstration of required levels of static strength, durability, and damage tolerance as well as the ability to predict stiffness properties. Demonstration of compliance for composite structure includes sustaining design ultimate loads with damage at the threshold of visual detectability—barely visible impact damage (BVID)—and sustaining design limit loads with clearly visible damage. In addition, it must be demonstrated that levels of damage smaller than those that reduce the residual strength to design limit load capability will not experience detrimental growth under operational loading conditions. For instance, considering the applied strains, materials, and design concepts, a no-growth approach for damage tolerance has been adopted in the case of Boeing B777 empennage [125]. This approach is based on demonstrating that any damage undetectable during visual inspection will not grow under operational loads. This means that a damaged component must be capable of carrying ultimate load for the operational life of the airplane. The advisory circular [139] includes acceptable means of compliance in the following areas: (i) effects of environment (including design allowables and impact damage); (ii) static strength (including repeated loads, test environment, process control, material variability, and impact damage); (iii) fatigue and damage tolerance evaluation; (iv) other items—such as flutter, flammability, lightning protection, maintenance, and repair. According to such

items, the no-growth behaviour of B777 composite structure has been demonstrated in numerous subcomponent tests. Following the typical building block approach in use within the aeronautical field, two full-scale cyclic load tests were performed inserting damage sites during several test sequences. In addition, the full-scale tests demonstrated the following characteristics required for damage tolerance compliance [125]:

- manufacturing anomalies allowed according to process specifications do not grow in a time equivalent to more than two design service lives;
- visible damage due to foreign-object impact does not grow during the time of two major inspection intervals (i.e., two C-checks, 4000 flights per C-check);
- the structure residual strength after damage is enough to withstand loads that can reasonably occur in service.

The residual strength capability was again demonstrated, introducing visible impact-induced damage in the test box and conducting fatigue tests lasting two inspection intervals. Although visible damage is easily detected by scheduled maintenance inspections, a no-growth behaviour was achieved again. Finally, many means of compliance were verified including strength after barely detectable impact damage, called threshold of detectability (TOD) impact damage in FAA advisory material; flaw growth from TOD impact damage; strength after detectable damage; flaw growth rates from detectable damage; lightning strike resistance; flame resistance. As a result, the allowable design was a fair amount higher than that of the material.

Summarising what is emerging by analysing a real certification stage of an aeronautical composite structure, during the design phase, it is necessary to demonstrate that invisible and barely visible damage occurrences do not affect the safety of the aircraft between adjacent inspection checks. To detail how a safety design may be affected by unforeseen events, the typical trend of residual stress/strain versus impact energy level is schematised in Figure 32. A first low-energy range is connected to no-visible damage as it is not inducing any failure—namely, below the energy level ensuring the onset of a hidden failure. Then, the residual strain/stress deeply decreases, while the impact energy level leads to a slightly increasing damage which is barely visible. That failure is indeed characterised by a through-thickness delamination, where no indentation is visible (inner visibility) or together with a slightly visible indentation (external visibility), which is not always appreciable by visual inspection. Then, the damage appears increasingly evident according to the energy level. That is the range for a setting limit and ultimate design stress or strain, where any safety factor is not considered yet.
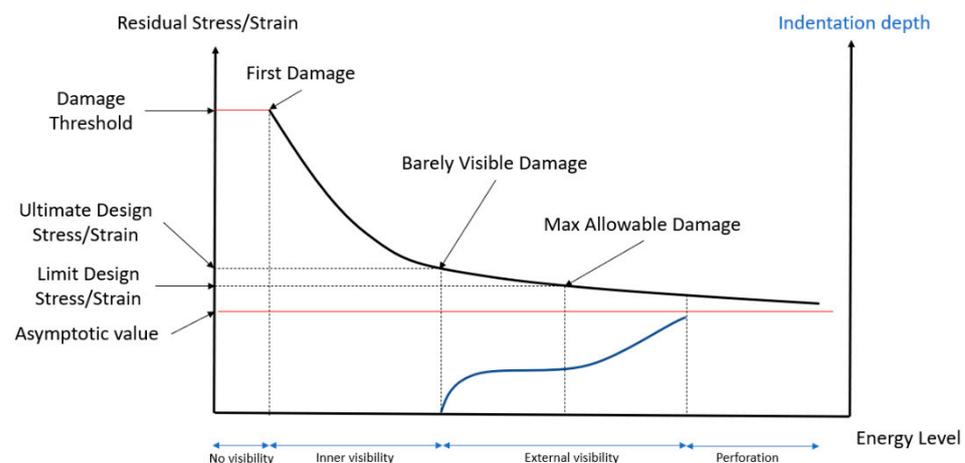
Figure 32. Schematic representation of residual strain versus energy level and derived design constraints.

Furthermore, as above mentioned, the damage is not the only event introducing knockdown factors. Other aspects that need to be accounted for are reported in Figure 33, whose scheme shows how they define the allowable design region merely with a reduction of allowable stress/strain. Composite structures are indeed sized using limited allowables,

which become appreciably lower than material ultimate stresses due to the introduced tolerance (see Figure 34). According to Boeing design manuals and military handbooks [125], the design limit allowable $\sigma_{d.l.a.}$ can be calculated for first approximation introducing a scatter to the ultimate material allowable $\sigma_{m.u.a.}$ as follows:

$$\sigma_{d.l.a.} = 0.5\ \sigma_{m.u.a.} \tag{8}$$
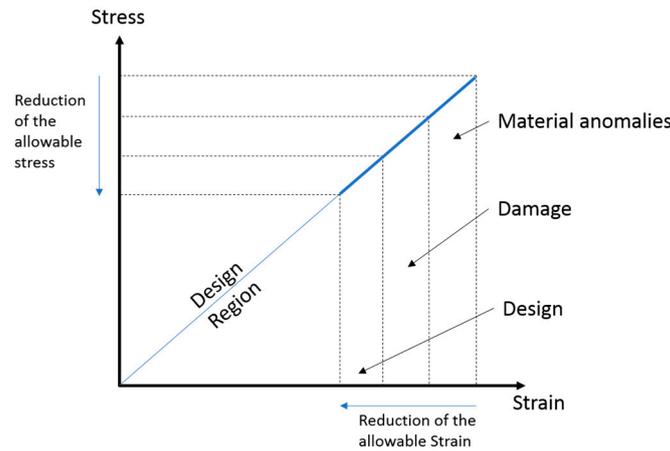
Figure 33. Schematic representation of scattering factors constraining the composite design.
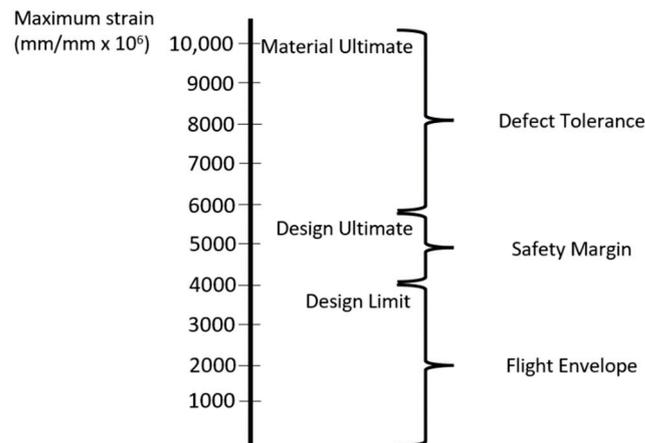
Figure 34. Typical design allowables for carbon fibres reinforced plastics (CFRP).

This definitely means that a huge amount of weight reduction expected introducing composite materials is wasted. That is where the SHM introduction may provide a more relaxed design, limiting the allowable to the residual stress or strain associated to the minimum damage detectable with an integrated system (i.e., the system target) capable of identifying emerging flaws where any other detection is not possible. As a matter of fact, the standardisation and reliability required to move from the damage tolerance to a condition-based design actually makes the possibility to account for SHM technology right from the structural design and avoid knockdown factors due to detection of inner visible damage far from application. However, due to the results that this type of system may potentially achieve, SHM appears to be the only way to design high performance and lighter components reaching the advantages fully expected up to now. For these reasons, the condition-based design is referred to here as the long-time perspective of SHM.

Otherwise, a short-time perspective introducing SHM is related to the damage assessment procedure adopted during lifetime and connected again with damage tolerance approach, which is based on scheduled inspections to ensure safety. The Paris law or similar approaches are useful to define the remaining life of airframe [140]. However,

structures subjected to cyclic loads show a particular evolution of the crack demanding for skilful inspection planning. As a matter of facts, the extreme conditions and harsh environments which aerospace structures are exposed to require the ability check of the component in supporting expected loads. This is primarily a flight safety consideration that damage tolerance tries to meet, ensuring the structure can continue carrying the agreed-upon regulation loads despite any damage or degradation (e.g., impacts-induced failures). Consequently, the concern with damage tolerance is ultimately with the damaged structure having adequate residual strength and stiffness to continue in-service safely at least until the damage can be detected by following scheduled maintenance inspections. The final goal is ensuring safety in every unforeseen event, not solely on likely scenarios of damage. Hence, it is worth defining the damage that the structure is capable of carrying at the various required load levels (ultimate, limit, etc.). Composite structures are certified with an approach allowing the presence of a damage, no matter how the damage onset and growth are. Hence, in-service inspection techniques are necessary and need to be capable of adequately detecting damage before it becomes critical. In addition, if the damage growth is allowed, it must be predictable that such inspection intervals can be reliably defined. In this context, in-service inspection procedures play a major role so that structural regions and elements are classified with respect to required non-destructive inspection (NDI) and NDE sensitivity. Inspection intervals are usually established on the basis of crack growth information, assuming a specified initial flaw size and a detectable crack size, the latter depending on the level of available NDI/NDE procedure and equipment. Cracks larger than that are presumed to be discovered and repaired with a defined confidence level. That is the target of the NDE equipment usually assessed with probability of detection approaches [141]. Furthermore, the inspection intervals must be such that an undetected flaw will not grow to critical size before the next inspection. Due to their key role, the use of NDI/NDE techniques and the establishment of appropriate inspection intervals have progressed considerably especially in the case of composites.

Non-destructive testing methods deal with the identification and characterisation of damage without altering (destroying) in any way the component inspected, whether they show inner or external visibility. Due to their characteristics, they provide a cost-effective approach to investigating the condition of a single component or for the in-service inspections of complex systems [142]. In the field of composites, numerous techniques are adopted, including ultrasonic testing [143], thermographic testing [144], infrared thermography testing [145,146], radiographic testing [147], visual testing [148], acoustic emission testing [149], acousto-ultrasonic [150], shearography testing [151], and electromagnetic testing [152]. As described above, each one of these methods has advantages and drawbacks, addressing specific problems in several types of flaw to be detected and different parts. As a consequence, although the great potentialities of several NDT techniques, some of their inherent limitations still persist. First of all, NDI/NDE inspection sensitivity and reliability while inspecting actual airframes are far from the standards within laboratory tests which include simpler coupons. However, the major concern of current NDI/NDE practices is that they cannot provide a continuous assessment of the structural condition. To practically perform these inspections, the aircraft has to be taken offline, disassembled in some parts and scanned. This process is time consuming and expensive, making necessary a detailed scheduling and preventing on-demand inspections. The implementation of an SHM system could improve such a situation due to the permanently attached transducers allowing structure interrogations as often as needed even when and where the accessibility is not possible [153,154]. The potential benefits introduced by operating SHM within aircraft inspections are detailed in the next section, where specific examples are given to justify the cost benefits achievable by introducing condition-based monitoring with integrated structures.

4.1.3. Benefit of SHM System within Aircraft Life Cycle

Unlike NDE inspections, the on-demand interrogations of an SHM system based on permanently attached sensors are always carried out in the same way. This continuous

process enables building up of an updated historical database that contains information about structural changes assisting in such a reasoning system. Advanced data analytics is then required for detecting characteristic changes in the material and then transferring that information for updating the prognosis system with the aim of estimating new residual life. That is possible where critical features extracted from raw data show significant changes in structural state relative to a reference condition. These features are then stored in the historical database which is uploaded at every SHM interrogation to define the current state of the structure. The monitoring process can be performed in combination with existing NDI/NDE procedures. SHM diagnosis populates the information about structural condition within several inspection intervals, increasing safety. In addition, most of the prognosis techniques currently operated are based on linear assumptions, which are far from the real mechanics of composites and the actual operational conditions. That is where the historical database populated by NDI outcomes and densified by SHM interrogation can compensate the prediction errors allowing adjustment and improvements of the crack-growth prediction laws [155].

Structural health monitoring could have a major contribution to the structural diagnosis and prognosis, not only increasing the safety by introducing a continuous monitoring. As a matter of fact, the introduction of an effective SHM system may completely change the maintenance strategies increasing safety level of operations. The damage assessment process is really complicated by the necessity of inspections targeted to ensure safety according to the damage tolerance design criteria. The complex environment in which aircrafts work, driven by the business of the operator, leads to the necessity of scheduled inspections between several flights that minimise the downtime. In fact, the damage assessment process is based on different levels of inspection and oriented to either releasing the aircraft or requiring its repair, as schematised in Figure 35. The walk-around operated by the aircraft captain is the first way to detect damage by visual inspection. However, the first detailed inspection is operated by the Level 1 inspectors according to rigorous visual inspection criteria and it is usually available at larger airports. When the release is not obtained during this phase, the inspection operated using sophisticated NDT approaches is required to obtain the release or repair response. However, the Level 2 inspectors, in charge of such type of tests, are available only in certain bases and it is necessary to move the aircraft in most cases. In fact, the inspection procedures are complicated and often introduce additional downtime. In this context, the principal aim of SHM is to reduce operative costs moving from the actual maintenance approach (based on two different levels of inspection) towards a condition-based philosophy (exploiting an autonomous and integrated sensing system) to decide about release or repair of the aircraft.
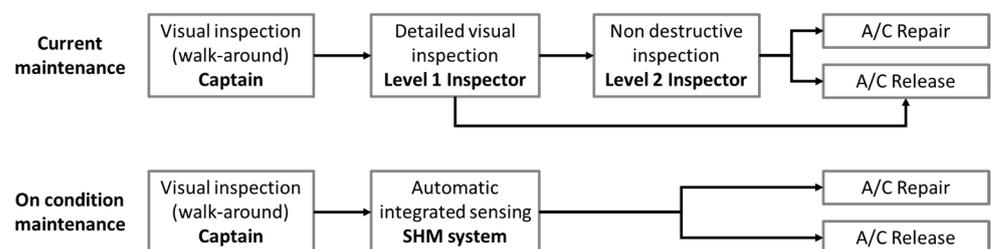
Figure 35. Possible maintenance approaches suited for aircraft operators.

According to the International Air Transport Association (IATA) benchmark for direct operating costs per flight depicted in Figure 36, the 17% of the operative costs of a recent aircraft are demanded for maintenance tasks and they can increase up to 25% for ageing vehicles. In the specific case of the 19-passengers aircraft De Havilland Canada DHC-6 Twin Otter, the maintenance costs—based on a combination of labour costs and parts costs—are about 21% of the total direct operative costs, while airframe and propeller maintenance cost assumes an annual utilisation of 1200 flight hours (FH) and a cycle to FH ratio of 2, which is the typical mission of that aircraft [156].

Direct Operative Costs
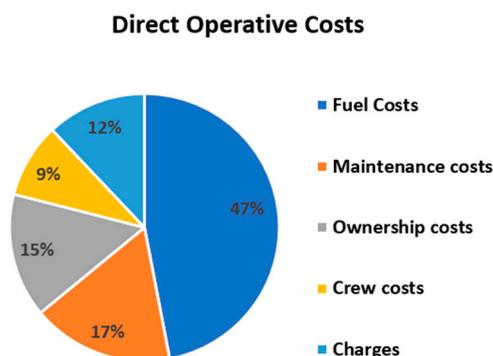
Figure 36. Typical cost breakdown for commercial aircraft according to International Air Transport Association (IATA) [157,158].

The scheduled maintenance levels for a commercial aircraft are reported in Table 9 along with typical frequency and man-hours required for each of them. This summary easily explains the complexity of maintenance procedures, step by step becoming heavier, to ensure the safety of aircraft lightweight structures. Check A is usually performed overnight every 500–800 FHs at an airport gate while check B requires 1 to 3 days at an airport hangar to be completed. More complex but very crucial is check C, usually performed less than every 2 years requiring 1 to 2 weeks of work in a maintenance base. Check D is usually operated every 6 years, where the paint may need to be completely removed for further inspection on the fuselage skin. For this reason, it requires a suitable maintenance base and about 2 months of work.

Table 9. Scheduled maintenance levels for commercial aircraft [159].

Check Type	Frequency	Man-Hours
A	500–800 FH	20–50
B	4–6 months	150
C	20–24 months	6000
D	6 years	50,000

Such data are variable and indeed depend on how much the aircraft is devoted to maintenance, as reported in Table 10 for check C. Its cost depends on the maintenance required (it may be light or heavy) starting from 60,000 USD for a small narrow-body aircraft up to 1 M\$ for a wide-body aircraft [160]. Again, considering the case of the 19-pax aircraft De Havilland Canada DHC-6 Twin Otter, the maintenance programme contemplates the check C being performed after 4000–6000 FHs and it is usually anticipated by 48 scheduled inspections of 100–125 FH interval. Only the C-check could cost up to 30,000–40,000 USD (the C-check lifetime plan is about 5–6% of the direct operative cost of that aircraft) while the total maintenance cost needed before is approximately equal to 100,000–120,000 USD.

Table 10. Approximate costs for C-check inspection for a variety of aircraft categories [159].

Aircraft Type	Interval	C-Light Cost (USD)	C-Heavy Cost (USD)
B737-800	20 months	120,000–160,000	220,000–320,000
B747-400	18 months	600,000–800,000	1.0–1.2 million
B767-300ER	16–18 months	450,000–550,000	600,000–700,000
B777-300ER	16–20 months	375,000–475,000	550,000–650,000
A320-200	18 months	150,000–180,000	250,000–350,000
A330-300	18 months	375,000–475,000	550,000–650,000
E190	6000 FH	70,000–90,000	110,000–180,000
CRJ-700	4000–6000 FH	60,000–80,000	100k–170,000
DH TwinOtter	4000–6000 FH	20,000–28,000	30,000–40,000

Starting from these considerations, to reduce such costs, it is possible to limit non-destructive inspections and disassembly of aircraft just in case of negative response claimed by a SHM system. It is indeed estimated that in this way SHM allows to reduce a relevant percentage—up to 3–4% maintenance costs—of operative costs for airlines by modifying the damage assessment process (short-time perspective). As a consequence of such aspects, the introduction of a reliable SHM system can increase the safety (continuous monitoring) and reduce costs (maintenance just in time).

On the latter perspective, it is possible to quantify such reduction estimating inspection costs and SHM system benefits instrumenting the door surrounds of a passenger airplane with two doors. The area under investigation is about three square-metres and the standard design flight goal of the fuselage is about 100,000 FH. The costs of inspection and instrumentation can be divided in NDT inspections, SHM weight, sensor installation, and sensors cost. The first is demanded for actual maintenance operation and consists of inspection for barely visible damages (BVID) and visible damages (VID) operated by a Level 2 inspector. Each inspection may cost around 22,000 USD. The other costs are demanded for SHM-based maintenance by avoiding any NDT inspection. To instrument one door surround, about 3 kg of sensors, 7 kg of electronic parts, and 16 kg of cables and miscellaneous are needed, for a total mass of 26 kg per door. The operational cost derived by further introducing one kilogram is about 0.07 USD per each FH. The sensor installation cost depends on how the sensor are bonded: (i) bonded on the cured structure or (ii) co-cured. In the first case, the cost is about 26,000 USD per each door surround ensuring 200M FH of durability, while it decreases to about 8000 USD for a co-bonded installation. This means 58,000 USD or 16,000 USD for instrumenting all door surrounds of the fuselage. The sensors will cost approximately 12,000 USD per door, with a total cost of 24,000 USD. For an ageing airplane, it is estimated that 1000 damage occurrences will happen on the fuselage operating for 500,000 FHs [161]. About 75% of these occur at the door surround and 80% of them have a dent depth d between 0.3 mm and 1.3 mm, which requires inspection. For a composite, it can be assumed that $d < 0.3$ mm is not visible, 0.3 mm $< d <$ 1.3 mm visible but less than the allowed size, and $d > 1.3$ mm is visible but with non-admissible damage. In conclusion, the occurrence of damage requiring inspection is 1.1×10^{-3} per FH. The resulting cost for inspecting door surrounds is about 2.4 million USD per 100,000 FH. According to the estimation given above, a fuselage integrated with sensors around the doors will cost in the worst case about 0.438 million USD with a benefit of about 1.9 million USD if no inspection is carried out during continuous monitoring of the structure.

It is possible to quantify the reduction of costs even considering a composite panel with an area of one square meter and making a few assumptions again for the benefit and cost calculation. In this case, it is possible to get to a benefit overcoming costs when the probability to have a damage event $P(E)$ is greater than 0.53×10^{-5}. Just to give an impression, probable events that are likely to occur at least one time during the operational life of a number of airplanes of the same type corresponds to a probability of occurrence $P(E) > 10^{-5}$. That is to say, considering 40 m^2 surface wing of a 19-passengers aircraft, 20 impacts during the whole lifetime are enough to have benefits achieved costs for instrumenting the wing. However, it is statistically identified that up to 1300 impacts due to bird strike may occur at the wing surface with damage requiring inspection occurring in many of those cases [161].

The impressive benefit obtained based on certain assumptions [160,162,163] and affected by an uncertainty of 10% does not account the cost for SHM maintenance and the inspections required for clarifying some system responses (combined NDE-SHM). However, also including scatter factors, the promising benefits introduced by integrating SHM during damage assessment process (short-time perspective) are remarkable and not negligible. By extending this calculation to the whole aircraft with a scatter factor equal to 4, it is possible to achieve about 4% reduction of maintenance costs, that is to say, about 0.8% of direct operative costs.

In addition, SHM must be considered during the structural design: monitoring, inspection, and damage detection become an integral part of structures at the design level reducing the knockdown factors introduced by actual damage tolerance approach (long-term perspective) for further decrease operational costs. Considering the limitation schematised in Figure 33, the damage tolerance approach introduces about 15% reduction in allowables calculation due to damage, whose contribution can be divided among safety factors need to address holes and repairs (which decrease the material allowables because of stress intensity factors around the affected region), visible damage, and barely visible damage, if one is considering ultimate or limit load, respectively. That is to say, the thickness of the structure will be increased by about 15% to address the presence of a damage which can be statistically expected among two C-Check intervals. The use of continuous monitoring technology, warning the presence of damage immediately after occurring, can reduce this gap significantly. Imprinting wing and fuselage takes approximately 8–14% and 7–12% of the maximum take-off weight and considering the effect on the design limit allowable only, in the worst case, the maximum take-off weight can be directly reduced by 0.75%. That is where SHM directly reduces take-off weight. However, then it enables the snowball effect with further reduction of weight and costs.

It is worth noting that, although these calculations are reported here to address the case of a commuter aircraft, they can be extended to other aircraft types and categories. In fact, either the number of doors or the airframe surface increases, with greater benefit in terms of costs. However, the percentage benefit remains very similar. As a matter of fact, although it will take several years before entry into service for commercial aircraft, SHM actually appears to be the major key-enabling technology in designing safer and lighter airframes.

4.2. Subsect Integrated Landing Gear Health Management

As demonstrated above, integrated health management is one of the few technologies that will help in reducing operational cost while increasing safety. In addition, it also moves away from conservative design philosophies. The health management requires a multidisciplinary approach bringing together advanced principles of mechanical engineering, sensor technologies, signal processing, and data analytics. Aircraft landing gear, which has not been considered in the previous discussion, is one of the most critical aircraft systems with a maintenance task programme requiring much effort, almost like engines. The health of the landing gear system depends on the proper functionality of each component. Several parts can have many failure modes and potential failure can be detected through the analysis of data collecting by distributed sensors. While some failure modes can be critical, others may only degrade the performance. The failure can be classified as [164]:

1. Incipient—hard to detect;
2. Slow progressive—hard to detect;
3. Intermittent;
4. Cascading;
5. Fast progressive.

System health is monitored measuring every deviation of useful parameters affected by the specific failure monitored from the corresponding reference. The remaining useful life is specified by the number of duty cycles and should be predicted based on the value of information given by the health management system. According to Ref. [165], a few probable failures of a landing gear systems are:

1. Failing to retract;
2. Failing to extend;
3. Failing to get-up locked after retraction;
4. Failing to get down-locked after extension;
5. Exceeding retraction/extension time limits;
6. Failing to provide feedback to cockpit of down locking, transit, and up locking.

The retraction and extension activities are quite a complex mechanics and are possible only when several conditions allowing those mechanisms to be activated are met. For instance, the retraction can be operated only when:

1. Aircraft hydraulics power and electrical power are "ON";
2. All weight-on-wheel switches are "OFF";
3. Select landing gear "UP" on the landing gear selector switch;
4. Hydraulic pressure flows correctly;
5. All down locks are unlocked;
6. Actuator stroke retracts the landing gears individually.

Hence, a retraction failure can occur when one of those conditions are not met and the reasons why this could happen are summarised in Table 11.

Table 11. Landing gear failure modes and suited detection approach [165].

Failure Mode	Detection Approach
No hydraulic power	Monitoring the pressure transducer in the system
No electrical power	Sensed by the system voltage sensor
Weight on wheel signal failure	Monitoring the electrical signal which needs to be tapped
Failure of down locks	Monitoring the signals from the down locks
Gear unlocked, but not going up to up lock	Monitoring the signals from the up lock
Retraction failure	Monitoring the time elapsed between selector switch operation, down lock release and up locking when each gear is beyond limits
Electro-selector switch failure	Monitoring the solenoid voltage
Electro-selector valve failure	Monitoring the pressure in the up line

In addition to all those aspects related to retractable system architecture functionalities, the landing induces overloads to the main structure and is subject to critical fatigue failure. As a matter of fact, landing gear represents an expensive maintenance item and this fact pushed many manufacturers of small aircraft to opt for non-retractable landing gears to limit maintenance to landing load induced damage (e.g., Tecnam P2012, DH Twin Otter, Cessna Caravan, etc.). This design is approved without any concern even of the cost of accepting huge aerodynamic drag increasing. Setting an integrated health management system at landing gear level can thus reduce maintenance costs of retractable systems by implementing predictive philosophy and reduce drag at aircraft level. The technical benefits rely on the ability of the system to monitor the operational and standard functional status of the landing gear; providing the necessary warnings in case functional anomalies following limited landings, hard landings, landings in particular critical conditions, or reaching fatigue life. As for the last aspect, the management system can count the real operation cycles of the gear components useful to compute the actual fatigue of the landing gear to be compared with respect to the theoretical fatigue loads used to qualify and approve the system during the design and certification stages. This allows a proactive action with regard to the ordinary maintenance program, possibly extending the inspection intervals or the specification, with considerable savings in terms of time and maintenance costs while returning an increased safety level as well. In particular, the benefits obtained are:

- reduction of global development costs;
- reduction in the number of fatigue tests and operating costs;
- increased reliability of the landing gear system;
- higher flight safety;
- reduction of maintenance costs through the elimination or simplification of scheduled and preventive maintenance "tasks", avoiding replacements of still intact parts and frequent inspection tasks.

4.2.1. Maintenance Tasks for a Landing Gear System

As mentioned in the previous section, landing gear systems are among most complex aircraft systems to be inspected during lifecycle management. To give an impression, the following considerations refer to a nose landing gear of a 19-pax aircraft according to standard procedures, therefore without any monitoring system integrated within the structure. Scheduled maintenance for this landing gear consists mainly of the tasks reported in Table 12.

Table 12. Landing gear failure modes and suited detection approach [165].

Inspection Interval	Action
100 FHs	Check that there are no external leaks, breakages, cracks, and the static attitude of the aircraft is guaranteed.
600 FHs	Check the correct tightening torques, and check that there are no external leaks, breakages, permanent deformations, and the static attitude of the aircraft.
1st time: 1800 FHs or 6 years Following times: 600 FHs	Perform eddy current on the body (there is no need to completely disassemble the truck) and visual inspection only on the shock absorber rod, checking for the absence of corrosion and the condition of the chromed surface.
12 years	Disassembly for visual inspection of the structural components, replacement of the rubber/gasket kits, verification of the absence of corrosion, and condition of the chromed, cadmium-plated, anodised surfaces. Run NDT by eddy current on the body.

Operations (1) and (2) do not involve a significant commitment of time and costs and are therefore neglected as a precaution; for phases (3) and (4) the aircraft must be on ground, even if the complete disassembly of the landing gear is not necessary. Operation (5) involves complete disassembly. If the landing gear returns for general overhaul, as agreed with the customer, it is necessary to completely disassemble and proceed to the inspection phases provided in the maintenance manual. If the trolley returns due to a malfunction, before disassembling it is necessary to carry out a complete functional test which consists of:

- deformation test;
- seal tightness test;
- check of operation of the charge valves (oil and nitrogen);
- polytropic execution by hydraulic press;
- testing the "anti-shimmy" system.

Instead, during the revision it is necessary to:

- Disassemble the landing gear completely;
- Paint off the painted components;
- Perform and ensure thorough cleaning of all parts;
- Carry out visual inspection to verify that there are no evident signs of wear, deformation, indentations, corrosions, scratches, surface state of the chromed and cadmium-plated or anodically oxidised parts, and check the integrity of the gaskets. This inspection must be carried out mandatorily on all the components of the shock-absorbing part as rod, piston, gasket holder, cylinder, oil scraper, leak plug (metering pin), etc.;
- Non-destructive testing as follows:
  - Penetrating liquids on the compasses (torque links)
  - Penetrating liquids on the stem;
  - Magnetoscopy on the articulation axes and on the wheel axle and valve seat, leak plug;
  - Penetrating liquids on the supports, bushings, spacers;
  - Penetrating liquids on the container;
  - Penetrating liquids on the shock piston;
- Rework and replacements with new parts:
  - Replace all parts that do not pass the visual inspection test;

      ○   Replace all the rubber/gasket kits, and the "consumables" (standard small parts, screws, washers, nuts, braking wire, cotter pins, spacers, plastic elements);

      ○   Rework the areas of the non-compliant parts in compliance with the tolerances required by the construction drawings and the maximum increases shown therein;

- Restoration of special processes (chrome plating, cadmium plating, anodic anodising, etc.) and of the roughness required on drawing;
- Re-painting of the painted components;
- Re-assembly;
- Verification of the correct application of the tightening torques and functional gaps required by the project;
- Perform full functional test according to applicable test report;
- Carry out finishing operations (identification plate, braking wire, paint retouches, etc.);
- Storage.

The previous action list gives an impression of the complex maintenance the landing gear is going through. Based on that task, in the following section, a calculation regarding the maintenance costs associated to a classical land gear and the same landing gear integrated with health management system is reported.

4.2.2. Cost Benefits Integrating Health Management System

As previously done for the airframe structures, several hypotheses can be proposed to estimate the return of investments in implementing an integrated vehicle system even for landing gear systems [162,163]. To find out the benefit, it is important to estimate the costs given by both classic system (inspection costs) and integrated system (system cost and added weight cost).

Inspection costs for classic landing gear: an accurate NDT requires a Level 2 category technician, for a cost of approximately 15,000 USD, including the costs of taking the aircraft on the ground. The whole cost of inspections is 15,000 USD after the first 1800 FHs and every 600 FHs thereafter, and therefore for 100 k FHs (design life) it will be approximately $100,000/600 \times 15,000$ USD = 2.5 million USD.

Costs for integrating health management system: the monitoring system adds a mass to the aircraft that has to be included in computation of the direct operative cost. The weight can be estimated as follows:

- Sensors: 0.5 kg,
- Electronics: 8 kg,
- Cables and other items; 5 kg

for a total of 13.5 kg per landing gear and a total weight added to the aircraft which corresponds approximately to 40.5 kg. The cost of the mass added to the aircraft can be estimated as 0.07 USD per FH per kg. Those values return an impact on direct operative costs of approximately 283,000 USD for 100,000 FHs if no cost is associated with the maintenance of the monitoring system. In addition to that cost, it is necessary to consider the integration costs as:

- Sensor installation: 5000 USD per landing gear (worst case, 50 man-hours necessary) for a total of 15,000 USD
- Cost of sensors: 4000 USD per landing gear for a total of 12,000 USD
- Electronic cost: 80,000 USD

The integrated landing gear will impact the direct operative cost of the aircraft as follows: 283,000 + 15,000 + 12,000 + 80,000 = 390,000 USD. Although the estimate is approximate and although it envisages having to restore some components of the SHM system, the benefit in terms of cost reduction in the life cycle is evident.

However, let us also consider also the costs that could be needed to maintain the monitoring system. If the landing gear returns for a general overhaul, the operations

described in the previous paragraph are estimated to affect approximately 15,000 USD per landing gear and therefore 45,000 USD for the aircraft. If they are inspected four times, they will require about 90,000 USD. Hence, the total maintenance of the landing gear system integrated with health management system during 100 FHs will have a cost equal to:

$$390,000 + 90,000 = 480,000 \text{ USD}$$

That is equal to 1/5 of the corresponding inspections and maintenance without any SHM and OLM approach mounted. The benefit can be calculated as:

$$\text{BENEFIT} = 2.5 \text{ million USD} - 0.48 \text{ million USD} = 2.02 \text{ million USD} \tag{9}$$

which is valid for a life cycle, or 100,000 flight hours. That results in approximately 80% saving of costs. Even considering that half of the inspection tasks only can be skipped, a 40% saving is still obtained. It is worth noting that this percentage calculation reported here is quite general, no matter the aircraft type. Hence, the analysis can be easily scaled up to wide-body aircraft.

Given all the above considerations, introducing a health management system for aircraft landing gear can be made more advantageous by introducing a retractable configuration for this aircraft category, because of the reduced maintenance costs. In addition, the landing gear induced drag and noise could further reduce costs and emissions strongly. That is to say, integrated health management of aircraft landing gear is not only a future challenge but even a key-enabling technology for this category of aircraft in order to achieve a near-zero emission vehicle.

4.3. Aeroelastic Tailoring of Distributed Propeller Wing

Distributed propulsion is barely a new concept and has captured the attention of major players in the aviation landscape to increase propulsion system efficiency along with better aerodynamic flow. However, such a non-conventional aircraft requires updated configuration to be effectively introduced in commercial aviation. Within the scope of the exploration of commuter aircraft key-enabling technologies, it is crucial to mention the need for new and better preliminary design approach which can strongly improve the impact of such a non-conventional architecture on the aircraft weight. That is also useful to address the potential outcomes after the implementation of such innovative concept on the selected aircraft configuration.

Within preliminary design concepts, it is necessary to figure out the aircraft performance limits and the overall reconfiguration that the airframe experiences when switching to distributed propulsion. It is essential to understand how to include such distributed subsystems in the aircraft model to perform a proper analysis. In general, the preliminary design framework strongly depends upon several aircraft parameters among which the weight characteristic is crucial for performance estimation. From a structural point of view, the mass breakdown analysis requires specific models assessing the weight of each aircraft component in order to compute several aircraft weight parameters, including Maximum Take-off Weight. Although a reference aircraft database is usually an efficient way to predict such overall characteristics, a novel aircraft featuring radically new technologies represents a challenge when existing knowledge does not provide a solution for preliminary estimation. As a consequence, the accuracy of normally used empirical methods and statistical data collected from previously constructed aircraft decreases strongly. However, the structural mass of an aircraft has a big influence on the overall performance and its optimisation from early design phase is worth achieving. Reducing structural weight lowers the operative empty weight and increases payloads that can be carried on as well as the corresponding range of the aircraft. One of the heaviest structural components of modern aircraft is the wing, on which a particular focus has always been placed. This is even more important in the case of distributed propulsion technologies, where the mass distribution (and the overall mass consequently) is highly affected by the position and mass

of the engines. In particular, the use of tip-mounted propellers can make quite challenging the design and the result can be far from optimal due to dynamic instability issues. That is where an accurate preliminary tool can be quite crucial to improve the design layout and return the optimal configuration without attempting too many resources and expensive experimental trials.

Generally, different methods are available in literature to estimate the mass of the airframe as well as the overall aircraft weight. It is possible to broadly divide those methods according to the approach adopted in:

- empirical and semi-empirical methods;
- analytical and quasi-analytical based methods; and
- finite element-based methods.

Empirical methods consist mostly of statistical evaluation based on existing aircraft. Although great and valuable results have been obtained by Raymer [166], Roskam [167], and Torenbeek [168], whose empirical mass estimation methods are still in use, the prediction accuracy depends primarily on the amount of data available from similar existing aircraft and how close they are to the aircraft under investigation in terms of design, configuration, and mission profile. Hence, the statistics-based methods are of limited practical use where a novel aircraft configuration or material is introduced [169]. Purely analytical methods make use of theoretical wing mass derivation based on structural mechanics to calculate the amount of material needed to withstand specific loads. However, they usually rely on simplified models when providing overall aircraft estimation or on very complex theories limited to single components. The design requires holistic approaches able to account for aerodynamic effects and aeroelasticity. To overcome these limits, several approaches have been introduced using beam model representation and analytical methods for the analysis and sizing of the wingbox structure, while considering the effects of static aeroelasticity [170]. However, they are still limited to the estimation of the material needed for the primary structure. Finite Element Methods (FEM) have been increasingly adopted in the last decades as general-purpose approach and can return quite reliable mass estimation. Different attempts have been made in the literature to define accurate modelling strategies with low computation efforts needed [170]. Although the major advantage of numerical simulation is the possibility to introduce as many details as needed in the model, including non-linear behaviours, they may increase the computational costs, or may not be available at the preliminary design stages [171].

Moving from empirical to finite element methods and passing through analytical approaches, different results may be achieved according to the fidelity of the model. In the same way as the previous classification, it is possible to group several adopted techniques according to the level of estimation achieved [171]:

- class I methods;
- class II methods;
- class II and a $\frac{1}{2}$ methods;
- class III methods.

Class I methods are also known as fractions methods, because the mass of each aircraft component is defined as a fraction of the maximum take-off mass of the aircraft. Class II methods further include aircraft parameters into the computation enabling the calculation of the mass of principal components by a set of equations. Class II and a $\frac{1}{2}$ methods are based on estimation of the mass of material required to withstand loads applied to a particular aircraft component. In order to calculate the required amount of material, basic strength/stiffness analysis is applied to simplified structural model of the load-carrying component. Finally, Class III methods allow the refinement of the mass breakdown prediction by incorporating FEM to calculate the aircraft primary structure.

Moving back to the specific application, it is worth achieving further advancements in the establishment of accurate class II and a $\frac{1}{2}$ methods and class III methods to optimise the airframe design. In particular, those approaches require advancements in setting formulae

for aeroelastic compensation while dealing with high aspect ratio aircraft and distributed propeller wing. The use of high aspect ratio paves the way to the application of really flexible wings, which may undergo to very large deformation due to the low twisting resistance of the outer wingbox. In addition, the presence of tip propeller mounting may generate dynamic instability, strongly reducing the flutter speed. This is such an underestimated topic in the literature and the knowledge of the mechanics of structures under such a complicated wing configuration is quite needed to address the optimal configuration in terms of weight penalties and aerodynamic improvement. While the high aspect ratio can be compensated by introducing a strut, the engine mounting over the wingspan may actually be a big issue due to lower flutter speed expected when moving the engine outboard. However, Mardanpour and Hughes [172] demonstrated that engine placement at certain locations has the potential to increase the flutter speed. That may be induced in two ways. One is the location where lower frequency flutter mode could be relegated to a higher frequency mode and the other is the location where the fluid structure interaction is decreased. Both criteria could be met at the area of minimum kinetic energy of the mode. That is to say, engine placement at the area of minimum kinetic energy of the modes has the potential to decrease fluid-structure interaction and enforce the structure to flutter at a higher mode [173]. In case of the high-aspect ratio wing presented by the authors, the area of minimum kinetic energy density of the bending and torsion modes of the wing, in the absence of engines, gravitational, and aerodynamic forces, may present different minimum levels. While the first bending mode has a minimum value at the root, the second bending mode shows the minimum kinetic energy density outboard of the 85% span, and for second torsion mode, this minimum moves to the region between 70% and 90% span. To further explore this possibility, the authors performed the same analysis for two-engine and four-engine configurations. In the first case, the point of the minimum kinetic energy was just outboard of 60% span [174]. In case of the four-engine configuration, for engine placement ahead of the elastic axis, the unstable mode contained a combination of first, second, and third bending modes [175]. When the engines were placed from about 60% to 80% span, there was a noticeable increase in flutter speed. This area is close to the area of minimum kinetic energy of the first three bending modes.

These results are summarised in Figure 37, which shows the normalised flutter speed while moving the engine placement along the wingspan for a two-engine wing (a) and a four-engine wing (b). In the first case, one engine is integrated in each wing side, placing the engine at about 60% wingspan ($\eta_1 = 0.6$) which would significantly increase the flutter speed with respect to the isolated wing ($\eta_1 = 0$). This amplification factor further increases if the engine is placed ahead of the wing axis. Instead, a tip-mounted engine would reduce the flutter speed by about 15%. While the first result would be beneficial for the design, the second is quite negative and requires a stiffer structure. However, the balancing effect given by both possibilities can be the right solution, with a certain mass used to compensate the negative effect and return to the design flutter speed. That is to say, the negative effect of the tip-mounted engine can be compensated by installing another engine onto the wing, whose mass is equal to that of the tip-mounted engine. Furthermore, if that adjunct mass is located around the location of minimum kinetic energy, a 25% increasing of flutter speed is experienced. A similar conclusion can be made looking at the four-engine configuration results in Figure 37b where one engine is fixed and the second engine is moved on the same semi-span. Indeed, the effect of having one tip propeller (blue line) is compensated by installing another engine along the span in the optimal position. This opens a new challenge in the preliminary design of distributed propellers aircraft, which deals with aeroelastic tailoring of wing. Keeping flutter speed constant while introducing outer wing propellers would mean keeping the benefits of distributed propulsion at all.
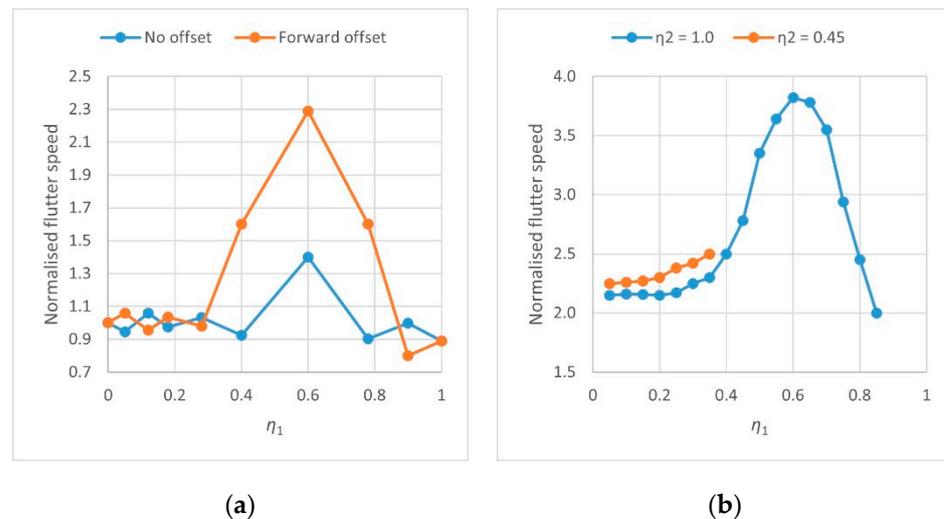
Figure 37. Normalised flutter speed: (**a**) for engine placement along the span for two values of chordwise offset; (**b**) in four-engine configuration with one engine fixed ($\eta 2$) and the other moving ($\eta 1$).

Another dynamic issue relies on the coupling of wing modes and engine modes, which may lead to a very critical instability. That is the case of the X-57 Maxwell, a prototype aircraft designed by NASA from the two-propeller Tecnam P2006T. Thanks to the hybrid configuration consisting of twelve wing-integrated propellers, the X-57 has a reduced wing area compared to the parent aircraft [171]. Generally, the design of a new aircraft must prevent any aeroelastic instabilities occurring inside the flight envelope. What is critical for an aircraft like the X-57 is the potential for whirl flutter, caused by the propeller aerodynamics, which drives the airframe/pylon motions to become unstable. The design went through a multi-step analysis where different wing versions were investigated thoroughly. In particular, the whirl flutter stability analysis revealed that improvement can be obtained without excessively compromising the airframe. The critical issue is the pylon mount flexibility, which allows the engine pitching mode to enable whirl flutter. Among several wing design versions, different changes were carried out to achieve flutter safety [172]. The second version showed two substantial changes in the structural design and model. The former design led to a very close spacing of the first two modal frequencies, which is an aeroelastic concern from a wing flutter perspective. Hence, unidirectional fibres were incorporated in the spar caps to increase the gap between natural frequencies. The second improvement dealt with the refinement of the tip propeller mount, including a firewall that served as a faceplate for mounting the motor. This faceplate, which provides much of the structural mounting stiffness, strongly influences the in-plane behaviour of the component and affects the whirl flutter. For that reason, it was modified in the third design version of the aircraft to stiffen the component, substantially reducing the faceplate deformations, and increasing engine mount rigidity.

Summarising, the design of X-57 Maxwell demonstrated that both wing aeroelastic concern and whirl flutter instability can be addressed by tailored aeroelastic properties of the wing. Generally, it is worth noting that structural optimisation may lead to improved stability performances at the cost of a very low weight increase. That is to say, the necessity of preliminary tools including such critical aspects for distributed propeller aircraft is quite crucial to enable the full exploitation of aerodynamic advantages introduced by this unconventional configuration.

4.4. Strut-Braced Wing

Strut-braced wing configuration is a design concept far from new for this category of aircraft. However, it was mostly used in the early days of aviation, becoming today more

common in small airplanes. Specifically, the use of thin airfoil sections requires a structural support for the wing to sustain the aerodynamic loads by decreasing the stress between the wing root and the wing support mounting. However, the use of external structures introduces a drag penalty that dramatically increases with the airspeed. Gradually, the external bracing was replaced in favour of a cantilever wing, ensuring lower drag with an appropriate wing-box and thickness-to-chord ratios. However, although the cantilever wing configuration was massively adopted with its aerodynamic advantages, the concept of the truss-braced wing configuration also survived due to other intrinsic advantages. Compared to a cantilever beam-like wing, the structural support allows increasing the wing aspect ratio with a consequent significant reduction of the induced drag. In addition, the design of a lower wing thickness becomes feasible with small transonic wave drag which requires the introduction of smaller sweep. Combining higher aspect ratios together with lower sweep enables natural laminar flow and a significant increase of the overall aircraft performance [176].

The advantages of strut-braced wing led to a number of specific and comprehensive investigations in the past. Many preliminary studies were conducted at the Boeing Company to evaluate the performance and economics of a large subsonic military airplane comparing cantilever and strut-braced configuration [177]. Specifically, Boeing researchers performed structural analysis in two load conditions relying on a 2.5-g manoeuvre and 1.67-g taxi bump. The results of optimisation and sensitivity analyses demonstrated that the second layout positively affects the fuel consumption thanks to a high aspect ratio wing with low thickness-to-chord ratio. In addition, the strut made it possible to solve ground strike problems arising during taxiing with the cantilever configuration. The analysis showed that the resulting configuration requires 1.6% less fuel with a reduction of 1.8% in MTOW and 3% in OEW compared to the standard cantilever wing aircraft. As a consequence, the direct operative costs were slightly lower. Another investigation performed at the Boeing Company compared strut and cantilever wing configuration for a transport aircraft in terms of block fuel consumption [178]. Again, the strut effectively saved structural wing weight. However, the thickness necessary to cope with buckling failure increased the drag with a higher fuel consumption compared to the cantilever layout. Instead, a practical use of a strut-braced wing was revealed in Ref. [179], where the authors focused on a business jet. They compared the novel configuration with aspect ratio 25 with an equivalent conventional wing business jet with the same payload and range and designed with a cantilever wing. The strut-braced wing design resulted in a higher weight of the wing. However, the aerodynamic advantage of having such a high aspect ratio led to a MTOW reduction and 20% fuel weight savings.

Previously mentioned works investigated the use of a strut rigidly attached to the wing. Therefore, strut buckling achieved in case of negative load factors drives the design and likely results in a very heavy and aerodynamically inefficient component. To avoid this instability at all, an adaptive configuration is proposed in Ref. [180] with the strut actually working only in case of positive load factors. Otherwise, the wing acts like a cantilever wing for negative load factors without occurring in buckling condition. In addition, such a non-rigid arrangement allows to optimise strut position and ageing force to achieve maximum benefit possible. In addition to the buckling issue, it is worth noting that the strut-braced wing concept allows reducing wing thickness-to-chord ratio and even shortening the chord without any static weight penalty. However, the updated design returns a smaller wing-box dimension which results in a lower torsional stiffness. The wing is thus more sensitive to aeroelastic problems, which include greater static aeroelastic deformation and/or lower flutter and divergence speeds. However, the strut design paves the way to another means of optimisation, highlighting the possibility to face the increased aeroelastic deformations by exploiting the moment that the strut induces on the wing [180].

Generally, the research findings appearing in the literature reveal that the strut-braced configuration allows reducing the wingbox material devoted to bending withstanding. The airfoils result shorter and thinner without any weight penalty. However, the spanwise

aerodynamic loads change and the resulting deformations vary accordingly. Hence, an optimisation chain helps to achieve further weight savings by iterative resizing of the wing structure. In addition, it is worth noting that the strut force ageing on the wing may positively affect the twist loads and further increase structural weight savings. Although the design may be challenging for commercial aircraft of a certain dimension, small aircraft can strongly benefit from a strut-braced configuration. To look into those benefits, a simple calculation is reported below, considering the effect on the bending alleviation induced by a strut. While all the aspects mentioned above about the application of strut-braced configuration and other aerodynamic aspects pointed out in the relative section remain valid, it is worth highlighting that the following calculations take into consideration the structural aspects only to estimate the possible weight saving achievable keeping the same wing characteristics. It is understood that weight alleviation can then be adopted to further increase the aspect ratio of the wing.

In this context, a preliminary calculation is carried out to estimate the weight alleviation introduced by the strut. In this case, two different configurations were considered, as shown in Figure 38:

1. Cantilever beam with uniform load distribution q;
2. Strut-braced beam with connection at one third of the wingspan and load distribution q.
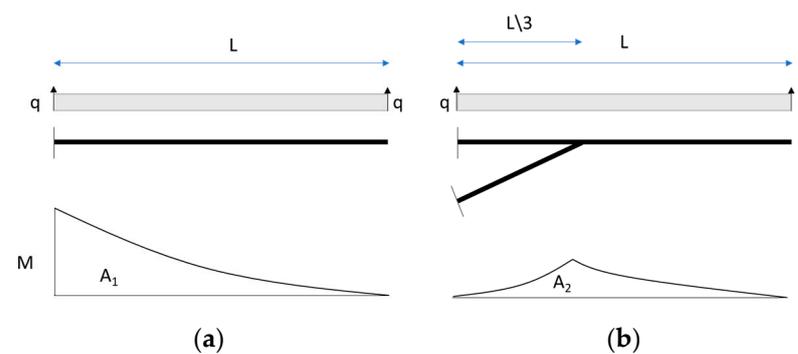
Figure 38. Comparison of beam models: (**a**) cantilever beam; (**b**) strut-braced model.

To estimate the weight ratio and give a first impression of the effect of the strut, the bending moment is estimated for both cases and the area under the weight is considered directly proportional to the area under the bending moment. As a consequence, the weight ratio is considered proportional to the ratio between those areas as explained afterwards. Firstly, A_1 and A_2 are approximately calculated as:

$$A_1 = 0.167 \, qL^3; \, A_2 = 0.111 \, qL^3.$$

The weight alleviation can then be estimated as 33.5%:

$$\Delta W = \frac{A_1 - A_2}{A_1} = 0.335$$

The bending moment is absorbed by the spar caps and the upper and lower panel. Neglecting the effect on the stiffened panels, it is possible to estimate the bending moment withstood by the caps as 80% of the total bending moment. Using a preliminary wing design algorithm, the caps have been estimated to be 14% of the overall wing weight, which is equal to 8–12% of the maximum take-off weight. Considering the relation chain, the strut-braced configuration can alleviate the maximum take-off weight of about 0.48%. In addition, a further alleviation can be introduced by the lighter panels, while the strut introduces a small penalty, which can be considered negligible as well.

In addition to the static alleviation factor, it is worth noting that the strut decreases the wing-free length with a positive effect on aeroelasticity. In particular, the aeroelastic penalty can be calculated for both configurations according to Torenbeek's formula [168]:

$$\Delta W_{aer} = \frac{\rho g}{G} q_D \frac{b^3}{\left(\frac{t}{c}\right)^2 \sqrt{1 - M}}. \tag{10}$$

The effect is proportional to b^3 with a weight penalty reduced by up to 70%. That contribution is estimated to be about 2% of the wing weight, which is approximately 8–12% of the maximum take-off weight. Applying again a rational relation chain, the alleviation factor ranges between 0.1% and 0.2% of the maximum take-off weight.

It is worth pointing out that the static and dynamic weight alleviation have been estimated by making a suitable assumption on two wing configurations with the same wingspan. The weight alleviation can be compensated to increase the aspect ratio. That is to say, the MTOW is kept constant, and the aerodynamic performances are improved.

4.5. Morphing Wing

Wing morphing relies on the idea of changing the body shape or geometry to adapt to different aerodynamic condition characterising a typical mission profile. This approach is far from new and Wright flyer already employed such a roll control enabled by changing wing twist using cables opportunely designed and actuated by the pilot during the flight. However, this is something that was easily approached dealing with such a flexible structure. Modern aircrafts are required to achieve higher cruise speed and payload, only possible making use of a rigid body, which is not compliant with a morphing attitude. This concept indeed requires an intrinsic high elasticity of the structure for smoothly changing the wing shape. That is where the morphing technology is quite difficult to implement without facing structural stability problem. Hence, high-lift devices have been widely implemented so far because they allow achieving higher lift without compromising structural rigidity. However, they suffer from aeroelastic problems and work properly only in fixed conditions, preventing their use for smoothly adapting the aerodynamics. That is the reason why morphing structures have a great potentiality, with the possibility to decrease parasite drag up to 22%, posing the challenge even for smaller aircraft [181].

Morphed wings have been investigated for decades in a large number of research activities aiming at matching the optimal aerodynamic shape in every flight condition. In fact, current projects deal mostly with the maturation of materials and structural mechanics. Instead, multiple unconventional architectures have been designed and tested in the past. Such adaptive systems can be categorised into two main groups:

- mechanised mechanisms and
- compliant mechanisms,

whose remarkable distinction relies on the use of different architectures. The former group of systems achieves morphing capability enabling rigid roto-translation of several linkages interconnected by kinematic chains [182]. Each sub-component is designed to: (i) withstand the external loads exerted in a real application, and (ii) achieve target shape-configuration. The former constraint is satisfied by solving stress relations. The latter request is targeted by designing the actuator and the transmission line to get to the specific configurations. Finally, the mechanical torques are defined to balance the aerodynamic loads with as little power consumption as possible [183]. Instead, the compliant mechanisms rely on a more sophisticated architecture opportunely shaping the wing through the deformation of structural elements. This system is equipped with a variable mechanical resistance distribution throughout the structure specifically designed to achieve the prescribed shapes. Although the compliant architectures guarantee a more uniform shape change, the robot-like mechanisms adopted in mechanised solutions is of more practical use. The real paradox of morphing the wing is indeed that the structure has to be stiff enough to withstand external loads and simultaneously flexible enough to accommodate

different shapes with as little energy as possible. As a consequence, the application of mechanised structures is mandatory in large aircraft and still advantageous in smaller air vehicles. As for high-speed cruising, high lift performance of the aircraft could be achieved by means of morphing technology. Low-speed conditions, mostly take-off and landing, can benefit from morphed solution with a performance improvement. High-lift devices are used for this purpose and can be also considered part of the family of morphing systems. However, some drawbacks still remain. Specifically, without any flow control, best performance in low-speed conditions is achieved by combining a fowler flap and a leading edge slat. The selection of a high-lift system indeed depends on the required take-off and landing performance. Generally, the maximum lift and the stall angle are the most important parameters to be maximised. The specificity of high-lift systems is that, depending on the needs, one system has to be used [184]. When the stall incidence has to be increased, the leading-edge device is the suited solution. Instead, the trailing edge device allows increasing lift at a certain flight angle, but at the cost of decreasing the stall angle. Hence, the combination of both systems increases both maximum lift and stall angle increases. However, they require heavy complex mechanisms to be moved to the design positions. In addition, they produce friction and lift-induced drag in cruise configuration, demanding for opportune fairings covering the kinematic mechanisms. In light of these considerations, introducing morphing technologies for both types of devices can strongly increase the overall performances.

As a matter of fact, morphing technologies remain a key-enabling technology for all aircraft categories where the emission is the first key driving design constraint. However, many challenges from the airframe standpoint remain open and require an improved system and much effort to achieve a step forward, looking at potential application of such technology to innovative green airliners. For instance, where large shape changes are necessary (e.g., STOL configuration), it is worth designing a suitable skin able to withstand the aerodynamic loads while satisfying the requirements for the underlying morphing structure. That is a huge challenge and a key issue, together with the improvement of actuators. Indeed, the weight required for morphing actuators or necessary to opportunely stiffer the structure is currently reducing the benefits coming from introducing morphing technologies.

4.6. Novel Composite Technologies, Nano- and Multi-Functional Materials

Improving material properties has been an increasingly challenging goal within the scientific community for many years. However, the introduction of composite technologies opened many ways to improve material performance by addressing criticalities and without affecting the overall weight or even reducing the weight impact of the resulting component/system at aircraft level. Generally speaking, the composites' performance is highly demanding and they are currently able to withstand high loads in harsh environments too. However, there are some aspects that can be improved by introducing advanced and more controlled manufacturing technologies. In addition, the tailored production of fully composite-made structures paved the way to the introduction of multifunctional materials with enhanced performance obtained by introducing different or novel materials within the structure. Hereinafter, three different key-enabling technologies are introduced, briefly describing how they can positively affect the aircraft design towards a near-zero emission air vehicle.

4.6.1. Automatic Fibre Placement

Composite manufacturing is a challenging technology due to the intrinsic lack of replicability. Very low tolerance typical of metallic components cannot be matched by composite products, whose manufacturing involves layout assembling of resin and fibres, fibres with different directions, or even the combination of sheets and cores in case of sandwich structures. In addition, the different manufacturing stages, along with the necessity to have tailored products, increases the production costs. Indeed, repeated processes are needed, and the final product likely fails the quality control with the consequence to be rejected

due to a lack of specification matching. In particular, the current processes including resin infusion and autoclave require a continuous monitoring of manufacturing parameters such as temperature and pressure, whose field distribution is worth it in order to achieve the expected mechanical properties of the final product. In this context, a promising technology consists of robotised placement of fibres and the absence of autoclave processes. In contrast to classic technologies, the automatic fibre placement with out-of-autoclave manufacturing [185] is able to return tailored configurations with a less expensive process and better quality of component. In particular, the use of automatic placement of fibres guarantees the positioning of dry fibres without using prepreg materials. All in all, it returns a specific tolerance requirement with a few further advantages listed as follows:

- lean manufacturing;
- simplified configuration;
- tailored material configuration/weight reduction;
- longer material shelf life;
- controlled resin to fibre content;
- low void content;
- suitable for large part production and sandwich structures;
- low energy consumption;
- special heated tools allow to build any composite shape.

Particularly promising is the manufacturing of coupons as complex as possible by rapid automated dry preforming process (AFP) followed by liquid resin infusion (LRI). However, it is rather difficult to address some challenges yet:

- manufacturing process parameters setup;
- development of a system for online monitoring of LRI process parameters;
- technology characterisation;
- allowable determination along with flammability and conductivity, and thermal and lightning strike properties.

Nonetheless, the use of novel and more reliable manufacturing technology can reduce the knockdown factors, reducing the gap between material and design allowables. In addition, the costs and emissions of production lines can be reduced with a strong impact on both cost of the aircraft and its overall emissions. That is to say, new emerging technologies can strongly impact the aircraft design of near-zero emission aircraft and are good candidates as key-enabling technologies.

4.6.2. Carbon Nanotubes

Carbon fibre-reinforced polymer composite laminates have been increasingly used in aerostructures because of the superior strength-to-weight ratio when compared to metallic materials. However, they show some criticalities in ensuring lower electrical and thermal conductivities and in the lack of efficient approaches for anti–icing/de–icing, lightning strike protection, and, as widely discussed above, condition monitoring. Moreover, CFRP laminates are characterised by extremely poor strength through the thickness and weak interlaminar fracture toughness (ILFT). Those intrinsic characteristics make them quite susceptible to delamination development, even under relatively low-energy impact. In this context, the use of carbon nanotubes (CNTs) has been receiving much attention in the last years because they are able to imbue the composite where they are introduced with multifunctional properties, including enhanced electrical/thermal conductivity and intrinsic structural health monitoring attitude. The addition of CNTs within the resin is a promising option because it does not alter structural integrity and enhance mechanical, thermal and electrical properties [186], providing multifunctionality to advanced hierarchical CFRP composites [187].

Within the last ones, nanotubes can be distributed throughout the matrix, placed around individual fibres or even spread between several layers. The last possibility is quite promising because it allows to control the amount and orientation of CNTs, enabling the

design of multiple functionalities in a specific location and direction, further increasing the tailoring parameters and integration capabilities of the resulting structure. One example is given in Ref. [188], where highly conductive CNT webs, drawn directly from specially grown CNT forests produced by chemical vapour deposition and characterised by negligible weight, are interleaved with several carbon layers to enhance thermal and electrical properties of the laminate. In addition, CNT webs may prevent the nesting between several plies with different directions, increasing the interlaminar fracture toughness without any weight penalty. Furthermore, ILFT can benefit from the interaction of nanotubes with specific epoxy resins. For instance, Bhanushali and Bradford [189] investigated the use of CNT webs in glass fibre composites integrating different numbers and orientation of CNT layers, finding out that ILFT is either marginally degraded or enhanced. Another study [190] showed that placing an ethylenediamine-functionalised multilayer CNT web characterised by negligible density between carbon fibre plies resulted in a 13% enhancement of the shear mode ILFT, while providing a further benefit in electrical conductivity. The investigation carried out in Ref. [191] shows again that the integrating a mixture of carbon nanotubes and epoxy resin through plain-woven glass fabric reinforcement returns a hierarchical composite exhibiting increased mechanical properties with a rather limited weight penalty. In detail, adding a 2% weight of carbon nanotubes leads to increase the storage modulus (56%), flexural modulus (50%), flexural strength (55%), tensile modulus (14%), and tensile strength (24%). Scanning electron microscope images indeed revealed the presence of strong anchoring of CNT with fibres and epoxy resin around the fibres, further demonstrating the ability of CNTs in strengthening the composite interface.

The introduction of such a zero-weight reinforcement strongly reduces some drawbacks of composite structure, inducing to close the gap between material allowables and ultimate and limit design allowables. Reducing 5% of these values only for the wing could reduce by up to 0.6% the max take-off weight of the aircraft. In addition to that, such multifunctional materials introduced can be adopted for de-icing and anti-icing purposes and SHM, further increasing the achievable benefits.

4.6.3. Structural Batteries

Another multifunctional property, that can be particularly suited for electric aircraft, consists of replacing load-bearing components with such a structural battery. Combining energy-storage capabilities along with load-bearing can minimise the detrimental impact of battery weight on the aircraft. Nonetheless, this technology is not mature enough yet to be integrated within the airframe and many challenging aspects have to be properly addressed to close technological gaps preventing their introduction for commercial aeronautical applications.

In detail, the structural batteries, also referred to as multifunctional electrochemical energy storage systems, are characterised by the combination of mechanical properties, such as carbon-based composites, and energy storage capabilities, such as conventional lithium-ion (Li-ion) batteries. According to the functional integration level, this type of component relies on the multifunctional properties of either the structure or the material. In the former case, either conventional batteries or thin film energy storages can be integrated into the structure. They are decoupled systems whose integration returns multifunctional structures. This architecture can be achieved by introducing a special structural layout where batteries are installed within the components—as shown in Figure 39—both ensuring the energy storage and fulfilling the required mechanical stiffness. In the latter case, multifunctional properties are ensured at material level, either with single ply functionalisation or through material constituent functionalisation. In this way, a coupled system is achieved with inherent multifunctional properties.

(a)   (b)
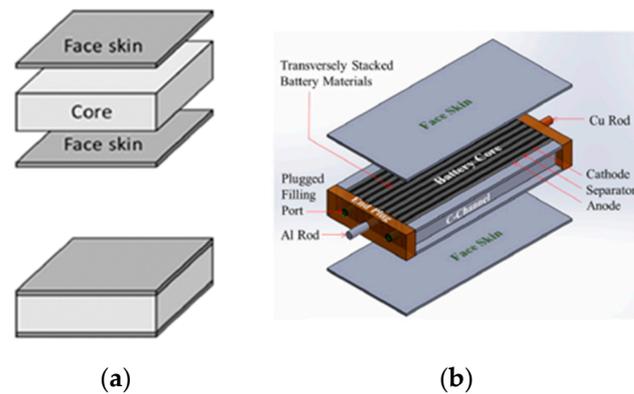
Figure 39. Schematic concept of sandwich structural battery: (**a**) sandwich panel with a foam core and two face skins; (**b**) sandwich panel with battery core and two face skins [192].

Multifunctional structural batteries capable of fulfil energy and mechanical requirements have been proposed in various applications such as satellites [193], spacecraft [194], unmanned air vehicles, and marine systems [195]. Lithium-ion batteries are particularly suitable for this application because of their high energy density, long cycle life, and environmental friendliness with zero emissions. Two main approaches have been proposed in the literature so far to develop structural batteries. The former consists of integrating conventional lithium-ion batteries into composite structures (multifunctional structure) [196]. The latter is rather devoted to developing structural electrodes [197], and even structural electrolyte [198] into lithium-ion batteries (multifunctional material). Generally, both energy density and structuralperformance are needed for structural batteries in electric vehicles. That is where the proposed approaches failed as not capable to achieve the intended energy performance. That is a highly demanding characteristic and reduces the field of application strongly.

Nonetheless, the structural battery concept shows a promising perspective for applications where sandwich structures and batteries are used thanks to the available volume for energy storing. The sandwich application presented in Ref. [192] showed a measured bending stiffness reduced by only 3% upon filling with electrolyte and after 50 charge-discharge cycles. However, lap-shear strength E-120HP epoxy strongly decreased (31%) after exposure to the battery electrolyte for 3 months. Nonetheless, the significant degradation did not lead to any structural damage or leakage during the charge-discharge cycling of structural battery. It is worth noting that a mechanics analysis showed that sandwich beam theory is able to predict the stiffness of the sandwich structural battery with 10% deviation respect to experimental findings. Hence, the battery behaves as a sandwich and the battery core is also very stiff. This approach was recently proposed even for aircraft vehicles because it shows promising results. Basically, it may reduce the weight of the batteries, which became part of the load-carrying mass. In addition, lighter vehicles need smaller batteries and electric motors enabling again the snowball effect. As a consequence, this design could reduce the weight and cost of electric aircraft and it is understood as a key-enabling technology, although much work is needed to achieve a reliable implementation within aircraft.

A recent review on the structural batteries for aeronautic applications is given in Ref. [199]. As a general principle, multifunctional structures can ensure good energy performance when conventional batteries are integrated. Specific energy densities between 20 and 139 Wh/kg and volumetric energy densities between 20 and 276 Wh/L could be achieved. However, the weight savings obtained with this approach are rather limited and the processing cost does not return enough performance gain compared to simply casing conventional batteries. Instead, a better structural performance is achieved introducing thin-film energy storage, but the achievable energy density is rather limited and assessed in between 35–3500 μWh/cm^2. Combined with the cost of thin-film energy storages, the result does not fit the aeronautical large-scale application. Another degree of performance is achieved by introducing multifunctional materials. Indeed, the structural performance

is generally very good and comparable to some aeronautical composites. However, the energy storage capabilities are not impressive. For the case of single ply functionalisation, a specific energy in the range 12–58 Wh/kg can be expected and elastic modulus in the GPa range. When working on functionalising material constituent, better energy storage capabilities can be theoretically achieved (up to 146 Wh/kg) but the structural performance decreases with storage properties.

Hence, as a general trend, structural batteries can show excellent properties in either structural or electrical function and the best trade-off should be designed according to the specific application. Indeed, structural performance returns very good weight saving, increased by the snowball effect. However, the low-energy storage capabilities limit the replacement of energy storage cells discussed in Section 2.5. This type of structural integration can be more suited for compensating small energy requirements, such as local electrical power units. On the other hand, high-energy storage capabilities ensured by multifunctional structures are well suited to replace aircraft energy sources, but they show very low structural performance and small weight saving.

However, another critical aspect emerging from the structural batteries' integration lies in the durability and certification aspects. They are strongly correlated, as the certification process in aeronautics aims to ensure safety over the entire aircraft lifetime. This issue arises mostly when the multi-functional integration is at structural level, which raises concerns in the way to estimate design life due to reduction in the interlaminar shear strength of the coupon. Indeed, batteries can be seen as inserted within the structure, with inherent negative impact on the structural strength. Hence, airworthiness requires testing the structural batteries at different coupon levels (from specimen to real scale subsystem and components) and load-scenario. In fact, according to FAA advisory circulars, it is worth demonstrating the compliance of these inclusions with static test, fatigue tests on primary structures, and damage tolerance compliance. In addition, health monitoring for safe storage and operation is demanding, is flammability prevention. Certification issues have not been addressed yet and require attention along with the end-of-life strategies, which have still not been considered thoroughly. However, as to this latter aspect, promising results are achieved approaching the problem with a life cycle assessment [200]. As a matter of perspectives, although many aspects require either being tuned or investigated further, structural batteries show promising results and can return optimised energy storage systems at aircraft level with a positive impact on life-cycle assessment of the whole platform.

5. Concluding Remarks

This paper has reviewed a number of key-enabling technologies for the future goal of designing and deploying near-zero emission aircraft. The aim is to bring together power and energy storage possibilities, novel aerodynamic findings, and innovative airframe technologies, whose efficient integration has the potential to move a further step in the design of environmentally friendly aircraft. In each field, the most promising technologies are discussed, highlighting the possible benefits at aircraft level, pointing out current criticalities and improvements needed to achieve the desired performance. The paper focused on the technologies that could be easily integrated into a commuter aircraft, since it is opinion of the European Community, who financed several projects on this topic, that a small air transport (SAT) demonstrator could be used to assess the feasibility of the new technologies and the overall results in terms of CO_2, NO_X, and noise emissions. Moreover, the results obtained at SAT level will be a milestone in the roadmap to the application of such technologies in the large passenger transport segment. Clearly, the integration of selected technologies and their impact on aircraft performance, including fuel saving, is left to the designer. For instance, the application of a morphing wing technology shall improve the aerodynamics without penalising the structural weight, thus reducing the aircraft energy demand without compromising the structural integrity. However, the impact on the overall sustainability will also depend on how the source materials have been produced

and how aircraft will be depleted at end-of-life. In other words, a life-cycle-analysis will be performed.

The need for significant emissions reduction in aviation pushes research into developing outstanding technologies, as well as manufacturing and operational strategies. However, with the current state-of-the-art, it is unlikely that we will soon get a large electric aircraft on the market, in contrast with the case of the electric car. This is probably due to the requirements of lightness, reliability, safety, comfort, and operational capability of fast air transport, which are not completely achieved yet. For instance, recent investigations on new aero-propulsive technologies have shown that they do not provide significant fuel burn reduction, unless the operational ranges are limited to short regional routes or the electric storage capability is unrealistically high, and that this little advantage comes at increased gross weight and operational costs.

For this reason, given the complexity of an aircraft with its performance and safety requirements, it is appropriate to face the problem of emissions abatement through a multi-disciplinary approach and be aware that the new eco-friendly air transport should be a revolutionary concept, not necessarily different from the classic tube-and-wing layout, but certainly with outstanding aero-propulsive technologies integrated within the airframe and with subsystems providing accurate power management and distribution, as well as fault-tolerant strategies. Moreover, it is worth noting that many improvements are still possible at airframe level, enabling higher aircraft performance by mostly integrating health management approaches, tailored wing architectures, and multi-functional materials.

The fast air transport requires both high energy and high power to perform its mission. The kerosene-based fuels, producing greenhouse and poisonous gases—such as carbon dioxide and nitrogen oxide—and soot when burned, are still attractive because of their high specific energy, which is actually roughly 60 times higher than the current commercial Li-ion batteries and will be still 20 times higher by 2035 in an optimistic forecast. It is clear that, by only considering batteries, electric motors, and main powerplant subsystems, the full-electric flight will be feasible only for short range, small aircraft. Even considering only the pollutants emissions' reduction, the snowball effect on gross weight cannot be neglected. It is unreasonable to perform the same mission with a large transport aircraft weighing 15–20 times the actual in-service airplane, as it would be an economic failure and probably would also require bigger airport infrastructure. Therefore, alternatives to the simple switch of conventional engines to electric motors and fuel to batteries must be sought.

The evolution of conventional propulsive systems, in particular of gas turbines, could provide thermodynamic efficiencies up to 70% with new materials and better cooling. In practice, this is not achievable by simply upgrading the existing engines, as the whole thermodynamic cycle must be optimised and the results must be evaluated at least at airframe level, not on the engine alone. In addition, even pushing the propulsive efficiency to 90%, it will be impossible to go much further from the current overall engine efficiency, as improvements will be made to the inherently low values of a thermal machine. Moreover, a high thermal efficiency, typical of high thrust settings, favours NO_X emissions, while low thrust settings produce significant amounts of carbon monoxide and hydrocarbons. The emissions of CO_2 follow the same trend of thrust-specific fuel consumption with engine ratings. Therefore, improvements of current gas turbine technology are welcomed, but largely insufficient alone in providing a quasi-zero emissions aircraft.

An interesting alternative is the utilisation of sustainable aviation fuels (SAFs), which are fuels compatible with both the existing engines and infrastructures. They are shortly named "drop-in" fuels for the reasons just stated. They are completely miscible with the conventional fossil fuel and provide the same performance because their base molecule is a hydrocarbon. Thus, when burned, they will produce nearly the same amount of CO_2 per unit of fuel as conventional jet fuel, yet the net life-cycle carbon emissions are reduced, since SAFs recycle carbon that is already present in the biosphere where most of the emitted carbon is absorbed by new biomass. SAFs are obtained by cultivation of specific crops or recycling organic wastes, giving a potential equivalent CO_2 reduction from 50% to 80%.

Yet, the social impact of land use change must be accounted for, while the European Union already stated that raw materials cannot be sourced from land with high biodiversity or high carbon footprint. The actual crops provide for a tiny availability and the final product may costs 50% to 60% more of conventional jet fuel. Yet, almost all of the six approved bio-based fuels are ready to be used and constitute a proven product to reduce the aviation climate impact.

As for electric propulsion alone, it is not sufficient to fulfil the requirements of regional and large transport aviation; however, it is still worth exploiting the many possibilities that the electric propulsion offers, since the link between the power source and the propulsors is no longer only mechanical but also electric. Moreover, the high efficiency of electric motors, with their seamless scalability, offers advantages on every aircraft class. Many different architectures are possible, which can be grouped into full and hybrid-electric configurations. The advantages and drawbacks of full-electric powerplant architectures have already been discussed. The hybrid-electric layout combines the advantage of both thermal and conventional systems, at the expense of a higher complexity and weight. The hybrid layout also includes the turbo-electric configuration, which is entirely powered by the thermal engine, not having an electric energy source. Clearly, the adoption of the turbo-electric chain alone generates a minor overall efficiency, since in the powerplant there are additional components with their mechanical and thermal losses. Therefore, the turbo-electric layout, but in general all the electric powerplants, are more attractive if integrated with new aerodynamic technologies, which are more difficulty enabled with a conventional powerplant.

The electric energy on a commuter aircraft could be easily stored in batteries or hydrogen tanks for fuel cells. Hydrocarbon fuel cells are also possible, since their use eliminates NO_X, but not carbon emissions. Liquid nitrogen fuel tanks as well as solar panels are excluded from the possible utilisation on the SAT segment. Batteries may achieve 500 W/kg specific energy by 2035, yet higher values towards 1500–2000 W/kg are desirable for the electric propulsion to become attractive on larger aircraft. PEM fuel cells using hydrogen as fuel are a viable alternative to batteries, but the authors did not find a clear historical trend on the specific energy (also depending on the storage technology) and specific power (accounting for fuel cell plus tank and subsystems) to draw a forecast of this technology. Recently, it has been stated that minor adaption of gas turbines may provide hydrogen to be directly fuelled into thermal engines—from a cryogenic tank through a heat exchanger—providing a net specific energy very close to the jet fuel and reducing climate impact by 75%.

Improvements in aerodynamics have a direct impact on aircraft performance. In the last decade, distributed electric propulsion (DEP) has been widely investigated to exploit the possibility to increase the wing maximum lift capability. The scalability and power line connections of electric drives enable an easier accommodation for DEP, whose main function is to blow on the wing at low airspeed. The increased local airspeed at a given angle of attack increases the maximum lift coefficient, just like an advanced high-lift device. This benefit should be used to size the wing for the cruising condition, hence allowing for a higher wing loading (reduced wing area for a given aircraft gross weight), while it is usually sized for landing condition, which sets a large wing area to limit take-off run and landing speed. Several experimental aircraft are being designed with this technology, the most famous is the NASA X-57. The key success for such technology will be the perfect integration of airframe, aerodynamics, and propulsion, where the above-mentioned advantages must not be offset by increased weight and installation or cooling drag.

Since the beginning of the airplane age, one of the objectives of aerodynamic technologies is the reduction of both viscous and non-viscous drag. As concerns the former, the establishing of laminar airflow, natural or forced, is an active thematic from the 1980s. As the laminar flow is unstable, protections must be enabled against ice, rain, and generally any kind of flow contamination that may promote transition. Another fascinating topic

is the boundary layer ingestion, which would allow for wake cancelling and hence drag reduction, while simultaneously producing thrust.

Parasite drag is not only laminar, but also turbulent. Devices such as riblets, which provide anisotropic roughness, constitute a passive technique to reduce turbulent drag. The accurate physics of riblets is still unknown, as they seem to interact with the turbulent flow structure. They would provide less fuel savings than laminar flow control or natural laminar flow and also imply additional operative costs due to their maintenance (shape adherence to the body). Nonetheless, they have been proven to be an effective method for drag reduction.

Non-viscous, subsonic drag, also known as vortex drag or lift-induced drag, is due to the vortex system established from the wing downstream. The pressure differential between upper and lower wing surface decreases towards the wing tips, where the two zones at different pressure interact, releasing wing tip vortices. This well-known phenomenon is visible in moist air, especially at high lift coefficients. As these vortices are due to the wing finiteness, the first proposal to mitigate such vortices is the increase of wing aspect ratio, usually increasing the wingspan by keeping the same wing area, hence reducing the three-dimensional aerodynamic effects. As this has significant structural drawbacks, until now wing tip vortices have been mitigated with the installation of winglets, which are wing tips appendices with profiles twisted and planform canted in such a way to counteract the induced drag vector.

A further improvement in induced drag reduction may come from propellers installed at wing tips and ultra-high aspect ratio wings. Although the idea is not new, the recent propulsive and structural advances could enable such layouts. A wing-tip propeller should operate so as to counteract the induced velocity vector with its flow swirl. By rotating the propeller in the opposite direction of the tip vortex, i.e., inner-up direction, it is possible to reduce the induced angle of attack and hence the induced drag. This has been shown by both numerical analyses and experimental tests, which have shown an equivalent aspect ratio increase of 35% or a reduction from 20 to 40 drag counts. Clearly, with the extreme position of wing-tip propellers, engine-out operations would be impossible or very difficult, while aero-elastic effects must be accurately predicted to avoid, for instance, whirl flutter.

Ultra-high aspect ratio wings, meaning aspect ratio larger than 20, can improve an aircraft aerodynamic efficiency with the most straight-forward solution and could also provide an easier establishment of laminar flow, because of the reduced cross-flow component. As in the case of wing-tip propellers, a larger wingspan enlarges the aero-elastic effects, which must be mitigated with an advanced wing structure adding little weight and drag penalties. In this sense, innovative configurations of transport aircraft such as strut-braced wing or truss-braced wing are being designed to get high aerodynamic efficiency, decreasing fuel burn by 10% to 20%. For short-range aircraft, spending a significant amount of mission time in climb and descent, at high lift coefficients, the impact on fuel burn should be even more beneficial. These advantages could be achieved if the wing structural weight is decreased from 50% to 90% with respect to the actual design and manufacturing techniques.

As airframe design impacts the aircraft weight, many technologies have been introduced and new ones are being investigated to get a lighter airframe. In fact, both aircraft acquisition and maintenance costs, as well as pollutant emissions, are proportional to aircraft weight. However, each new technology has many drawbacks that prevent its full exploitation in structural design while complying to performance and safety requirements. Again, a multi-disciplinary approach is needed to account for the numerous factors affecting the characteristics of interest.

Composite materials are inherently lighter and stiffer than the conventional materials employed in aircraft manufacturing (i.e., metals). They can also be manufactured as one-piece barrels, providing a significant weight saving due to missing fittings among smaller parts. However, there are other aspects limiting these advantages. For instance, random events such as low-velocity impacts may induce almost invisible failures due to the complex

mechanics behaviour of the anisotropic and multi-layered structure. The usual response is a constrained design and strict maintenance schedule, offsetting the advantage of the use of composite materials. To limit such drawback, structural health monitoring (SHM) can be used to provide continuous or on-demand structural monitoring, enabling on-condition maintenance and enabling smart intelligent composite structures. The complete adoption of SHM to provide a condition-based structural design is a long-term perspective since the standardisation and reliability of such a system requires time. In the short term, SHM should support damage-tolerant design with damage assessment, still relying on scheduled inspections with non-destructive techniques to ensure safety. The examples of aircraft life cycle and landing gear maintenance are given in this paper.

As concerns unconventional aircraft configurations, weight estimation cannot rely on statistics since currently there are no such aircraft in service. Therefore, higher fidelity methods also covering a multi-disciplinary approach must be included in the preliminary design phase. Since Class I methods, based on empirical data, are out of discussion, an acceptable weight estimation should start with a Class II method, which derives the aircraft main components mass through semi-empirical formulations based on the component geometry and the limit load factors. The use of Class III methods, i.e., FEM, provides the maximum freedom and accuracy, but requires a relatively high computational cost and may require geometric details that may be not available in the preliminary design phase. A feasible alternative may be the adoption of the Class II and a $\frac{1}{2}$ methods which are based on the estimation of the mass of material required to withstand loads applied to a particular aircraft component. Clearly, they must be integrated in the design loop to be effective.

A typical and trending example of non-conventional aircraft configuration is the wing with distributed propellers. Apart from the mass breakdown needed to estimate the aircraft maximum take-off weight, aeroelastic tailoring is needed to design a safe and performant innovative architecture. Flutter speed, propeller whirl flutter, structural stability, and modal frequencies are some of the concerns for a wing with multiple propulsors installed. The example of the NASA X-57 Maxwell is given in the paper.

The strut-braced wing is another unconventional configuration back on the scene of aviation research, because with the modern design and manufacturing techniques, the disadvantage of the additional aerodynamic drag due to the wing struts may be beneficially offset by increasing the wing aspect ratio to a value higher than 20 and adopting a thinner airfoil shape, enabling higher aerodynamic efficiencies at high Mach numbers. Consequently, MTOW may be reduced and fuel savings of 20% are theoretically possible, as claimed by the Boeing. Moreover, non-rigid wing struts may be installed to avoid buckling with negative load factors. In this case, the wing will behave as a cantilever structure in that condition, while the strut would work only in case of positive load factor.

Morphing wings have been an active object of research since the beginning of aviation. The idea is to change the geometry to adapt to different aerodynamic conditions. As an example, roll control may be achieved—as the Wright brothers did at the beginning of aviation era—by twisting the wing instead of deflecting the ailerons. Moreover, high lift may be achieved by changing the wing profile curvature instead of relying on rigid high-lift devices such as slats and flaps, which require complex and heavy mechanisms to be actuated. According to some studies, morphing structures have the potential to decrease parasite drag up to 22%. Morphing systems are categorised into two main groups using different architectures. One type consists of multiple rigid elements interconnected by kinematic chains like a robot. The other type relies on the deformation of structural elements. The first is of more practical use, while the latter usually provides uniform shape changes. For both, there is the inherent difficulty to be stiff enough to withstand external loads and simultaneously flexible enough to accommodate different shapes with as little energy as possible.

Finally, novel composite manufacturing technologies, as well as nano- and multi-functional materials, should provide additional benefits in terms of costs, weight, and performance. For instance, the automatic composite fibre placement with out-of-autoclave

manufacturing leads to a less expensive process and better component quality. Carbon nanotubes shall enhance mechanical, thermal, and electrical properties of composites. Structural batteries, which would be installed as sandwich panels, may enable a beneficial snowball effect by integrating the electric energy source within aircraft structure, which should be lighter, hence requiring less power, smaller motors, and eventually smaller batteries. As research progresses, these integrated concepts should provide negligible structural degradation after numerous charge/discharge cycles. Certification and end-of-life disposal are open issues. As a consequence, this design could reduce the weight and cost of electric aircraft and it is highlighted as a key-enabling technology, although much work is needed to achieve a reliable implementation within aircraft.

Author Contributions: Conceptualisation, D.C.; methodology, D.C.; validation, D.C., P.D.V. and V.M.; formal analysis, D.C., P.D.V. and V.M.; investigation, D.C., P.D.V., V.M., F.R. and G.W.; resources, F.N.; data curation, D.C.; writing—original draft preparation, D.C., P.D.V., V.M. and G.W.; writing—review and editing, D.C., P.D.V. and V.M.; visualisation, D.C., P.D.V. and V.M.; supervision, D.C.; project administration, F.N.; funding acquisition, F.N. All authors have read and agreed to the published version of the manuscript.

Institutional Review Board Statement: Not applicable.

Informed Consent Statement: Not applicable.

Data Availability Statement: Not applicable.

Conflicts of Interest: The authors declare no conflict of interest. The funders had no role in the design of the study; in the collection, analyses, or interpretation of data; in the writing of the manuscript, or in the decision to publish the results.

Abbreviations

The following abbreviations and symbols are used in this manuscript:

AC	Alternate Current
ACARE	Advisory Council for Aeronautics Research in Europe
AFloNext	Aircraft Flow Control Technologies
AFP	Automated dry Performing Process
ALTTA	Application of hybrid Laminar flow Technology on Transport aircraft
APU	Auxiliary Power Unit
ASTM	American Society for Testing and Materials
ATAG	Air Transport Action Group
ATJ	Alcohol-to-Jet
ATJ-SPK	Alcohol-to-Jet Synthetic Paraffinic Kerosene
BLADE	Breakthrough Laminar Aircraft Demonstrator
BLI	Boundary Layer Ingestion

BMS	Battery Management System
BVID	Barely Visible Impact Damage
CAI	Compression After Impact
CFRP	Carbon fibres Reinforced Plastics
CMC	Ceramic Matrix Composite
CNT	Carbon Nanotube
CS2	Clean Sky 2
DC	Direct Current
DEP	Distributed Electric Propulsion
DP	Distributed Propulsion
ELFIN	European Laminar Flow Investigation
ELICA	ELectric Innovative Commuter Aircraft
FAA	Federal Aviation Authorities
FEM	Finite Element Methods
FH	Flight Hours
FT-SPK	Fischer–Tropsch Synthetic Paraffinic Kerosene
FT-SPK/A	Fischer–Tropsch Synthetic Paraffinic Kerosene and Aromatics
GEN	Generator
HEFA	Hydroprocessed Fatty Acid Esters and Free Fatty Acid
HFC	Hydrogen Fuel Cell
HFS-SIP	Hydroprocessing of Fermented Sugars—Synthetic Iso-Paraffinic kerosene
HLFC	Hybrid Laminar Flow Control
IATA	International Association of Air Transport
ICAO	International Civil Aviation Organisation
ICE	Internal Combustion Engine
ILFT	Interlaminar Fracture Toughness
IMD	Insulation Monitor Devices
IoT	Internet of Things
LFC	Laminar Flow Control
LRI	Liquid Resin Infusion
MIL	Minimum Induced Loss
MOT	Motor
MTOM	Maximum Take-Off Mass
NDE	Non-Destructive Evaluation
NDI	Non-Destructive Inspection
NLF	Natural Laminar Flow
PEM	Proton Exchange Membrane
RANS	Reynolds-Averaged Navier–Stokes
SAF	Sustainable Alternative Fuel
SAT	Small Air Transport
SBW	Strut-Braced Wing
SFWA	Smart Fixed Wing Aircraft
SHM	Structural Health Monitoring
SiC	Silicon Carbide
SOFC	Solid-Oxide Fuel Cell
TBW	Truss-Braced Wing
TOD	Threshold Of Detectability
UAV	Unmanned Aerial Vehicle
UHAR	Ultra-High Aspect Ratio
UNINA	University of Naples "Federico II"
VAC	Volt in Alternate Current
VDC	Volt in Direct Current
VID	Visible Impact Damage
CO	Carbon monoxide
CO2	Carbon dioxide
LH2	Liquid hydrogen
NOX	Nitrogen oxide
ap	Propeller axial induction factor

apt	Propeller tangential induction factor
AR	Wing aspect ratio
ARe	Wing effective aspect ratio
b	Wingspan
c	Wing chord
CD	Drag coefficient
CD0	Parasite drag coefficient
CDi	Induced drag coefficient
CL	Lift coefficient
CM	Pitching moment coefficient
CT	Propeller thrust coefficient
d	Dent depth
Dp	Propeller disk diameter
e	Oswald factor for lift-induced drag
G	Shear modulus
g	Gravitational acceleration
J	Propeller advance ratio
L	Structural beam length
M	Mach number
P(E)	Probability of occurrence of the event E
q	Structural load distribution (force per unit length)
R	Propeller radius
r	Propeller blade station
Re	Reynolds number
Rec	Reynolds number based on wing chord
ReD	Reynolds number based on propeller diameter
t/c	Thickness ratio
Tp	Propeller thrust
V∞	Free-stream flow speed
Vp	Flow speed at the propeller
w	Wing-induced downwash
W	Aircraft gross weight
wp	Propeller-induced downwash
wswirl	Flow tangential speed downstream of the propeller
α	Angle of attack
αiw	Induced angle of attack due to the wing
η	Non-dimensional wingspan station
ρ	Material density
ρ∞	Free-stream flow density
σ	Structural element stress
ω	Flow angular speed downstream of the propeller
Ω	Propeller angular speed

References

1. National Academies of Sciences, Engineering, and Medicine. *Commercial Aircraft Propulsion and Energy Systems Research*; The National Academies Press: Washington, DC, USA, 2016; ISBN 9780309440967.
2. Darecki, M.; Edelstenne, C.; Enders, T.; Fernandez, E.; Hartman, P.; Herteman, J.P.; Kerkloh, M.; King, I.; Ky, P.; Mathieu, M.; et al. *European Commission, Directorate-General for Mobility and Transport, Directorate-General for Research and Innovation, Flightpath 2050: Europe's Vision for Aviation: Maintaining Global Leadership and Serving Society's Needs*; European Union Publications Office: Luxembourg, 2011; ISBN 9789279262296.
3. Conceptual Design of a 19-Passenger Commuter Aircraft with Near Zero Emissions. Available online: https://ec.europa.eu/info/funding-tenders/opportunities/portal/screen/opportunities/topic-details/jti-cs2-2018-cfp09-tht-03 (accessed on 24 February 2022).
4. European Aeronautical Industry. *Clean Sky 2-Joint Technical Programme*; European Aeronautical Industry: Brussels, Belgium, 2015.
5. Advisory Council for Aeronautics Research in Europe (ACARE). *2008 Addendum to the Strategic Research Agenda*; ACARE: Chandigarh, India, 2008.

6.   Small Air Transport. Available online: https://clean-aviation.eu/clean-sky-2/programme-overview-and-structure/clean-sky-2-structure/small-air-transport-ta (accessed on 24 February 2022).

7.   ELectric Innovative Commuter Aircraft. Available online: https://cordis.europa.eu/project/id/864551 (accessed on 24 February 2022).

8.   Della Vecchia, P.; Malgieri, D.; Nicolosi, F.; De Marco, A. Numerical Analysis of Propeller Effects on Wing Aerodynamic: Tip Mounted and Distributed Propulsion. *Transp. Res. Procedia* **2018**, *29*, 106–115. [CrossRef]

9.   Patterson, M.D.; German, B.J.; Daskilewicz, M.J. Simplified Aerodynamics Models to Predict the Effects of Upstream Propellers on Wing Lift. In Proceedings of the 53rd AIAA Aerospace Sciences Meeting, Kissimmee, FL, USA, 5–9 January 2015; American Institute of Aeronautics and Astronautics: Reston, VA, USA, 2015; pp. 1–15.

10. Borer, N.K.; Patterson, M.D.; Viken, J.K.; Moore, M.D.; Bevirt, J.B.; Stoll, A.M.; Gibson, A.R.; Clarke, S.; Redifer, M.E.; Christie, R.J.; et al. Design and Performance of the NASA SCEPTOR Distributed Electric Propulsion Flight Demonstrator. In Proceedings of the 16th AIAA Aviation Technology, Integration, and Operations Conference, Washington, DC, USA, 13–17 June 2016; American Institute of Aeronautics and Astronautics: Reston, VA, USA, 2016; pp. 1–20.

11. Stoll, A.M.; Mikic, G.V. Design Studies of Thin-Haul Commuter Aircraft with Distributed Electric Propulsion. In Proceedings of the 16th AIAA Aviation Technology Integration Operations Conference, Washington, DC, USA, 13–17 June 2016; pp. 13–17. [CrossRef]

12. Orefice, F.; Nicolosi, F.; Della Vecchia, P.; Ciliberti, D. Conceptual Design of Commuter Aircraft Including Distributed Electric Propulsion. In Proceedings of the AIAA Aviation 2020 Forum, Virtual Event, 15–19 June 2020; American Institute of Aeronautics and Astronautics (AIAA): Reston, VA, USA, 2020; p. 18.

13. Orefice, F.; Della Vecchia, P.; Ciliberti, D.; Nicolosi, F. Correction: Aircraft Conceptual Design Including Powertrain System Architecture and Distributed Propulsion. In Proceedings of the AIAA Propulsion and Energy Forum, Indianapolis, IN, USA, 19–22 August 2019; American Institute of Aeronautics and Astronautics: Reston, VA, USA, 2019.

14. Epstein, A.H. Aeropropulsion for Commercial Aviation in the Twenty-First Century and Research Directions Needed. *AIAA J.* **2014**, *52*, 901–911. [CrossRef]

15. European Union Aviation Safety Agency (EASA). *Certification Specifications and Acceptable Means of Compliance for Normal, Utility, Aerobatic, and Commuter Category Aeroplanes*; EASA: Cologne, Germany, 2015.

16. 3D Printing in Aerospace & Aviation | GE Additive. Available online: https://www.ge.com/additive/additive-manufacturing/industries/aviation-aerospace (accessed on 28 February 2022).

17. Ranasinghe, K.; Guan, K.; Gardi, A.; Sabatini, R. Review of Advanced Low-Emission Technologies for Sustainable Aviation. *Energy* **2019**, *188*, 115945. [CrossRef]

18. Ruijgrok, G.J.J.; van Paassen, D.M. *Elements of Aircraft Pollution*; Delft University Press: Delft, The Netherlands, 2005; ISBN 9040726027.

19. European Environment Agency (EASA). *European Aviation Environmental Report 2019*; EASA: Cologne, Germany, 2019; ISBN 9789292101978.

20. International Air Transport Association (IATA). *Fact Sheet 2: SAF Technical Certification*; IATA: Geneva, Switzerland, 2019.

21. Commercial Aviation Alternative Fuels Initiative (CAAFI). *Fuel Readiness Level*; CAAFI: Haymarket, VA, USA, 2010.

22. Felder, J.L. *NASA Electric Propulsion System Studies Outline*; NASA Presentation; National Aeronautics and Space Administration (NASA): Washington, DC, USA, 2015.

23. de Vries, R.; Brown, M.T.; Vos, R. A Preliminary Sizing Method for Hybrid-Electric Aircraft Including Aero-Propulsive Interaction Effects. In Proceedings of the 2018 Aviation Technology, Integration, and Operations Conference, Atlanta, Georgia, 25–29 June 2018.

24. Ciliberti, D.; Orefice, F.; Della Vecchia, P.; Nicolosi, F.; Corcione, S. An Approach to Preliminary Sizing of Turbo-Electric Aircraft with Distributed Propulsion. In Proceedings of the AIDAA XXV International Congress, Rome, Italy, 9–12 September 2019.

25. Siemens Unveils 260 kw Electric Engine. Available online: https://www.flyingmag.com/aircraft-siemens-unveils-260-kw-electric-aircraft-motor/ (accessed on 28 February 2022).

26. Benefits of 270 VDC in the Aviation Industry. Available online: https://fcxinc.com/benefits-of-270-vdc-in-the-aviation-industry/ (accessed on 28 February 2022).

27. Cotton, I.; Nelms, A.; Husband, M. Higher Voltage Aircraft Power Systems. *IEEE Aerosp. Electron. Syst. Mag.* **2008**, *23*, 25–32. [CrossRef]

28. Michaelides, E.E. *Alternative Energy Sources*; Springer: Berlin/Heidelberg, Germany, 2012; ISBN 9783642209505.

29. Ohiostandard Galvanic Cell with No Cation Flow. Available online: https://commons.wikimedia.org/w/index.php?curid=84049705 (accessed on 2 March 2022).

30. Strack, M.; Chiozzotto, G.P.; Iwanizki, M.; Plohr, M.; Kuhn, M. Conceptual Design Assessment of Advanced Hybrid Electric Turboprop Aircraft Configurations. In Proceedings of the 17th AIAA Aviation Technology, Integration, and Operations Conference, Denver, Colorado, 5–9 June 2017; American Institute of Aeronautics and Astronautics: Reston, VA, USA, 2017.

31. German, B.; Bradley, M.; McDonald, R.; Vos, R. Design of Electric and Hybrid-Electric Aircraft. In Proceedings of the AIAA Aviation 2018 Forum, Atlanta, GA, USA, 25–29 June 2018; AIAA: Atlanta, GA, USA, 2018.

32. Scrosati, B.; Garche, J. Lithium Batteries: Status, Prospects and Future. *J. Power Sources* **2010**, *195*, 2419–2430. [CrossRef]

33. Gerssen-Gondelach, S.J.; Faaij, A.P.C. Performance of Batteries for Electric Vehicles on Short and Longer Term. *J. Power Sources* **2012**, *212*, 111–129. [CrossRef]

34. How Lithium Ion Batteries Grounded the Dreamliner. Available online: https://www.scientificamerican.com/article/how-lithium-ion-batteries-grounded-the-dreamliner/ (accessed on 28 February 2022).

35. Zamboni, J. *A Method for the Conceptual Design of Hybrid Electric Aircraft*; TU Delft: Delft, The Netherlands, 2018.

36. Gallagher, K.G.; Goebel, S.; Greszler, T.; Mathias, M.; Oelerich, W.; Eroglu, D.; Srinivasan, V. Quantifying the Promise of Lithium-Air Batteries for Electric Vehicles. *Energy Environ. Sci.* **2014**, *7*, 1555–1563. [CrossRef]

37. Blurton, K.F.; Sammells, A.F. Metal/Air Batteries: Their Status and Potential-a Review. *J. Power Sources* **1979**, *4*, 263–279. [CrossRef]

38. Rajashekara, K.; Grieve, J.; Daggett, D. Hybrid Fuel Cell Power in Aircraft. *IEEE Ind. Appl. Mag.* **2008**, *14*, 54–60. [CrossRef]

39. Santin, M.; Traverso, A.; Massardo, A. Technological Aspects of Gas Turbine and Fuel Cell Hybrid Systems for Aircraft: A Review. *Aeronaut. J.* **2008**, *112*, 459–467. [CrossRef]

40. Dunn, J.P. Fuel Cell Powered Electric Aircraft. U.S. Patent No. US006568633B2, 27 May 2003.

41. Bradley, T.H.; Moffitt, B.A.; Mavris, D.N.; Parekh, D.E. Development and Experimental Characterization of a Fuel Cell Powered Aircraft. *J. Power Sources* **2007**, *171*, 793–801. [CrossRef]

42. Verstraete, D.; Lehmkuehler, K.; Gong, A.; Harvey, J.R.; Brian, G.; Palmer, J.L. Characterisation of a Hybrid, Fuel-Cell-Based Propulsion System for Small Unmanned Aircraft. *J. Power Sources* **2014**, *250*, 204–211. [CrossRef]

43. Bradley, T.H.; Moffitt, B.A.; Fuller, T.F.; Mavris, D.N.; Parekh, D.E. Comparison of Design Methods for Fuel-Cell-Powered Unmanned Aerial Vehicles. *J. Aircr.* **2009**, *46*, 1945–1956. [CrossRef]

44. Bradley, T.H.; Moffitt, B.A.; Mavris, D.N.; Fuller, T.F.; Parekh, D.E. Hardware-in-the-Loop Testing of a Fuel Cell Aircraft Powerplant. *J. Propuls. Power* **2009**, *25*, 1336–1344. [CrossRef]

45. Rhoads, G.D.; Wagner, N.A.; Taylor, B.J.; Keen, D.B.; Bradley, T.H. Design and Flight Test Results for a 24 Hour Fuel Cell Unmanned Aerial Vehicle. In Proceedings of the 8th Annual International Energy Conversion Engineering Conference, Nashville, TN, USA, 25–28 July 2010.

46. Renouard-Vallet, G.; Saballus, M.; Schumann, P.; Kallo, J.; Friedrich, K.A.; Müller-Steinhagen, H. Fuel Cells for Civil Aircraft Application: On-Board Production of Power, Water and Inert Gas. *Chem. Eng. Res. Des.* **2012**, *90*, 3–10. [CrossRef]

47. Motapon, S.N.; Dessaint, L.A.; Al-Haddad, K. A Comparative Study of Energy Management Schemes for a Fuel-Cell Hybrid Emergency Power System of More-Electric Aircraft. *IEEE Trans. Ind. Electron.* **2014**, *61*, 1320–1334. [CrossRef]

48. Motapon, S.N.; Dessaint, L.A.; Al-Haddad, K. A Robust H_2-Consumption-Minimization-Based Energy Management Strategy for a Fuel Cell Hybrid Emergency Power System of More Electric Aircraft. *IEEE Trans. Ind. Electron.* **2014**, *61*, 6148–6156. [CrossRef]

49. Kim, K.; Kim, T.; Lee, K.; Kwon, S. Fuel Cell System with Sodium Borohydride as Hydrogen Source for Unmanned Aerial Vehicles. *J. Power Sources* **2011**, *196*, 9069–9075. [CrossRef]

50. Nicolay, S.; Karpuk, S.; Liu, Y.; Elham, A. Conceptual Design and Optimization of a General Aviation Aircraft with Fuel Cells and Hydrogen. *Int. J. Hydrogen Energy* **2021**, *46*, 32676–32694. [CrossRef]

51. Dudek, M.; Tomczyk, P.; Wygonik, P.; Korkosz, M.; Bogusz, P.; Lis, B. Hybrid Fuel Cell-Battery System as a Main Power Unit for Small Unmanned Aerial Vehicles (UAV). *Int. J. Electrochem. Sci.* **2013**, *8*, 8442–8463.

52. Herwerth, C.; Chiang, C.; Ko, A.; Matsuyama, S.; Choi, S.B.; Mirmirani, M.; Gamble, D.; Paul, R.; Sanchez, V.; Arena, A.; et al. *Development of a Small Long Endurance Hybrid PEM Fuel Cell Powered UAV*; SAE Technical Papers; SAE International: Los Angeles, CA, USA, 2007.

53. Yang, C.; Moon, S.; Kim, Y. A Fuel Cell/Battery Hybrid Power System for an Unmanned Aerial Vehicle. *J. Mech. Sci. Technol.* **2016**, *30*, 2379–2385. [CrossRef]

54. Hydrogen-A Future Fuel for Aviation. Available online: https://www.rolandberger.com/en/Insights/Publications/Hydrogen-A-future-fuel-for-aviation.html (accessed on 28 February 2022).

55. European Commission. Clean Sky 2. In *Hydrogen-Powered Aviation*; European Union: Brussels, Belgium, 2020; ISBN 9789292463410.

56. HY4 Aircraft. Available online: https://www.aerospace-technology.com/projects/hy4-aircraft/ (accessed on 2 March 2022).

57. HES Unveils Element One Hydrogen-Electric Passenger Aircraft. *Fuel Cells Bull.* **2018**, *2018*, 4–5. [CrossRef]

58. Alcock, C. Alaka'i Seeks Partner as Skai Hydrogen EVTOL Prototype Prepares to Fly. Available online: https://www.futureflight.aero/news-article/2021-09-25/alakai-seeks-partner-skai-hydrogen-evtol-prototype-prepares-fly (accessed on 2 March 2022).

59. Warwick, G. Germany's Apus Developing Zero-Emission Four Seater. Available online: https://aviationweek.com/special-topics/sustainability/germanys-apus-developing-zero-emission-four-seater (accessed on 2 March 2022).

60. Podlaski, M.; Vanfretti, L.; Khare, A.; Nademi, H.; Ansell, P.; Haran, K.; Balachandran, T. Initial Steps in Modeling of Cheeta Hybrid Propulsion Aircraft Vehicle Power Systems Using Modelica. In Proceedings of the AIAA Propulsion and Energy Forum, Virtual Event, 24–28 August 2020; American Institute of Aeronautics and Astronautics (AIAA): Reston, VA, USA, 2020; pp. 1–16.

61. Alcock, C. Pipistrel to Supply Electric Propulsion for Airflow's ESTOL Proof-of-Concept Aircraft. Available online: https://www.futureflight.aero/news-article/2021-11-12/pipistrel-supply-electric-propulsion-airflows-estol-proof-concept-aircraft (accessed on 5 May 2021).

62. Manthey, N. ZeroAvia Completes Maidenflight with Hydrogen Aircraft. Available online: https://www.electrive.com/2020/09/30/zeroavia-completes-maidenflight-with-hydrogen-aircraft/ (accessed on 2 March 2022).

63. The ZEROe Demonstrator Has Arrived. Available online: https://www.airbus.com/en/newsroom/stories/2022-02-the-zeroe-demonstrator-has-arrived (accessed on 2 March 2022).

64. Guynn, M.D.; Freh, J.E.; Olson, E.D. *Evaluation of a Hydrogen Fuel Cell Powered Blended-Wing-Body Aircraft Concept for Reduced Noise and Emissions*; National Aeronautics and Space Administration (NASA): Washington, DC, USA, 2004.

65. Corchero, G.; Montañés, J.L. An Approach to the Use of Hydrogen for Commercial Aircraft Engines. *Proc. Inst. Mech. Eng. Part G J. Aerosp. Eng.* **2005**, *219*, 35–44. [CrossRef]

66. International Civil Aviation Organization (ICAO). *Guidance on the Development of States' Action Plan on CO₂ Emissions Reduction Activities (Doc 9988)*; ICAO: Montreal, QC, Canada, 2019.

67. Kim, H.D.; Perry, A.T.; Ansell, P.J. A Review of Distributed Electric Propulsion Concepts for Air Vehicle Technology. In Proceedings of the AIAA/IEEE Electric Aircraft Technologies Symposium, Cincinnati, OH, USA, 9–11 July 2018.

68. Van, E.N.; Troillard, P.; Jézégou, J.; Alazard, D.; Pastor, P.; Döll, C. Reduction of Vertical Tail Using Differential Thrust: Influence on Flight Control and Certification. Presented at the Advanced Aircraft Efficiency in a Global Air Transport System (AEGATS'18), Tolouse, France, 23–25 October 2018; Available online: https://oatao.univ-toulouse.fr/21801/ (accessed on 2 March 2022).

69. Van, E.N.; Alazard, D.; Pastor, P.; Döll, C. Towards an Aircraft with Reduced Lateral Static Stability Using Electric Differential Thrust. In Proceedings of the 2018 Aviation Technology, Integration, and Operations Conference, Atlanta, GA, USA, 25–29 June 2018.

70. Van, E.N.; Alazard, D.; Döll, C.; Pastor, P. Co-Design of Aircraft Vertical Tail and Control Laws Using Distributed Electric Propulsion. *IFAC-PapersOnLine* **2019**, *52*, 514–519. [CrossRef]

71. Freeman, J.L.; Klunk, G.T. Dynamic Flight Simulation of Spanwise Distributed Electric Propulsion for Directional Control Authority. In Proceedings of the AIAA/IEEE Electric Aircraft Technologies Symposium (EATS), Cincinnati, OH, USA, 12–14 July 2018; pp. 1–15. [CrossRef]

72. Snyder, M.H.; Zumwalt, G.W. Effects of Wingtip-Mounted Propellers on Wing Lift and Induced Drag. *J. Aircr.* **1969**, *6*, 392–397. [CrossRef]

73. Patterson, J.C.; Bartlett, G.R. *Evaluation of Installed Performance of a Wing-Tip-Mounted Pusher Turborprop on a Semispan Wing*; National Aeronautics and Space Administration (NASA): Washington, DC, USA, 1987.

74. Deere, K.A.; Viken, S.A.; Carter, M.B.; Viken, J.K.; Derlaga, J.M.; Stoll, A.M. Comparison of High-Fidelity Computational Tools for Wing Design of a Distributed Electric Propulsion Aircraft. In Proceedings of the 35th AIAA Applied Aerodynamics Conference, Denver, CO, USA, 5–9 June 2017; pp. 1–22.

75. Veldhuis, L.L.M. *Propeller Wing Aerodynamic Interference*; TU Delft: Delft, The Netherlands, 2005.

76. Dimchev, M. *Experimental and Numerical Study on Wingtip Mounted Propellers for Low Aspect Ratio UAV Design*; Delft University of Technology: Delft, The Netherlands, 2012.

77. Sinnige, T.; Van Arnhem, N.; Stokkermans, T.C.A.; Eitelberg, G.; Veldhuis, L.L.M. Wingtip-Mounted Propellers: Aerodynamic Analysis of Interaction Effects and Comparison with Conventional Layout. *J. Aircr.* **2019**, *56*, 295–312. [CrossRef]

78. Patterson, M.D. *Conceptual Design of High-Lift Propeller Systems for Small Electric Aircraft*; Georgia Institute of Technology: Atlanta, GA, USA, 2016.

79. Deere, K.A.; Viken, S.A.; Carter, M.B.; Viken, J.K.; Wiese, M.R.; Farr, N. Computational Analysis of Powered Lift Augmentation for the LEAPTech Distributed Electric Propulsion Wing. In Proceedings of the 35th AIAA Applied Aerodynamics Conference, Denver, CO, USA, 5–9 June 2017; pp. 1–20.

80. Murray, J.; Lechniak, J. *The LEAPTech Experiment: Approach, Results, Recommendations 2016*; National Aeronautics and Space Administration (NASA): Washington, DC, USA, 2016.

81. Orefice, F.; Della Vecchia, P.; Ciliberti, D.; Nicolosi, F. Preliminary Design to Fulfil Future Market Demand of Electric. *Int. Rev. Aerosp. Eng.* **2021**, *14*, 294. [CrossRef]

82. Budziszewski, N.; Friedrichs, J. Modelling of a Boundary Layer Ingesting Propulsor. *Energies* **2018**, *11*, 708. [CrossRef]

83. Valencia, E.; Alulema, V.; Rodriguez, D.; Laskaridis, P.; Roumeliotis, I. Novel Fan Configuration for Distributed Propulsion Systems with Boundary Layer Ingestion on a Hybrid Wing Body Airframe. *Therm. Sci. Eng. Prog.* **2020**, *18*, 100515. [CrossRef]

84. Hartuç, T. *Boundary Layer Ingestion Theoretical and Experimental Research*; TU Delft: Delft, The Netherlands, 2015.

85. Isikveren, A.T.; Seitz, A.; Bijewitz, J.; Hornung, M.; Mirzoyan, A.; Isyanov, A.; Godard, J.L.; Stückl, S.; Van Toor, J. Recent Advances in Airframe-Propulsion Concepts with Distributed Propulsion. In Proceedings of the 29th Congress of the International Council of the Aeronautical Sciences, St. Petersburg, Russia, 7–12 September 2014; pp. 1–14.

86. Corte, B.D.; Van Sluis, M.; Rao, A.G.; Veldhuis, L. Experimental Investigation of the Flow Past an Axisymmetric Body at Low Speed. *Proc. Int. Soc. Air Breath. Engines* **2019**, *49*, 540–546.

87. Nasoulis, C.P.; Protopapadakis, G.; Gkoutzamanis, V.G.; Kalfas, A.I. The Impact of Propulsive Architecture on the Design of a 19-Passenger Hybrid-Electric Aircraft. *IOP Conf. Ser. Mater. Sci. Eng.* **2022**, *1226*, 012074. [CrossRef]

88. Ashcraft, S.W.; Padron, A.S.; Pascioni, K.A.; Stout, G.W., Jr.; Huff, D.L. *Review of Propulsion Technologies for N + 3 Subsonic Vehicle Concepts*; National Aeronautics and Space Administration (NASA): Washington, DC, USA, 2011.

89. Synodinos, A.; Self, R.; Torija, A. Preliminary Noise Assessment of Aircraft with Distributed Electric Propulsion. In Proceedings of the 2018 AIAA/CEAS Aeroacoustics Conference; American Institute of Aeronautics and Astronautics, Atlanta, GA, USA, 25–29 June 2018.

90. Rizzi, S.A.; Palumbo, D.L.; Rathsam, J.; Christian, A.W.; Rafaelof, M. Annoyance to Noise Produced by a Distributed Electric Propulsion High-Lift System. In Proceedings of the 23rd AIAA/CEAS Aeroacoustics Conference, Denver, Colorado, 5–9 June 2017; AIAA AVIATION Forum. American Institute of Aeronautics and Astronautics: Reston, VA, USA, 2017.

91. Fink, M.R. Approximate Prediction of Airframe Noise. *J. Aircr.* **1976**, *13*, 8–9. [CrossRef]

92. Huff, D.L.; Henderson, B.S.; Envia, E. Motor Noise for Electric Powered Aircraft. In Proceedings of the 22nd AIAA/CEAS Aeroacoustics Conference, Lyon, France, 30 May–1 June 2016.

93. Pascioni, K.A.; Rizzi, S.A.; Schiller, N.H. Noise Reduction Potential of Phase Control for Distributed Propulsion Vehicles. In Proceedings of the AIAA Scitech Forum, San Diego, CA, USA, 7–11 January 2019.

94. Posey, J.W.; Tinetti, A.F.; Dunn, M.H. The Low-Noise Potential of Distributed Propulsion on a Catamaran Aircraft. In Proceedings of the Collection of Technical Papers-12th AIAA/CEAS Aeroacoustics Conference, Manchester, UK, 10–12 May 2004; 2006; Volume 5, pp. 2865–2877.

95. Joslin, R.D. *Overview of Laminar Flow Control*; National Aeronautics and Space Administration (NASA): Washington, DC, USA, 1998.

96. Beck, N.; Landa, T.; Seitz, A.; Boermans, L.; Liu, Y.; Radespiel, R. Drag Reduction by Laminar Flow Control. *Energies* **2018**, *11*, 252. [CrossRef]

97. Abbas, A.; De Vicente, J.; Valero, E. Aerodynamic Technologies to Improve Aircraft Performance. *Aerosp. Sci. Technol.* **2013**, *28*, 100–132. [CrossRef]

98. Collier, F. An Overview of Recent Subsonic Laminar Flow Control Flight Experiments. In Proceedings of the 23rd Fluid Dynamics, Plasmadynamics, and Lasers Conference, Nashville, TN, USA, 6–8 July 1992; American Institute of Aeronautics and Astronautics: Reston, VA, USA, 1993.

99. Williams, G. *Progress and Achievements in CleanSky SFWA*; Airbus Operations GmbH: Buxtehude, Germany, 2018.

100. Fujino, M.; Yoshizaki, Y.; Kawamura, Y. Natural-Laminar-Flow Airfoil Development for a Lightweight Business Jet. *J. Aircr.* **2003**, *40*, 609–615. [CrossRef]

101. Fujino, M. Design and Development of the HondaJet. *J. Aircr.* **2005**, *42*, 755–764. [CrossRef]

102. Pe, T.; Thielecke, F. Synthesis and Topology Study of HLFC System Architectures in Preliminary Aircraft Design. In Proceedings of the 3rd CEAS Air & Space Conference, Venice, Italy, 24–28 October 2011.

103. Bottemanne, M.; Atkin, C. Tool for Sizing Suction Pumps for Hybrid Laminar Flow Control Concepts. *Int. J. Mech. Eng. Robot. Res.* **2018**, *7*, 1–8. [CrossRef]

104. Schmitt, V.; Archambaud, J.P.; Hortstmann, K.H.; Quast, A. Hybrid Laminar Fin Investigations. In Proceedings of the RTO AVT Symposium on Active Control Technology for Enhanced Performance Operational Capabilities of Military Aircraft, Land Vehicles and Sea Vehicles, Braunschweig, Germany, 8 October–5 November 2000. RTO MP-051.

105. Schrauf, G.H.; Horstmann, K.H. Simplified Hybrid Laminar Flow Control. In Proceedings of the ECCOMAS 2004-European Congress on Computational Methods in Applied Sciences and Engineering, Jyväskylä, Finland, 1 February 2004.

106. Parikh, P.G. Passive Removal of Suction Air for Laminar Flow Control, and Associated Systems and Methods. U.S. Patent No. US7866609B2, 2011.

107. Risse, K.; Schueltke, F.; Stumpf, E.; Schrauf, G. Conceptual Wing Design Methodology for Aircraft with Hybrid Laminar Flow Control. In Proceedings of the 52nd Aerospace Sciences Meeting, National Harbor, MD, USA, 13–17 January 2014.

108. Risse, K.; Anton, E.; Lammering, T.; Franz, K.; Hoernschemeyer, R. An Integrated Environment for Preliminary Aircraft Design and Optimization. In Proceedings of the 53rd AIAA/ASME/ASCE/AHS/ASC Structures, Structural Dynamics and Materials Conference, Honolulu, HI, USA, 23–26 April 2012.

109. Jiménez, J. Turbulent Flows over Rough Walls. *Annu. Rev. Fluid Mech.* **2004**, *36*, 173–196. [CrossRef]

110. Catalano, P.; de Rosa, D.; Mele, B.; Tognaccini, R.; Moens, F. Effects of Riblets on the Performances of a Regional Aircraft Configuration in NLF Conditions. In Proceedings of the AIAA Aerospace Sciences Meeting, Kissimmee, FL, USA, 5–9 January 2018.

111. García-Mayoral, R.; Jiménez, J. Drag Reduction by Riblets. *Philos. Trans. R. Soc. A Math. Phys. Eng. Sci.* **2011**, *369*, 1412–1427. [CrossRef]

112. McLean, J.D.; George-Falvey, D.N.; Sullivan, P.P. Flight-Test of Turbulent Skin Friction Reduction by Riblets. In Proceedings of the International Conference on Turbulent Drag Reduction by Passive Means, London, UK, 15–17 September 1987; pp. 1–17.

113. Szodruch, J. Viscous Drag Reduction on Transport Aircraft. In Proceedings of the 29th Aerospace Sciences Meeting, Reno, NV, USA, 7–10 January 1991; American Institute of Aeronautics and Astronautics: Reston, VA, USA, 1991.

114. Torrigiani, F.; Bussemaker, J.; Ciampa, P.D.; Fioriti, M.; Tomasella, F.; Aigner, B.; Rajpal, D.; Timmermans, H.; Savelyev, A.; Charbonnier, D. Design of the Strut Braced Wing Aircraft in the Agile Collaborative MDO Framework. In Proceedings of the 31st Congress of the International Council of the Aeronautical Sciences, ICAS 2018, Belo Horizonte, Brazil, 9–14 September 2018; pp. 1–16.

115. Zhao, W.; Kapania, R.K.; Schetz, J.A.; Coggin, J.M. Nonlinear Aeroelastic Analysis of SUGAR Truss-Braced Wing (TBW) Wind-Tunnel Model (WTM) Under In-Plane Loads. In Proceedings of the 56th AIAA/ASCE/AHS/ASC Structures, Structural Dynamics, and Materials Conference, Kissimmee, FL, USA, 5–9 January 2015; American Institute of Aeronautics and Astronautics: Reston, VA, USA, 2015.

116. Bradley, M.K.; Droney, C.K. *Subsonic Ultra Green Aircraft Research: Phase I Final Report*; NASA/CR–2011-216847; National Aeronautics and Space Administration (NASA): Washington, DC, USA, 2011.

117. Rajpal, D.; De Breuker, R.; Timmermans, H.; Lammen, W.F.; Torrigiani, F. Including Aeroelastic Tailoring In The Conceptual Design Process of A Composite Strut Based Wing. In Proceedings of the 31st Congress of the International Council of the Aeronautical Sciences, ICAS 2018, Belo Horizonte, Brazil, 9–14 September 2018; pp. 1–12.

118. Model Testing of High Lift System. Available online: https://cordis.europa.eu/project/id/865267 (accessed on 28 February 2022).

119. Ciobaca, V.; Wild, J. An Overview of Recent DLR Contributions on Active Flow-Separation Control Studies for High-Lift Configurations. *AerospaceLab* **2013**, *6*, 1–12.

120. Viken, J.K.; Viken, S.; Deere, K.A.; Carter, M. Design of the Cruise and Flap Airfoil for the X-57 Maxwell Distributed Electric Propulsion Aircraft. In Proceedings of the 35th AIAA Applied Aerodynamics Conference, Denver, CO, USA, 5–9 June 2017; pp. 1–41.

121. Memmolo, V. *Structural Health Monitoring of Complex Structures Based on Propagation and Scattering of Guided Ultrasonic Waves in Composite Media*; University of Naples "Federico II": Naples, Italy, 2018.

122. Cusati, V.; Corcione, S.; Memmolo, V. Impact of Structural Health Monitoring on Aircraft Operating Costs by Multidisciplinary Analysis. *Sensors* **2021**, *21*, 6938. [CrossRef]

123. Memmolo, V.; Monaco, E.; Boffa, N.D.; Maio, L.; Ricci, F. Guided Wave Propagation and Scattering for Structural Health Monitoring of Stiffened Composites. *Compos. Struct.* **2018**, *184*, 568–580. [CrossRef]

124. Dillingham, G.L. *Aviation Safety: Status of FAA's Actions to Oversee the Safety of Composite Airplanes*; US Government Accountability Office: Washington, DC, USA, 2011.

125. US Department of Defense. In *Composite Materials Handbook: Volume 3, Polymer Matrix Composites Guidelines for Characterization of Structural Materials*; MIL-HDBK-17-3F; US Department of Defense: Washington, DC, USA, 2002.

126. US Department of Defense. *DoD JSSG-2006 Aircraft Structures*; US Department of Defense: Washington, DC, USA, 1998.

127. Abrate, S. *Impact on Composite Structures*; Cambridge University Press: Cambridge, UK, 1998; ISBN 9780511574504. [CrossRef]

128. Kim, E.H.; Rim, M.S.; Lee, I.; Hwang, T.K. Composite Damage Model Based on Continuum Damage Mechanics and Low Velocity Impact Analysis of Composite Plates. *Compos. Struct.* **2013**, *95*, 123–134. [CrossRef]

129. Maio, L.; Monaco, E.; Ricci, F.; Lecce, L. Simulation of Low Velocity Impact on Composite Laminates with Progressive Failure Analysis. *Compos. Struct.* **2013**, *103*, 75–85. [CrossRef]

130. Wang, H.; Vu-Khanh, T. Fracture Mechanics and Mechanisms of Impact-Induced Delamination in Laminated Composites. *J. Compos. Mater.* **1995**, *29*, 156–178. [CrossRef]

131. Bouvet, C.; Castanié, B.; Bizeul, M.; Barrau, J.J. Low Velocity Impact Modelling in Laminate Composite Panels with Discrete Interface Elements. *Int. J. Solids Struct.* **2009**, *46*, 2809–2821. [CrossRef]

132. Wu, H.Y.T.; Springer, G.S. Measurements of Matrix Cracking and Delamination Caused by Impact on Composite Plates. *J. Compos. Mater.* **1988**, *22*, 518–532. [CrossRef]

133. Guynn, E.G.; O'Brien, T.K. Influence of Lay-up and Thickness on Composite Impact Damage and Compression Strength. In Proceedings of the Collection of Technical Papers-AIAA/ASME/ASCE/AHS/ASC Structures, Structural Dynamics and Materials Conference, Washington, DC, USA, 16–19 April 1985; pp. 187–196.

134. Takeda, S.; Minakuchi, S.; Okabe, Y.; Takeda, N. Delamination Monitoring of Laminated Composites Subjected to Low-Velocity Impact Using Small-Diameter FBG Sensors. *Compos. Part A Appl. Sci. Manuf.* **2005**, *36*, 903–908. [CrossRef]

135. Memmolo, V.; Maio, L.; Boffa, N.D.; Monaco, E.; Ricci, F. Damage Detection Tomography Based on Guided Waves in Composite Structures Using a Distributed Sensor Network. *Opt. Eng.* **2015**, *55*, 011007. [CrossRef]

136. Dorey, G. Impact Damage in Composites Development, Consequences and Prevention. In Proceedings of the ICCM 6: Sixth International Conference on Composite Materials ECCM 2: 2nd European Conference on Composite Materials, London, UK, 20–24 July 1987; pp. 3.1–3.26.

137. Lee, J.; Soutis, C. Experimental Investigation on the Behaviour of CFRP Laminated Composites under Impact and Compression after Impact (CAI). In *EKC-2008 Proceedings of the EU-Korea Conference on Science and Technology*; Springer: Berlin/Heidelberg, Germany, 2008; Volume 124, pp. 275–286.

138. U.S. Department of Transportation. *AC 20-107B: Composite Aircraft Structure*; Federal Aviation Administration: Washington, DC, USA, 2010; Volume 1, pp. 1–2.

139. FAA, AC. *Federal Aviation Administration AC 25.571-1D Damage Tolerance and Fatigue Evaluation of Structure*; U.S. Government Publishing Office: Washington, DC, USA, 2011.

140. Pugno, N.; Ciavarella, M.; Cornetti, P.; Carpinteri, A. A Generalized Paris' Law for Fatigue Crack Growth. *J. Mech. Phys. Solids* **2006**, *54*, 1333–1349. [CrossRef]

141. U.S. Department of Defense. *MIL-HDBK No: 1823A. Nondestructive Evaluation System Reliability Assessment*; U.S. Department of Defense: Washington, DC, USA, 2009.

142. Liew, C.K.; Veidt, M.; Rajic, N.; Tsoi, K.; Rowlands, D.; Morton, H. Inspections of Helicopter Composite Airframe Structures Using Conventional and Emerging Nondestructive Testing Methods. *J. Test. Eval.* **2011**, *39*, 6. [CrossRef]

143. Peng, W.; Zhang, Y.; Qiu, B.; Xue, H. A Brief Review of the Application and Problems in Ultrasonic Fatigue Testing. *AASRI Procedia* **2012**, *2*, 127–133. [CrossRef]

144. Kroeger, T. Thermographic Inspection of Composites. *Reinf. Plast.* **2014**, *58*, 42–43. [CrossRef]

145. Vavilov, V.P.; Budadin, O.N.; Kulkov, A.A. Infrared Thermographic Evaluation of Large Composite Grid Parts Subjected to Axial Loading. *Polym. Test.* **2015**, *41*, 55–62. [CrossRef]

146. Maio, L.; Memmolo, V.; Boccardi, S.; Meola, C.; Ricci, F.; Boffa, N.D.; Monaco, E. Ultrasonic and IR Thermographic Detection of a Defect in a Multilayered Composite Plate. *Procedia Eng.* **2016**, *167*, 71–79. [CrossRef]

147. Tan, K.T.; Watanabe, N.; Iwahori, Y. X-ray Radiography and Micro-Computed Tomography Examination of Damage Characteristics in Stitched Composites Subjected to Impact Loading. *Compos. Part B Eng.* **2011**, *42*, 874–884. [CrossRef]

148. Bossi, R.H.; Giurgiutiu, V. Nondestructive Testing of Damage in Aerospace Composites. In *Polymer Composites in the Aerospace Industry*; Woodhead Publishing: Sawston, UK, 2015; pp. 413–448. ISBN 9780857099181.

149. Sarasini, F.; Santulli, C. Non-Destructive Testing (NDT) of Natural Fibre Composites: Acoustic Emission Technique. In *Natural Fibre Composites: Materials, Processes and Applications*; Woodhead Publishing: Sawston, UK, 2014; pp. 273–302. ISBN 9780857095244.

150. Su, Z.; Zhou, C.; Hong, M.; Cheng, L.; Wang, Q.; Qing, X. Acousto-Ultrasonics-Based Fatigue Damage Characterization: Linear versus Nonlinear Signal Features. *Mech. Syst. Signal Process.* **2014**, *45*, 225–239. [CrossRef]

151. Hung, Y.Y.; Yang, L.X.; Huang, Y.H. 5 Non-Destructive Evaluation (NDE) of Composites: Digital Shearography BT-Non-Destructive Evaluation (NDE) of Polymer Matrix Composites. In *Non-Destructive Evaluation (NDE) of Polymer Matrix Composites*; Woodhead Publishing: Sawston, UK, 2013; pp. 84–115. ISBN 9780857093448.

152. Yang, S.H.; Kim, K.B.; Oh, H.G.; Kang, J.S. Non-Contact Detection of Impact Damage in CFRP Composites Using Millimeter-Wave Reflection and Considering Carbon Fiber Direction. *NDT & E Int.* **2013**, *57*, 45–51. [CrossRef]

153. Memmolo, V.; Boffa, N.D.; Maio, L.; Monaco, E.; Ricci, F. Damage Localization in Composite Structures Using a Guided Waves Based Multi-Parameter Approach. *Aerospace* **2018**, *5*, 111. [CrossRef]

154. Parodi, M.; Fiaschi, C.; Memmolo, V.; Ricci, F.; Maio, L. Interaction of Guided Waves with Delamination in a Bilayered Aluminum-Composite Pressure Vessel. *J. Mater. Eng. Perform.* **2019**, *28*, 3281–3291. [CrossRef]

155. Giurgiutiu, V. Structural Health Monitoring with Piezoelectric Wafer Active Sensors. In Proceedings of the 16th International Conference on Adaptive Structures and Technologies, Kuala Lumpur, Malaysia, 30–31 August 2006; DEStech Publications: Lancaster, PA, USA, 2006; pp. 94–100, ISBN 978-1932078572.

156. Twin Otter Series 400 Brochure. Available online: https://www.utilityair.com/wp-content/uploads/2019/12/TOSeries400_brochure_FEB2019_LOW.pdf (accessed on 2 March 2022).

157. Markou, C.; Cros, G.; Cioranu, A.; Yang, E. *Airline Maintenance Cost Executive Commentary*; International Air Transport Association (IATA): Geneva, Switzerland, 2011.

158. Ferjan, K. *Airline Cost Management Group (ACMG)*; International Air Transport Association (IATA): Geneva, Switzerland, 2015.

159. Ackert, S.P. *Basics of Aircraft Maintenance Programs for Financiers*; Aircraft Monitor: San Francisco, CA, USA, 2010.

160. Ricci, F.; Monaco, E.; Maio, L.; Boffa, N.D.; Memmolo, V. The Role of SHM in the Design and Maintenance of Modern and Aging Structures. Presented at the International Symposium on Dynamic Response and Failure of Composite Materials, Island of Ischia, Italy, 21–24 June 2016.

161. El-Sayed, A.F. *Bird Strike in Aviation: Statistics, Analysis and Management*; John Wiley & Sons: Hoboken, NJ, USA, 2019; ISBN 9781119529835.

162. SAE International. *ARP6275-Determination of Cost Benefits from Implementing an Integrated Vehicle Health Management System*; SAE International: Warrendale, PA, USA, 2019.

163. Kent, R.M.; Murphy, D.A. *Health Monitoring System Technology Assessments-Cost Benefits Analysis*; National Aeronautics and Space Administration (NASA): Washington, DC, USA, 2000.

164. Currey, N.S. *Aircraft Landing Gear Design: Principles and Practices*; American Institute of Aeronautics and Astronautics: Washington, DC, USA, 1988; ISBN 978-0-930403-41-6.

165. Srivastava, A.N.; Mah, R.W.; Meyer, C. Integrated Vehicle Health Management of a Transport Aircraft Landing Gear System. *Anim. Prod. Sci.* **2009**, *49*, 73.

166. Raymer, D. *Aircraft Design: A Conceptual Approach*; American Institute of Aeronautics and Astronautics: Washington, DC, USA, 2013; ISBN 0791847276.

167. Roskam, J. *Airplane Design Part III: Layout Design of Cockpit, Fuselage, Wing and Empennage: Cutaways and Inboard Profiles*; DARcorporation: Lawrence, KS, USA, 2002; ISBN 9781884885563/188488556X.

168. Torenbeek, E. *Synthesis of Subsonic Airplane Design*; Delft University Press: Delft, The Netherlands, 1982; ISBN 9024727243.

169. Dababneh, O.; Kipouros, T. A Review of Aircraft Wing Mass Estimation Methods. *Aerosp. Sci. Technol.* **2018**, *72*, 256–266. [CrossRef]

170. Van der Velden, A.; Kelm, R.; Kokan, D.; Mertens, J. Application of MDO to Large Subsonic Transport Aircraft. In Proceedings of the 38th Aerospace Sciences Meeting and Exhibit, Reno, NV, USA, 10–13 January 2000.

171. Elham, A.; Van Tooren, M.J.L. Tool for Preliminary Structural Sizing, Weight Estimation, and Aeroelastic Optimization of Lifting Surfaces. *Proc. Inst. Mech. Eng. Part G J. Aerosp. Eng.* **2016**, *230*, 280–295. [CrossRef]

172. Mardanpour, P.; Hodges, D.H. On the Importance of Nonlinear Aeroelasticity and Energy Efficiency in Design of Flying Wing Aircraft. *Adv. Aerosp. Eng.* **2015**, *2015*, 613962. [CrossRef]

173. Mardanpour, P.; Hodges, D.H.; Rezvani, R. Nonlinear Aeroelasticity of High-Aspect-Ratio Wings Excited by Time-Dependent Thrust. *Nonlinear Dyn.* **2014**, *75*, 475–500. [CrossRef]

174. Mardanpour, P.; Hodges, D.H.; Neuhart, R.; Graybeal, N. Engine Placement Effect on Nonlinear Trim and Stability of Flying Wing Aircraft. *J. Aircr.* **2013**, *50*, 1716–1725. [CrossRef]

175. Mardanpour, P.; Richards, P.W.; Nabipour, O.; Hodges, D.H. Effect of Multiple Engine Placement on Aeroelastic Trim and Stability of Flying Wing Aircraft. *J. Fluids Struct.* **2014**, *44*, 67–86. [CrossRef]

176. Joslin, R.D. Aircraft Laminar Flow Control. *Annu. Rev. Fluid Mech.* **1998**, *30*, 1–29. [CrossRef]

177. Kulfan, R.M.; Vachal, J.D. *Wing Planform Geometry Effects on Large Subsonic Military Transport Airplanes*; Boeing Commercial Airplane Company: Seattle, WA, USA, 1978.

178. Park, P. The Effect on Block Fuel Consumption of a Strutted versus Cantilever Wing for a Short-Haul Transport Including Strut Aeroelastic Considerations. In Proceedings of the Aircraft Systems and Technology Conference, Los Angeles, CA, USA, 21–23 August 1978; American Institute of Aeronautics and Astronautics: Reston, VA, USA, 1978.

179. Turriziani, R.V.; Lovell, W.A.; Martin, G.L.; Price, J.E.; Swanson, E.E.; Washburn, G.F. *Preliminary Design Characteristics of a Subsonic Business Jet Concept Employing an Aspect Ratio 25 Strut-Braced Wing*; National Aeronautics and Space Administration (NASA): Washington, DC, USA, 1980.

180. Gern, F.H.; Naghshineh-Pour, A.H.; Sulaeman, E.; Kapania, R.K.; Haftka, R.T. Structural Wing Sizing for Multidisciplinary Design Optimization of a Strut-Braced Wing. *J. Aircr.* **2001**, *38*, 154–163. [CrossRef]

181. Barbarino, S.; Bilgen, O.; Ajaj, R.M.; Friswell, M.I.; Inman, D.J. A Review of Morphing Aircraft. *J. Intell. Mater. Syst. Struct.* **2011**, *22*, 823–877. [CrossRef]

182. Pecora, R.; Concilio, A.; Dimino, I.; Amoroso, F.; Ciminello, M. Structural Design of an Adaptive Wing Trailing Edge for Enhanced Cruise Performance. In Proceedings of the 24th AIAA/AHS Adaptive Structures Conference, San Diego, CA, USA, 4–8 January 2016.

183. Amendola, G.; Dimino, I.; Concilio, A.; Pecora, R.; Amoroso, F.; Arena, M. Morphing Aileron. In *Morphing Wing Technologies: Large Commercial Aircraft and Civil Helicopters*; Butterworth-Heinemann: Oxford, UK, 2018; pp. 547–582. ISBN 9780081009697.

184. Moens, F. Augmented Aircraft Performance with the Use of Morphing Technology for a Turboprop Regional Aircraft Wing. *Biomimetics* **2019**, *4*, 64. [CrossRef] [PubMed]

185. Boffa, N.D.; Monaco, E.; Ricci, F.; Lecce, L.; Barile, M.; Memmolo, V. Hybrid Structural Health Monitoring on a Composite Plate Manufactured with Automatic Fibers Placement Including Embedded Fiber Bragg Gratings and Bonded Piezoelectric Patches. In *Health Monitoring of Structural and Biological Systems XIII*; Fromme, P., Su, Z., Eds.; SPIE: San Francisco, CA, USA, 2019; p. 27.

186. Ebert, L.B. Science of Fullerenes and Carbon Nanotubes. *Carbon N. Y.* **1997**, *35*, 437–438. [CrossRef]

187. Qian, H.; Greenhalgh, E.S.; Shaffer, M.S.P.; Bismarck, A. Carbon Nanotube-Based Hierarchical Composites: A Review. *J. Mater. Chem.* **2010**, *20*, 4751–4762. [CrossRef]

188. Hawkins, S.C.; Poole, J.M.; Huynh, C.P. Catalyst Distribution and Carbon Nanotube Morphology in Multilayer Forests by Mixed CVD Processes. *J. Phys. Chem. C* **2009**, *113*, 12976–12982. [CrossRef]

189. Bhanushali, H.; Bradford, P.D. Woven Glass Fiber Composites with Aligned Carbon Nanotube Sheet Interlayers. *J. Nanomater.* **2016**, *2016*, 1–9. [CrossRef]

190. Nistal, A.; Falzon, B.G.; Hawkins, S.C.; Chitwan, R.; García-Diego, C.; Rubio, F. Enhancing the Fracture Toughness of Hierarchical Composites through Amino–functionalised Carbon Nanotube Webs. *Compos. Part B Eng.* **2019**, *165*, 537–544. [CrossRef]

191. Kumar, S.; Falzon, B.G.; Kun, J.; Wilson, E.; Graninger, G.; Hawkins, S.C. High Performance Multiscale Glass Fibre Epoxy Composites Integrated with Cellulose Nanocrystals for Advanced Structural Applications. *Compos. Part A Appl. Sci. Manuf.* **2020**, *131*, 105801. [CrossRef]

192. Zhang, Y.; Ma, J.; Singh, A.K.; Cao, L.; Seo, J.; Rahn, C.D.; Bakis, C.E.; Hickner, M.A. Multifunctional Structural Lithium-Ion Battery for Electric Vehicles. *J. Intell. Mater. Syst. Struct.* **2017**, *28*, 1603–1613. [CrossRef]

193. Roberts, S.C.; Aglietti, G.S. Satellite Multi-Functional Power Structure: Feasibility and Mass Savings. *Proc. Inst. Mech. Eng. Part G J. Aerosp. Eng.* **2008**, *222*, 41–51. [CrossRef]

194. Roberts, S.C.; Aglietti, G.S. Structural Performance of a Multifunctional Spacecraft Structure Based on Plastic Lithium-Ion Batteries. *Acta Astronaut.* **2010**, *67*, 424–439. [CrossRef]

195. Thomas, J.P.; Qidwai, S.M.; Pogue, W.R.; Pham, G.T. Multifunctional Structure-Battery Composites for Marine Systems. *J. Compos. Mater.* **2013**, *47*, 5–26. [CrossRef]

196. Pereira, T.; Zhanhu, G.; Nieh, S.; Arias, J.; Hahn, H.T. Energy Storage Structural Composites: A Review. *J. Compos. Mater.* **2009**, *43*, 549–560. [CrossRef]

197. Ekstedt, S.; Wysocki, M.; Asp, L.E. Structural Batteries Made from Fibre Reinforced Composites. *Plast. Rubber Compos.* **2010**, *39*, 148–150. [CrossRef]

198. Ding, J.; Tian, T.; Meng, Q.; Guo, Z.; Li, W.; Zhang, P.; Ciacchi, F.T.; Huang, J.; Yang, W. Smart Multifunctional Fluids for Lithium Ion Batteries: Enhanced Rate Performance and Intrinsic Mechanical Protection. *Sci. Rep.* **2013**, *3*, 2485. [CrossRef]

199. Kühnelt, H.; Beutl, A.; Mastropierro, F.; Laurin, F.; Willrodt, S.; Bismarck, A.; Guida, M.; Romano, F. Structural Batteries for Aeronautic Applications—State of the Art, Research Gaps and Technology Development Needs. *Aerospace* **2022**, *9*, 7. [CrossRef]

200. Zackrisson, M.; Jönsson, C.; Johannisson, W.; Fransson, K.; Posner, S.; Zenkert, D.; Lindbergh, G. Prospective Life Cycle Assessment of a Structural Battery. *Sustainability* **2019**, *11*, 5679. [CrossRef]